

Water redistribution at the soil surface

ponding and surface runoff in flat areas

Willemijn M. Appels

Thesis committee

Promotor

Prof. Dr *ir.* S. E. A. T. M. van der Zee
Personal chair at the Soil Physics and Land Management Group
Wageningen University

Co-promotor

Dr P. W. Bogaart
Researcher Environmental sciences
Utrecht University

Other members

Prof. Dr rer. nat. I. Neuweiler, Leibniz University Hannover (Germany)
Prof. Dr *ir.* O. Oenema, Wageningen University
Dr L. Pfister, CRP Gabriel Lippmann, Luxembourg (Luxembourg)
Prof. Dr *ir.* R. Uijlenhoet, Wageningen University

This research was conducted under the auspices of the Graduate School SENSE

Water redistribution at the soil surface

ponding and surface runoff in flat areas

Willemijn M. Appels

Thesis

submitted in fulfilment of the requirements for the degree of doctor
at Wageningen University

by the authority of the Rector Magnificus

Prof. Dr M.J. Kropff,

in the presence of the

Thesis Committee appointed by the Academic Board

to be defended in public

on Tuesday 19 March 2013

at 4 p.m. in the Aula.

CIP-data Koninklijke Bibliotheek, Den Haag

Water redistribution at the soil surface: ponding and surface runoff in flat areas

Appels, W. M., 2013

PhD thesis, Wageningen University, The Netherlands
With references - with summaries in English and Dutch

ISBN 978-94-6173-506-5

Contents

1	Introduction	1
1.1	Setting the stage	2
1.2	Terminology	2
1.3	Problem definition	3
1.4	Theoretical background	4
1.5	Goals and outline of the thesis	7
2	Influence of spatial variations of microtopography and infiltration on surface runoff and field scale hydrological connectivity	9
2.1	Introduction	10
2.2	Theory	13
2.3	Results and discussion	20
2.4	Conclusions	29
3	Observations of surface runoff on flat agricultural fields: interactions between driving mechanisms and surface topography and associated thresholds	31
3.1	Introduction	32
3.2	Material and methods	34
3.3	Results and Discussion	38
3.4	Discussion	45
3.5	Conclusions and recommendations	48
4	Effects of microtopography and shallow groundwater dynamics on ponding and surface runoff in flat areas	51
4.1	Introduction	52
4.2	System schematization	54
4.3	Model description	56
4.4	Numerical experiments	59
4.5	Results and discussion	62
4.6	General discussion and concluding remarks	71
5	Spatiotemporal variability of saturation excess surface runoff in flat fields due to interactions between meso- and microtopography	75
5.1	Introduction	76
5.2	Material and methods	78
5.3	Results	85

5.4	Conclusions	96
6	Microtopography as a driving mechanism for ecohydrological processes in shallow groundwater systems	99
6.1	Introduction	100
6.2	Microtopography and runoff	103
6.3	Microtopography and response time in shallow groundwater ecosystems . .	106
6.4	Microtopography and spatial distribution of groundwater quality parame- ters and site factors	112
6.5	Closing remarks	114
7	General Discussion	117
7.1	Summary of results	118
7.2	Synthesis	120
7.3	Perspectives for process oriented research	122
7.4	Perspectives for impact oriented research	123
7.5	Final conclusions	123
	Appendix A	125

Chapter 1

Introduction

1.1 Setting the stage

Within catchments, water travels through a variety of flow routes from the point where a raindrop hits the soil surface to the point where a stream transfers it to a larger catchment or the ocean. The ensemble of flow routes and transport mechanisms defines the catchment's unique response to a rainfall event, both in discharge and water quality (Hendriks, 2010; van der Velde et al., 2012). Surface runoff or overland flow, i.e. the water that does not infiltrate into the soil during or after a rainfall event, but moves over the soil surface towards ditches, streams, or rivers while not being concentrated in channels of a defined size, is the fastest flow route in a catchment and an important carrier of sediment, nutrients, and pesticides (Turtola and Jaakkola, 1995; Pärn et al., 2012). Surface runoff is the main transport route for phosphorus and it can therefore have an important role in the eutrophication of streams and channels in agricultural areas.

In The Netherlands, one of the most important targets for the improvement of surface water quality as aimed for in the European Water Framework Directive, is the reduction of nutrient concentrations (both nitrogen and phosphorus) (Noij et al., 2009). To identify the most suitable and effective measures for reducing the transport of nutrients from field to stream, it is important that the processes that control the transport are well identified and quantified. To this aim, the Dutch Ministry of Agriculture, Nature and Food Quality (now the Ministry of Economic Affairs) commissioned several large projects to investigate the interactions between ground- and surface water to answer questions such as: How can a better quantification of the cycles of water and nutrients be achieved? How can a better understanding of these cycles be translated into policy development and management measures?

The PhD research presented in this thesis was part of the Alterra project "Relationships between groundwater and surface water" (Project 5232870-06), that aimed to answer these questions. The PhD research was specifically oriented at quantification of the surface runoff flow route in The Netherlands.

1.2 Terminology

It is appropriate to shortly define the two most abundant terms in this thesis.

Overland flow is the spatially distributed phenomenon of water moving over the soil surface and **surface runoff** is the flux of this process at a point in space. The terms are often used interchangeably. Whereas this thesis deals with overland flow, the overall goal of the study was to quantify the flux of this phenomenon at designated points in agricultural catchments. Therefore, the term surface runoff will be used throughout this thesis, also when referring to the spatially distributed phenomenon itself.

Similarly, the term **relief** refers to the elevations or inequalities of a land surface and **topography** refers to the pattern of a surface, including both its relief and position of its natural and man-made features. These terms too, are used interchangeably in scientific literature. In order to remain consistent with some of the benchmark studies in

the behaviour of surface flow on heterogeneous surfaces, the word topography is used throughout this thesis.

1.3 Problem definition

Surface runoff is an important process that affects the local water balance and causes soil erosion and rapid solute transport towards ditches, streams, and rivers. It is highly variable in space and time, resulting in variable groundwater recharge patterns and local peak inputs towards the aforementioned surface water bodies. The water balance and water quality of these water bodies are affected by the fast reaction of the water levels to surface runoff and the rapid increase of the loads of sediments and solutes such as nutrients and pesticides.

Surface runoff studies have been performed over a wide range of ecosystems, ranging from hillslopes in (semi-) arid regions, e.g. Mueller et al. (2007); Abrahams et al. (1994), to riparian wetlands, e.g. Herron and Hairsine (1998); Vellidis et al. (2003), and peat areas in wetter climate regions, e.g. (Holden et al., 2008). Though water budget studies on surface runoff have been performed before in flat, agricultural areas, such as the ones found in The Netherlands, there has been little systematic investigation into controls on and relations between driving mechanisms of surface runoff in these areas. There are several reasons for this. Firstly, in these catchments, surface runoff is a relatively rare phenomenon (Church and Woo, 1999). Rainfall events generally occur at intensities lower than the infiltration capacity of the soil. Surface runoff generated from infiltration excess is rare, except on clay soils, and will mostly be restricted to the summer months during which convective rain storms give rise to the occasional high intensity rainfall event. In case of shallow groundwater levels, saturation excess surface runoff may occur during wet seasons when the soil is completely saturated, but less so if catchments are well (artificially) drained. The latter is the case for most agricultural catchments, except for peat grasslands, where the groundwater level is kept close to the soil surface to prevent the peat from oxidizing and compacting. Secondly, measuring and modelling surface runoff is not a trivial thing to do. Because of the highly variable nature of the surface runoff process and its spillpoints towards the ditches in both space and time, it can be very costly to set up a measurement installation only to measure a small amount of water. Modelling surface runoff involves coupling the equations for free surface water flow to those of a variably saturated medium. The interface between these zones is numerically stiff and complex due to the different magnitudes of the timescales involved. In the flat agricultural catchments, the direction of flow is not determined by a clear large scale gradient, but by local gradients of topographic features with dimensions ranging from centimeters to a couple of meters. The development of surface runoff in such topographies involves ponding of water in small ponds and flow directions that can change when a pond fills up and starts to spill water to another pond. Mathematically, this is quite complex. Thirdly, because of the spatial variability of the surface runoff process, observations of surface runoff at a chosen location or detailed process modelling

of a certain field or hillslope can be highly unrepresentative for what happens at another location.

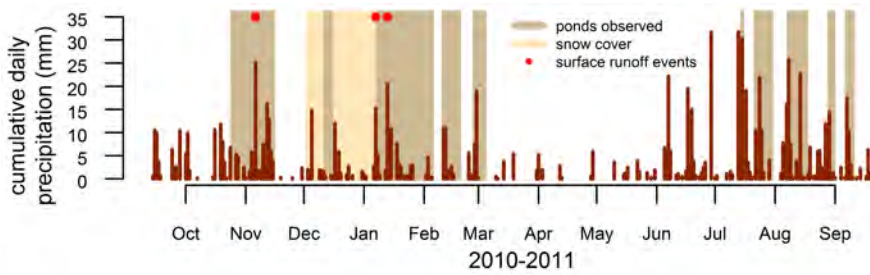
The estimation of surface runoff contribution in water balance studies in e.g. The Netherlands is rather inexact because of these issues. More specifically, the interactions between surface runoff controls and the role of the soil surface in transporting water to streams has not been given appropriate attention (Stolte et al., 2000).

1.4 Theoretical background

1.4.1 Surface runoff characteristics

Surface runoff is generated when the soil saturates from either above or below. From above, the rainfall rate and runoff from upslope areas exceed the infiltration capacity of the soil. This mechanism is known as infiltration excess or Hortonian surface runoff, named after Robert E. Horton, the first to describe the partitioning of rainfall between infiltration and runoff at the soil surface (Horton, 1933). From below, the groundwater table rises up to the soil surface until there is no more pore space available to store water. This mechanism is known as saturation excess or Dunne surface runoff, named after Thomas Dunne, the first to publish a study on non-Hortonian surface runoff generation (Dunne and Black, 1970). Infiltration and saturation excess are the limits of a larger spectrum of surface runoff generating mechanisms. In the field, the distinction may not always be so clear, as also at moderate rainfall intensities (lower than the infiltration capacity) and an unsaturated soil, surface runoff can occur when the rainfall rate exceeds the vertical percolation rate. This intermediate surface runoff generating process has been coined “Dunton” (Loague et al., 2010). The very definition of surface runoff, i.e. flow on the soil surface that does not occur in well-defined channels, indicates that it has a variable nature. The initiation of surface runoff is variable in space due to heterogeneity of 1) the soil and soil degradation processes such as compaction, sealing, and crust formation affecting the infiltration properties of the soil (Deasy et al., 2009) and of 2) saturation levels of the soil due to groundwater fluctuations affecting the subsurface storage capacity (Heathwaite et al., 2005). While the latter may occur from field scale size (order of magnitude 10^4 m^2), the former type of heterogeneity affects surface runoff initiation even at plot scales (order of magnitude $1\text{--}10 \text{ m}^2$). This spatial heterogeneity combined with temporal dynamics of precipitation create a large intra- and inter-field variability in the extent, volume, rate, and timing of surface runoff events within a catchment (Haygarth et al., 2000).

In hilly areas, the large scale topographical gradient is the dominant aspect in routing surface runoff. Steeper slopes increase the velocity of flow and thereby increase the risk of erosion (Hairsine and Rose, 1992). In areas with a negligible large scale elevation gradient, **microtopography**, consisting of (ir)regular topographical features such as soil clods, crop rills, clumps of vegetation or washed on sediments, is the main factor in routing non-infiltrating water. Surface runoff has an intricate relationship with vegetation: the phenomenon itself is responsible for a variable distribution of



(a)



(b)



(c)

Figure 1.1: Illustrations of temporal and spatial variability of surface runoff. Fig. a: rainfall time-series with ponding observations and surface runoff events connecting ponds with the ditch at Wageningen UR campus. Lower row: adjacent fields in the southern part of The Netherlands. Photos taken on the same day: surface runoff event on field (b), no ponding and no surface runoff on field (c).

micronutrients, creating microhabitats, whereas vegetation in general decreases surface runoff impact and volumes by dampening the impact of raindrops (De Baets et al., 2006), increasing the infiltration capacity of the soil (Weiler and Naef, 2003; Abrahams et al., 2003), and thereby allowing persistence of self-organized vegetation patterns (Rietkerk et al., 2002). These effects are mainly found in semi-arid areas. In wetlands, clumps and tussocks of plants create a microtopography that in turn affects the routing of surface runoff (Peach and Zedler, 2006; Pouliot et al., 2011).

1.4.2 Measurements

The distributed nature of surface runoff poses practical restrictions to large scale measurement of surface runoff in terms of equipment, labour, and money. Surface runoff events do not occur very often (Fig. 1.1a), so measurements should be conducted over periods of multiple years. The positioning of weirs or flumes in non-well-defined channels is another challenge. In general, surface runoff is therefore collected along a logical transect of either a plot, field, or hillslope. This means that only the spillpoint from a hillslope or field to a stream is monitored and no information on the spatial variation of

surface runoff generation within this unit is gathered. Though it may be desirable to surround a complete field with gutters or trenches, it is more common to place gutters along segments of a field, where surface runoff has been observed before (Deasy et al., 2009). The positioning of equipment at locations where surface runoff, if any, is known to occur, can lead to an overestimation of the surface runoff flux in a catchment when one takes these numbers as the base of one's calculations. Figures 1.1b and c are examples from the southern part of The Netherlands, where two adjacent fields have a very different appearance on the same day. The field in Fig.1.1b experienced surface runoff from the field to the surrounding ditch days before and after the photos were taken, whereas the other field did not give a sign of ponding during this period. However, also less extreme cases may still be variable in producing surface runoff discharge, as the actual overflow may depend on random or erratic features such as macrofauna burrows.

1.4.3 Modelling

Modelling surface runoff in relation with groundwater and unsaturated water flow is a recognized challenge in hydrology. Reasons are the heterogeneity of the soil and surface characteristics, the strong nonlinearity of the equations (which differ for the surface water, unsaturated zone, and groundwater), the complexity of boundary conditions, that link these zones, and quite different time constants. All in all, this leads to stiff problems and unstable numerical schemes (Sophocleous, 2002). Consequently, strong simplifications have been commonly adopted with regard to the degree of coupling of zones or the boundary conditions that are used (Smith and Hebbert, 1983). Still, significant advances have been made on coupled schemes. Hydrological models that feature two-dimensional surface flow coupled to infiltration or variably saturated media exist, e.g. ParFlow (Kollet and Maxwell, 2006), CATHY (Paniconi and Wood, 1993; Orlandini et al., 1996; Camporese et al., 2010), tRIBS (Ivanov et al., 2004), but these are not able to deal with heterogeneous surface topographies through which surface runoff must be routed. There is a handful of models that solve two-dimensional surface flow on heterogeneous surfaces (Antoine et al., 2009), also on infiltrating surfaces (Delestre et al., 2012). To date, only HydroGeoSphere (Therrien et al., 2008) has been reported being able to deal with saturation excess surface runoff in heterogeneous topographies (Frei et al., 2010). Due to the strong nonlinearity and complexity of the equations, simulations with these models take a lot of time (Frei et al., 2010), and developers prefer to use reduced-complexity (parsimonious) models when a larger set of simulations is desired (Antoine et al., 2009). Alternative strategies for the modelling of surface runoff through complex surfaces typically involve ignoring flow hydraulics, assuming instantaneous redistribution in every timestep (Darboux et al., 2001; Antoine et al., 2009; Appels et al., 2011).

To arrive at meaningful model simplifications, it is necessary to focus the model to be developed towards the system that is of primary importance, which, in turn, depends on the application. The system that is central to the present project comprises a

relatively flat area of limited horizontal extent and shallow groundwater level. The justification to limit the horizontal extent to typically 100 m² scale is that due to the area's flatness, surface runoff is expected to be approximately oriented towards surface water and follow rill and depressions of the soil surface with sizes ranging from decimeters to several meters.

1.5 Goals and outline of the thesis

The general aim of this thesis is to investigate and quantify the development of surface runoff on relatively flat soils of catchments in temperate climate zones. The questions at the basis of the research presented in this thesis are:

- What are the main driving mechanisms of surface runoff in these catchments?
- What rainfall conditions prevail during surface runoff events?
- How do flow routes develop during surface runoff events in various types of surface topography?

To answer these research questions, I measured surface runoff volumes at agricultural fields in The Netherlands and developed a numerical model for the redistribution of water over a heterogeneous soil surface. I applied this model to real and simulated soil surfaces, conducting sensitivity analyses under conditions of both infiltration excess and saturation excess surface runoff. With this approach, I intend to find generic processes and structures that underlay surface runoff generation from observed field characteristics. The ability to quantitatively estimate the contribution of surface runoff as a function of characteristics such as rainfall amount, soil type, dimensions of the microtopography, and groundwater conditions will contribute to the determination of surface runoff risk and impact throughout catchments. Based on this risk estimation, effective measures can be designed, selected, and implemented at those locations where surface runoff has a significant effect on the water quality of streams and ditches. The identification of the most important controls of surface runoff generation can be used to propose improved measurement schemes to acquire data that can be used for calibration and validation of regional and national hydrological models.

In Chapter 2, I investigate surface runoff development from the perspective of hydrological connectivity. The object-oriented ponding and redistribution model I developed, is used to simulate infiltration excess surface runoff generation in synthetic soil surfaces with varying statistical properties. Chapter 3 reports on the measurements at the agricultural fields in the eastern part of The Netherlands. I examined hydrological data obtained on two field sites in The Netherlands for a period of 1.5 years from several points of view to give an integrated narrative of surface runoff in the flat lowland agricultural catchments that are the subject of this thesis. Chapter 4 deals with an extended version of the ponding and redistribution model, which includes lateral groundwater flow as well as infiltration and redistribution of water on the soil surface.

With this model (FAST-Runoff), I quantify the generation of saturation excess surface runoff in fields with simulated microtopographies and mesotopographies for a large range of rainfall events, soil types and initial conditions. In Chapter 5 an attempt is made to apply the FAST-Runoff model to real fields with varying micro- and mesotopography. To this end, I used topographic data from three agricultural fields in the southern part of The Netherlands, where surface runoff measurements have been performed by the research institute Alterra. I discuss the results of model simulations on parts of the fields and compare them to the volume and nutrient loads of surface runoff that was measured at these sites. Chapter 6 is a collaborative effort that reviews the intricate relationships between microtopography, surface runoff, and ecohydrology in systems featuring shallow water tables. With the ponding and redistribution model, it is shown how microtopography could add flexibility to the acrotelm-catotelm concept in raised bog hydrology. Also, the effects of microtopography and surface runoff on the mixing of water with different chemical signatures and the subsequent results in variations of the occurrence of plant species are demonstrated. A synthesis of the research presented in this thesis is given in Chapter 7. Additionally, implications and applications of the results in larger scale hydrological models and perspectives for further research on surface runoff in complex landscapes are discussed.

Chapter 2

Influence of spatial variations of microtopography and infiltration on surface runoff and field scale hydrological connectivity

Abstract

Surface runoff on agricultural fields arises when rainfall exceeds infiltration. Excess water ponding in and flowing through local microtopography increases the hydrological connectivity of fields. In turn, an increased level of hydrological connectivity leads to a higher surface runoff flux at the field boundaries. We investigated the functional hydrological connectivity of synthetic elevation fields with varying statistical properties. For this purpose, we developed an object-oriented ponding and redistribution model to which Philip's infiltration model was coupled. The connectivity behaviour is determined by the presence of depressions with a large area and spatial organization of microtopography in rills or channels. The presence of microdepressions suppresses the effect of the spatial variation of infiltration properties. The connectivity behaviour of a field with a varying spatial distribution of infiltration properties can be predicted by transforming the unique connectivity function that was defined for a designated microtopography.

2.1 Introduction

In groundwater dominated lowland catchments the larger part of precipitation on drained agricultural fields recharges the groundwater or reaches surface waters through subsurface drains. However, shallow subsoil structure deterioration due to sealing or compaction, shallow groundwater tables and long and intense precipitation events facilitate ponding of water at the soil surface. During a rainfall event, the ponded area on the field expands and surface runoff reaches the field boundaries when one or more series of ponds form continuous flow paths to the channels and ditches surrounding the field. To understand catchment discharge characteristics it is important to quantify the relative contributions of different flow routes in a catchment (van der Velde et al., 2010). Surface runoff is not only important with regard to the water balance of a catchment. Also, substances that are applied to or reside at soil surfaces can be rapidly mobilised and transferred to channels and rivers by surface runoff and the sediment transport associated with it. It is the main contributor of pesticides to surface-water bodies and one of the main contributors of phosphorus to aquatic ecosystems (Blanchoud et al., 2007; Louchart et al., 2001; Probst, 1985; Turtola and Jaakkola, 1995; Simard et al., 2000; Heathwaite et al., 2005). Surface runoff therefore plays an important role with regard to the contamination, the eutrophication, and the implications for ecological functioning of these systems (van der Velde et al., 2009; Deasy et al., 2009; Bolinder et al., 2000). From the perspective of complying with European standards for surface water quality as incorporated in the EU Water Framework Directive, surface runoff may well be a crucial factor regarding success or failure of environmental measures aimed at protecting surface water quality.

The onset and duration of surface runoff depends on several aspects. It is obvious that precipitation intensity and duration, infiltration properties of the soil, which depend



Figure 2.1: Ponded water on a flat field (a) and flow of surface runoff through a biopore (mole burrow) (b). Photographs were taken in the East of The Netherlands, February 2010.

on e.g. the initial soil moisture condition, and height of the groundwater table affect the infiltration capacity of the soil and the amount of water available for ponding and surface runoff. The way in which ponds at the field surface combine and form flowpaths depends mainly on the spatial organization of the microtopography of the field, in particular when the area is flat.

The drivers of surface runoff are variable in space and time and extend over different spatial and temporal scales. Soil moisture conditions (or groundwater levels) fluctuate over time periods of e.g. weeks, whereas the actual beginning of surface runoff occurs in a couple of minutes. Similarly, excess water may pond on an area of several square meters (Fig. 2.1a), whereas the actual flowroute to the surface water can be determined by the coincidental presence of preferential flowpaths such as mole burrows (Fig. 2.1b).

Little is known about the magnitude of the contribution of surface runoff to the catchment water balance. In a recent experimental study the magnitudes of various flow routes in a tile-drained field were measured and quantified (van der Velde et al., 2010; Rozemeijer, 2010). The study illustrates the irregular occurrence of surface runoff in space and time: two events were observed during the measurement period of 1.5 years, and only a fraction of the field location contributed to the ponding and runoff event (van der Velde et al., 2010). Besides, it also illustrates the qualitative impact of surface runoff: the P-concentrations measured in the surface runoff samples were on average ten times as high as the concentrations of groundwater and tile-drain effluent reaching the ditch (Rozemeijer, 2010). However, the surface runoff flux was difficult to measure directly (van der Velde et al., 2010). A measurement campaign in the field specifically aiming at measuring surface runoff would require a dense network of sensors to be installed for a prolonged period of time in the hope of capturing surface runoff events. Moreover, considering the local character of the surface runoff process, it is not very likely that one field is representative for the catchment as a whole, thus requiring multiple campaigns in

a single catchment. As performing such campaigns throughout a catchment is not practically and financially feasible, numerical modelling can provide more generic insight on the effects of variability of the driving processes.

Adequate physical modelling of the processes involved in the development of surface runoff requires a fine spatial and temporal discretization (van der Velde et al., 2010; Bronstert and Bárdossy, 2003). This can be and has been done with brute numerical force on field and hillslope scale e.g. Fiedler and Ramirez (2000). When interested in a broader investigation of varying scenarios, physical modelling with fine discretization requires too much computational power and when modelling the catchment scale a subgrid approach is therefore desirable (Antoine et al., 2009). The concept of hydrological connectivity can be used to translate small scale dynamics to catchment studies (Lexartza-Artza and Wainwright, 2009). The development of ponding and surface runoff at small spatial scales has been investigated from a perspective of hydrological connectivity in several studies (Darboux et al., 2001, 2002a,b; Antoine et al., 2009). Hydrological connectivity in a landscape, though reported to lack a broadly accepted definition (Bracken and Croke, 2007), commonly refers to the continuous passage of water from one part of the landscape to another, thereby generating some catchment runoff response (Bracken and Croke, 2007). This passage depends on static or *structural* elements such as topography and soil surface properties on the one hand and dynamic or *functional* processes such as the capacity of water to move through the system in response to some forcing on the other hand (Antoine et al., 2009). In the case of surface runoff, structural connectivity results from the aforementioned microtopography and functional connectivity from the spatial variability of saturated areas, infiltration properties, vegetation, and flow resistance (Mueller et al., 2007). Structural and functional connectivity cannot be strictly separated. For instance, the organization of microtopography creates certain flowpaths at the surface, which, when carrying water, erode and alter the local microtopography. However, on the timescale of an event, it is common to assume that the elements that constitute structural connectivity do not change (Antoine et al., 2009). These elements are in general easier to measure than functional connectivity, therefore most indicators of connectivity require a fine digital elevation model (DEM) as input and are for example combined with other maps of spatially distributed hydraulic conductivity and vegetation (Mueller et al., 2007). With these data, connectivity length (a measure derived from percolation theory) (Darboux et al., 2002a) or a distribution of flowlengths along a hillslope (Mayor et al., 2008) may be calculated to determine connectivity of various surfaces. Measures derived from percolation theory have previously been used to assess subsurface hydrological connectivity (Western et al., 2001). Another static measure of connectivity proposed by Bracken and Croke (2007) is the volume of water required to start surface runoff to characterize the behaviour of two hillslopes. Antoine et al. (2009) compare several of these structural methods to a simplified hydrograph of microtopographic surfaces with different connectivity properties. The hydrograph is an indicator of functional

connectivity that is able to reflect structural connectivity differences, as the hydrographs of similar rainfall events are different for varying DEM settings. Lane et al. (2009) represent landscape hydrological connectivity with a topographically driven surface flow index (an adaptation of the topographic index (Kirkby, 1975)). The combined effect of infiltration and microtopography on functional connectivity at the field scale has not been quantified yet (Antoine et al., 2009).

In this study, we numerically investigate the development of hydrological connectivity as a function of microtopography and infiltration during a rainfall event. The analysis consists of three steps. First, we examine the effect of microtopographical statistics and configuration on depression storage and functional connectivity. Second, we develop a framework to integrate the effect of spatially uniform infiltration. Third, we analyze if the results of the second step still hold in the presence of non-uniform infiltration. The goal is to understand how indicators of hydrological connectivity respond to spatial heterogeneity in terms of microtopography and infiltration parameters. The analyses are based on numerical simulations of runoff on synthetic microtopographical fields with distinct spatial patterns.

2.2 Theory

We investigated the development of connectivity at fields without a regional gradient, with spatially heterogeneous microtopography and soil hydraulic properties, and surrounded by ditches as these are typical for the lowland areas we are interested in. For this purpose, we needed a flexible, versatile model that is able to simulate surface runoff using fine spatial and temporal resolutions (of the order of magnitude of centimeters and minutes). A fully coupled model for surface runoff and infiltration is prone to stability and convergence problems because of this heterogeneity. Therefore we developed a versatile, object oriented ponding and redistribution model and coupled it to a simple analytical infiltration model. The topographies and spatial distributions of soil hydraulic properties we used in the analysis are synthetic, so we were able to control all statistical properties of the topographies and investigate their effect on connectivity.

2.2.1 Topography

Though microtopography at the millimeter scale has been reported to be normally or lognormally distributed (Cremers et al., 1996), the spatial organization of e.g. rills, furrows, and animal tracks is not replicated when generating Gaussian random fields. Therefore, we generated topographies with different spatial organizations. Random topographies were generated in R Statistical Software (R Development Core Team, 2010) with the `RandomFields` package. We used an exponential covariance function for the definition of the semivariogram shape. By varying the variance σ^2 and integral scale l of this function, we modified the height variations and the average area of the depressions and hills of the topographies. The surfaces have no underlying trend (i.e. the microtopography is relative to a horizontal plane). To generate fields with a different

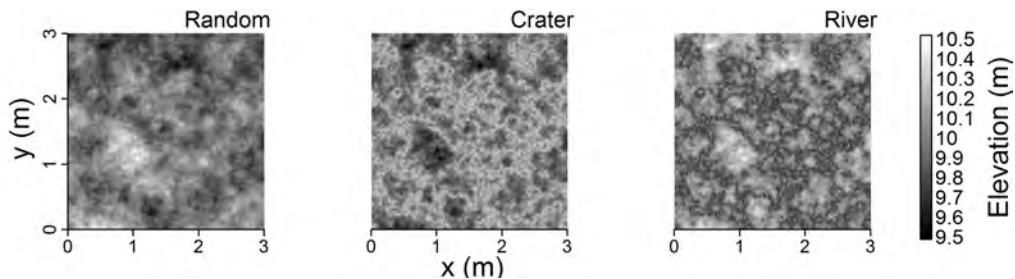


Figure 2.2: Detail of generated topographies with the same probability density function, but different spatial organization. From left to right: random, crater, and river topography. Statistics used are mean $\mu = 10$ m, standard deviation $\sigma = 0.03$ m, integral scale $l = 0.3$ m, plot size $L = 3$ m, and cell size $\Delta x = 0.01$ m

spatial organisation, we used the method developed by Zinn and Harvey (2003) to transform random topographies to topographies with a distinct crater structure and to topographies with a distinct channel (river) structure (illustrated in Fig. 2.2). This method, originally designed to generate conductivity fields with different patterns of connectivity, preserves the probability density function of a distribution and features near-identical isotropic spatial covariance functions. It has been used before to transform synthetic topographies by Antoine et al. (2009).

2.2.2 Flow routing

We developed an algorithm that explicitly deals with the filling, merging, and connecting of depressions in a field. In the DEM of each field, the location of sinks is found from the steepest gradient of the soil level in a four-neighbour scheme. The depressions belonging to the sinks are defined and saved as objects in a database. In the database, characteristics of each depression are collected including area, storage capacity, and spill points to neighbouring depressions. In every timestep of the simulation of a rainfall event a water balance is calculated for all depressions in the database under the assumption of instantaneous water transfer. When the amount of rainfall and runoff in a certain depression exceeds the capacity of the depression, water spills over the lowest spillpoint to a neighbouring depression. When the capacity of this neighbouring depression is exceeded as well, the excess water is routed over the lowest spillpoint of this depression. If the two depressions share their lowest spillpoint, they merge to form a new depression with a new storage capacity and new lowest spillpoint to the surroundings. Water that spills over the field boundary is added to the total runoff volume of the field. Runoff is allowed to drain freely at all sides of the fields. The algorithm is illustrated in pseudocode in Fig. 2.3. As all information regarding the depressions is present from the beginning of the simulation, the redistribution phase of the algorithm is fast. The structure of the database with various spillpoints for each depression allows for changes of flow direction during the simulation of a rainfall event. This is illustrated in Fig. 2.4. Since we neglect the flow dynamics of the surface runoff, we neglect the amount of water stored in

Analysis of topography	READ digital elevation model find pits and outlets determine catchments of pits and outlets determine spillpoints and static characteristics of catchments WRITE catchment database
Simulation	<pre> DO for each timestep DO for each catchment Determine water input from precipitation and previous ponding Determine infiltrated volume per cell Update catchment water volume and height of ponding layer IF catchment storage capacity is reached Add catchment to redistribution list ENDIF ENDDO DO WHILE there are catchments on redistribution list Check lowest spillpoint of catchment C1 IF spillpoint == outlet Add excess water to surface runoff volume ELSEIF storage capacity of neighboring catchment C2 is reached IF catchments C1 and C2 share lowest spillpoint Merge C1 and C2 to new catchment C4 Add C4 to redistribution list ELSE Pass excess water to neighboring catchment C3 Add C3 to redistribution list ENDIF ELSE Pass excess water to neighbor C2 ENDIF ENDDO WRITE waterbalance, ponding depth, and contributing area to file ENDDO </pre>

Figure 2.3: Pseudocode of the ponding and redistribution algorithm

detention storage and only consider water stored in depression storage.

The assumption of instantaneous water transfer is justified by the observation that in a field that contains many small depressions, the transfer of water is controlled by the duration needed to fill the depressions and the time required by water to move from one depression to the other can be neglected. Furthermore, an instantaneous flow model is computationally much faster than a full 2D hydraulic model and is therefore more suitable for analysis of a large amount of elevation fields. This benefit is illustrated by Antoine et al. (2009) who developed a 2D hydraulic model for the simulation of surface runoff on a heterogeneous topography. For their connectivity analyses, however, they used an instantaneous flow model similar to the one described above as the hydraulic runoff model was 1000 times slower than the instantaneous flow model (Antoine et al., 2009). The versatile setup of the model allows for the incorporation of an infiltration rate in every cell of the DEM. We determine the infiltration rate of all cells of the DEM by looping through all depressions in the DEM from the cell with the highest elevation to the cell with the lowest elevation. As we route any excess water to the next cell downslope, infiltration excess runoff is considered within the timestep.

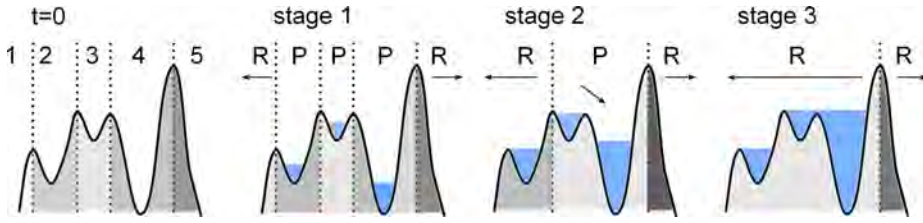


Figure 2.4: Redistribution concept: shading indicates various microcatchments, vertical dotted lines indicate spillpoints. In the first stage ponding occurs in microcatchments 2, 3, and 4 (P). Catchments 1 and 5 contribute their excess water directly to runoff flux at the field boundary (R). In the second stage catchments 3 and 4 have merged to one larger, ponding catchment; catchment 2 contributes all its excess water via catchment 1 to the runoff flux. In the third stage the newly formed catchment is also full and all excess water is routed via catchment 2 and 1 to the left field boundary.

2.2.3 Infiltration

As we want to compute the infiltration rate at every cell of our domains, calculating the infiltration rate by numerically solving the Richards equation is computationally quite demanding. We therefore chose to extend the routing algorithm with Philip's infiltration equation (Philip, 1957a). It is an infinite-series solution that provides an approximate solution to the Richards equation. Usually only the first two terms of the series are used, resulting in Philip's Two-Term infiltration equation:

$$i = \frac{S}{2\sqrt{t}} + K_v \quad (2.1)$$

in which i is the infiltration rate [$L T^{-1}$], S is the sorptivity [$L T^{-1/2}$] and K_v is the hydraulic conductivity [$L T^{-1}$]. Sorptivity S was defined by Philip (1957b) as a measure of the capacity of the medium to absorb or desorb liquid by capillarity. Sorptivity is the cumulative infiltration during the first unit of time; the dominant parameter in the early stage of infiltration and it depends on the soil type and the initial moisture content of the soil. The hydraulic conductivity K_v is the rate to which infiltration rate converges when t is large. Though it is often assumed to be equal to the saturated hydraulic conductivity of the medium (e.g. Ajayi et al. (2008)), this is technically not correct (Philip, 1957b). On the basis of experimental and theoretical work, it was proposed that its value should be half the saturated hydraulic conductivity $K_v \approx 0.5 \times K_s$ (Sharma et al., 1980). Here, we treated it as the saturated hydraulic conductivity of the upper soil layer, which in a uniform soil under a ponding layer is nearly equal to the saturated conductivity K_s (Hillel, 1980). As Eq. 2.1 assumes ponded conditions, a time correction is needed when the Eq. is applied to infiltration under rainfall conditions where the potential infiltration rate at the beginning of a rainfall event is higher than the rainfall rate. The time compression approximation (Salvucci and Entekhabi, 1994; Sivapalan and Milly, 1989) provides a time correction in two steps, under the assumption that the infiltration rate at a certain time depends on the cumulative infiltrated water up to that time. First, a

correction time t_c is calculated at which the potential infiltration rate i is equal to the effective precipitation rate p_e [$L T^{-1}$].

$$t_c = \frac{S^2}{4(p_e - K_v)^2} \quad (2.2)$$

Second, the ponding time t_p is calculated from the cumulative infiltration at t_c divided by the precipitation rate:

$$t_p = \frac{S\sqrt{t_c} + K_v t_c}{p_e} \quad (2.3)$$

The final expression for infiltration during a rainfall event then becomes:

$$i(t) = \begin{cases} p_e & \text{for } t < t_p \\ \frac{S}{2\sqrt{t-(t_p-t_c)}} + K_v & \text{for } t \geq t_p \end{cases} \quad (2.4)$$

In the case of spatially non-uniform infiltration, excess water from a certain cell can form runoff for a cell downslope that did not reach its ponding time yet. Hence, for each cell, precipitation rate, runoff rate, and the local value of $i(t)$ are combined in a water balance. The effective precipitation rate p_e in Eqs. 2.2, 2.3, and 2.4 is the local sum of precipitation rate and runoff rate.

2.2.4 Limited soil water storage capacity

The formulation of Philip's infiltration equation allows for an infinite amount of water to be infiltrated. In the lowland catchments that have our interest, the storage capacity of the soil is often limited due to shallow groundwater tables. When saturated, the infiltration capacity of the soil decreases strongly as the lateral groundwater flux is small due to the small gradient of the groundwater table. We investigated this phenomenon by making assumptions on the soil water storage capacity. For a uniform depth of the groundwater table, the depth of the unsaturated zone and hence the available water storage capacity is determined by the surface elevation of the cell. We determine the soil water storage capacity at the beginning of the rainfall event by assuming a hydrostatic equilibrium soil moisture profile, calculated with the Campbell water retention function (Campbell, 1974):

$$\psi = \psi_{ae} s^{-b} \quad (2.5)$$

in which ψ is the matric potential [L], ψ_{ae} is the air entry pressure [L], s is the relative saturation, the ratio between soil moisture content and saturated soil moisture content θ/θ_s [-], and b is the pore size distribution index [-]. Rewriting Eq. 2.5 to obtain s as a function of ψ and integrating this function from the elevation of the groundwater table Z_g to the elevation of the soil surface Z_s yields the total amount of moisture present in the column at the beginning of the rainfall event. For the integration of the function it should be kept in mind that while $\psi < \psi_{ae}$, $s = 1$. We disregard the development of the soil moisture profile during the rainfall event, but simply limit the cumulative infiltration to the initially available storage.

The value of saturation at the soil surface, that we derive from Eq. 2.5, can also be used to determine a value for the sorptivity parameter S (see Eq. 2.1). We use the equation of Rawls (Rawls, 1992) for this purpose:

$$S = \sqrt{\theta_s \psi_{ae} K_s (1-s) \frac{2b+3}{b+3}} \quad (2.6)$$

As the saturation is directly related to the surface elevation, sorptivity S is too.

2.2.5 Model parameterization

To make the analysis as general as possible, we redefined the model parameters in a dimensionless form where possible. We related cell size and integral scale of the elevation covariance function to the size of the field and the standard deviation of the elevation distribution to the integral scale of the elevation covariance function. The ranges are mentioned in Table 2.1. The conductivity parameter K_v is normalized to rainfall rate p and to the squared sorptivity S . The latter normalization does not result in a dimensionless parameter but provides a measure for the relation between initial moisture content and effective saturated conductivity. The basis for these ranges is a field size of 10 m. The field size L was chosen such that the number of cells (1 million) allowed for a reasonable computation time on a normal PC. The choice for cell size of 0.01 m implies that we ignore the redistribution effect at the scale of small soil aggregates, but include the effect of features with sizes that correspond to clumps of grass and wheel tracks. The non-dimensional ranges of the investigation translate to realistic values such as $\sigma = 0.075$ m and unrealistically large values such as $\sigma > 0.25$ m. To enable an analysis of the average behaviour of the elevation distribution and topography types, we made ten replicates of each set of properties. We performed a jackknife analysis on each set of fields with the same set of statistics for the variables 1) depression storage capacity DSC , 2) volume of water input required to fill the depression storage, and 3) the difference between mean elevation and mean water level in depressions at complete filling. For these three variables, the means and variances of the 45 combinations of 8 elevation

Table 2.1: Normalized variables and the ranges used in the analysis. x is DEM cell size [L], L is field size [L], l is integral scale of elevation covariance function [L], σ is standard deviation of elevation, K_v is hydraulic conductivity [L T⁻¹], and S is sorptivity [L T^{-1/2}].

Variable	Minimum	Maximum
$\Delta x/L$	0.001	0.001
l/L	0.01	3
σ/l	0.10	5
K_v/p	0.1	0.5
K_v/S^2 ^a	0.075	187.5

^a This ratio has unit [L⁻¹]

fields were not all similar to the confidence interval of the ensemble of 10 elevation fields, but all (10) combinations of 9 elevation fields were. From these results it was concluded that 10 realisations were sufficient for the analysis presented here.

The range of the ratio K_v/p included values for K_v ranging from 0.16 to 1.2 cm hr⁻¹, corresponding to realistic values for clay soils to sandy soils (Wösten et al., 2001), and values for p ranging from 0.5 cm to 12 cm hr⁻¹, corresponding to moderate rainfall events and a rainfall event with a return period of 25 years in the Netherlands. The range of the ratio K_v/S^2 included values for sorptivity S ranging from 0.08 to 4.0 cm hr^{-1/2}. A low sorptivity value corresponds to a higher soil moisture content at the beginning of an event. When microtopographic variation is significant, the sorptivity measured at a point will underestimate the sorptivity of a surface as the actual surface area (i.e. the absorptive area) is significantly larger than the surface area in the xy-plane (Thompson et al., 2010). In these situations a compensation factor should be applied, increasing the sorptivity for DEMs with a larger microtopographic variation. Thompson et al. (2010) found this compensation factor to be 1:1 related to the surface area ratio, the ratio between actual surface area of the DEM and the surface area of the DEM in the xy-plane. In our irregular topographies, the surface area ratio follows from the ratio between standard deviation and integral scale of the elevation distribution σ/l . This implies that for the simulations over the infiltrating surfaces the lower range of sorptivity values was only applied to fields with a relatively small σ/l and the higher range only to fields with a relatively high σ/l . In the simulations, we applied a duration of each rainfall event that guarantees to fill the maximum depression storage capacity of the topographies. We generated fields of K_v and S values with the spatial distribution independent of, perfectly positively correlated to, and perfectly negatively correlated to the elevation fields. The independent fields were generated similarly to the elevation fields (Paragraph 2.2.1) using the RandomFields package in R Statistical Software (R Development Core Team, 2010). The K_v fields were then transformed to have a lognormal distribution. The coefficient of variation after the transformation ranged from 0.05 to 0.5. The perfectly positively correlated K_v and S fields were generated by sorting the values from low to high and positioning them at the corresponding elevation points, sorted from low to high value. The perfectly negatively correlated K_v and S fields were generated by positioning the sorted values at the corresponding elevation points, sorted from high to low. The perfect positive correlation is the most likely to occur in reality, as lower spots are wetter (resulting in a low value for sorptivity S) and experience more sealing and compaction (resulting in a low value for effective conductivity K_v). For the parameterization of the analysis with the limited available soil moisture storage, we used values for the pore size distribution index $b = 7.12$, saturated water content $\theta_s = 0.42$, and air entry pressure $\psi_{ae} = -29.9$ cm and $K_s = 12$ cm hr⁻¹ from Clapp and Hornberger (1978) representative for sandy clay loam. We assume the lateral groundwater flux is negligible compared to the infiltration flux. A range of groundwater depths from 30 to 200 cm below the average soil surface was investigated for topographies with a standard deviation of 7.5 cm.

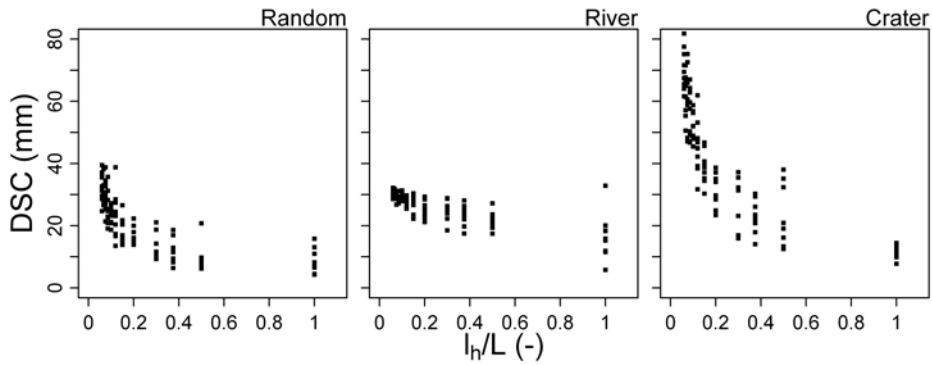


Figure 2.5: Depression storage capacity as a function of the ratio between integral scale and field size l_h/L of the elevation distribution for the three topography types. The standard deviation σ of the elevation distribution is 0.15 m.

2.3 Results and discussion

2.3.1 Depression storage capacity

The numerical topographies are characterized by 1) the properties of the used autocovariance function: zero mean μ , standard deviation σ and integral scale l and 2) the type of transformation they were subjected to. These properties influence both the development and the final state of connectivity. In the final state, all depressions are filled with water and maximum depression storage capacity (DSC) is reached. From this point on the entire field contributes to surface runoff.

The integral scale affects the area of the depressions and thus the number of depressions in the numerical topographies. When the area of the depressions is large compared to the field size, a boundary effect occurs because the relative area of depressions that immediately drain to the surrounding ditches increases. These depressions do not contribute to the DSC and the average DSC of fields with a large ratio l/L will therefore be smaller than that of fields with a small ratio l/L for a designated standard deviation σ , as is shown in Fig. 2.5. The range of observed DSC values decreases when the ratio l/L decreases up to the point where this ratio is no longer the determining factor for DSC value. The boundary effect has then become negligible. From this point, the standard deviation σ and the particular type of topography determine the DSC value. The boundary disappears from the value $l/L = 0.1$. When the ratio l/L is small and its effect can be neglected, the depression storage capacity DSC depends only on the standard deviation σ of the elevation distribution, as can be seen in Fig. 2.6a. Empirical relationships between DSC and standard deviation of microtopographic plots have been established by e.g. Onstad (1984), Kamphorst et al. (2000), Cremers et al. (1996), and Hansen et al. (1999). For a synthetic numerical field, as used in this analysis, the dependency is linear, its slope and correlation coefficient of fitting depending on the topography type (see Fig. 2.6 and Table 2.2).

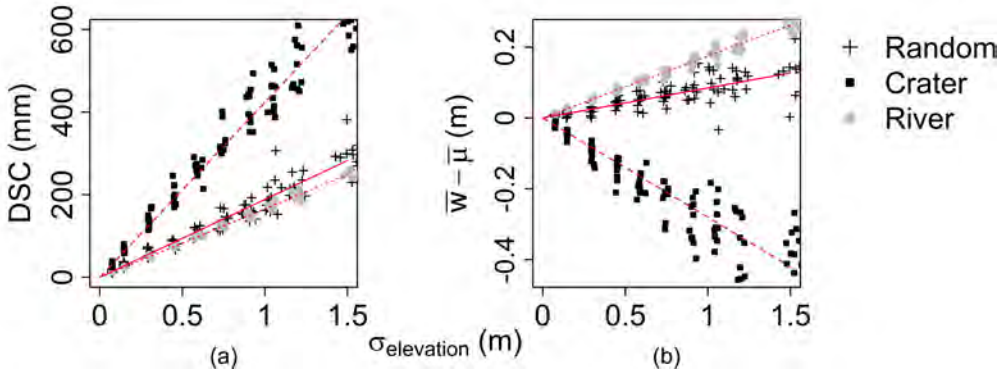


Figure 2.6: Dependence of depression storage capacity (a) and difference between mean elevation and mean waterlevel (b) on the standard deviation σ of the elevation distribution for each topography type. Lines indicate fitted linear relationships.

The range of standard deviation σ in Fig. 2.6 is unrealistically large. In field measurements values in the range 0.05–0.2 m were found. The range used in this theoretical analysis illustrates the general principles. As the fields have no slope, the difference between average water level in the depressions when DSC is reached and the mean of the elevation distribution depends linearly on σ too (Fig. 2.6b). The relative difference can be expressed as a percentile of the elevation distribution according to

$$x = \frac{w - \mu}{\sigma} \quad (2.7)$$

where w is the elevation of the average water level at DSC, μ is the mean and σ the standard deviation of the elevation distribution. For the 750 realisations of all σ/l and l/L , the x -value only differed for each topography type. This position is fixed for every topography type, illustrated in Fig. 2.7. The DSC and average water level of each depression in the numerical topographies are determined by the height of the overflow points of the depressions. In the river topographies, the elevation values are arranged such that the low values of the distribution form connected channels, thus the overflow points have a low elevation too. In the random topographies, the height of the overflow points is closer to the field mean elevation as extreme values occur in isolated patches and cells with an elevation close to the mean form connected bands. In the crater topographies, the high values of the elevation distribution form connected ridges and

Table 2.2: Slopes and correlation coefficients of fitting of linear dependencies in Fig. 2.6

Topography	α_1	R_1^2	α_2	R_2^2
Random	0.19	0.980	0.085	0.849
River	0.17	0.998	0.17	0.994
Crater	0.42	0.989	-0.28	0.951

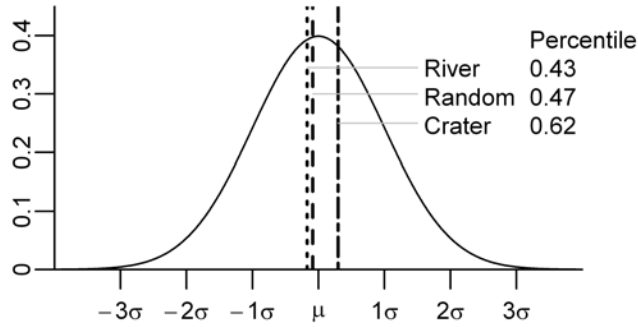


Figure 2.7: Relative position of water heights at maximum depression storage in the probability density function of the normal distribution for the three topography types.

overflow points have a higher elevation than in the other two topography types. As the average elevation of the overflow points is higher than the mean elevation, the slope of the linear relationship in Fig. 2.6b is negative. The different positions of the average water level imply that under conditions of maximum depression storage the topography types have different ponded areas, as all cells below the respective percentiles will be ponded.

2.3.2 Connectivity development of impermeable topographies

Following Darboux et al. (2001, 2002a,b), Antoine et al. (2009) proposed a simplified hydrograph as indicator of connectivity development, because it discriminates well between the three considered types of topography and contains information on the functional connectivity (i.e. the flow of water on the surface) as opposed to indicators that only analyze the microtopography. We prefer this type of connectivity metric over metrics from percolation theory (such as percolation threshold and evolution of percolation length) as our ultimate aim is to translate our small scale findings to field scale hydrological models.

The dependent variable of the hydrograph (vertical axis) is the cumulative surface runoff rate at all field boundaries normalized by division with the precipitation rate. The hydrograph is a function of the cumulative input of water, normalized by the depression storage capacity of the field (horizontal axis). By these two normalizations, the appearance of the simplified hydrograph does not depend on rainfall rate and field size anymore, enabling a focus on the connectivity behaviour of the microtopography and infiltration characteristics. In the absence of infiltration, the normalized runoff rate is equal to the relative area of the field that contributes to runoff, i.e. the area with a direct flowpath to the field boundaries divided by the total field area.

Within the topography types, the development of connectivity does not depend on the standard deviation σ of the elevation distribution. Parameter σ is linearly related to the depression storage capacity through a certain value of coefficient α (Table 2.2). The

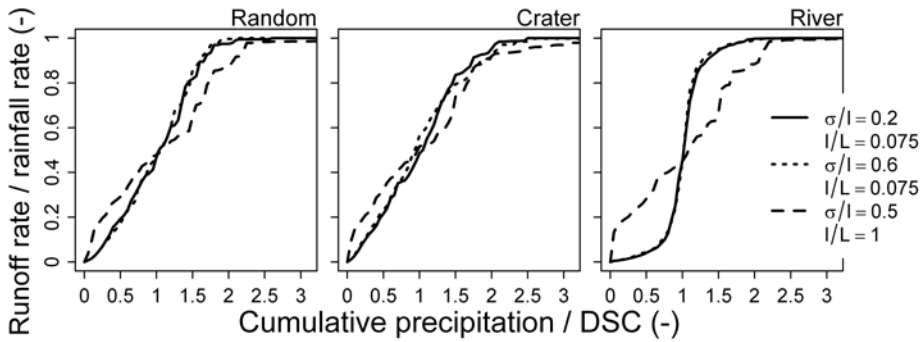


Figure 2.8: Normalized surface runoff rates (in absence of infiltration) as a function of normalized cumulative precipitation for topographies with varying standard deviation σ/l and the ratio between integral scale and field size l/L . Each curve is an average of ten topographies with identical statistics.

cumulative input of water needed to fill the depressions increases with the same order of magnitude. The net quantities of water required for establishing full hydrological connectivity increase as σ increases, but the relative quantities stay the same. Therefore, the simplified hydrograph does not change.

Unlike changing the ratio σ/l , changing the ratio l/L affects the simplified hydrographs (dashed lines in Fig. 2.8). Large values for the ratio l/L imply that the depressions in the field are relatively large compared to the field area and that there is a large area of the field that immediately contributes to the occurrence of surface runoff at the field boundaries. When l/L is large (> 0.25), there is hardly any difference between the connectivity development of the topography types. Darboux et al. (2002b) note that microtopographies will generally not have integral scales that are large compared to field size and therefore microtopography can be assumed to be normally distributed without correlation features. Considering elevation differences within an order of magnitude of decimeters however, these may be organised in patches that are large relative to field dimensions. Examples of such features are old filled ditches, parts of fields that have subsided due to heavy machinery or trampling of cattle. When the boundary effect is small ($l/L < 0.1$), the differences between connectivity of the three topography types are more pronounced. The river topographies experience little runoff at the first stages of the rainfall events, but combine this with a fast increase of hydrological connectivity. The random and crater topographies have a development that is linear for the major part of the curves. Like the differences in DSC and average water level, the differences in the simplified hydrographs can be explained from the position of the overflow points in the topographies. The depression storage capacity of a river topography is not only reached faster because the absolute storage capacity is smaller than that of the other topographies, but also because the ratio between ponded area and depression size is smaller. The increase of surface runoff rate of a river topography is therefore steeper

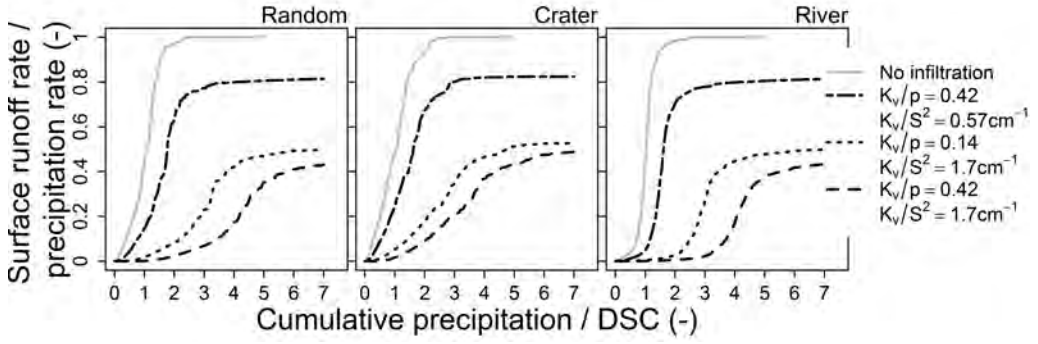


Figure 2.9: Normalized field area contributing to surface runoff as a function of normalized cumulative precipitation for three infiltration scenarios, characterized by the ratios between saturated conductivity and precipitation rate K_v/p and saturated conductivity and sorptivity K_v/S^2 , for the three topography types.

than that of random and crater topographies.

It is remarkable, that in Fig. 2.8 the curves of the random and crater topographies are relatively similar, whereas in Fig. 2.6 and 2.7 the crater topographies stand out compared to the random and river topographies.

2.3.3 Effects of infiltration

Uniform infiltration

As under infiltration excess conditions the rainfall rate is greater than the effective hydraulic conductivity, DSC can be reached and in due time all depressions will contribute to ponding and surface runoff. Because of infiltration, the fraction of the field contributing to surface runoff as a function of cumulative input of water is delayed (Fig. 2.9). When the infiltration parameters are spatially uniform, the relationship between the fraction of the field that contributes to runoff and the actual storage is exactly the same as that of an impermeable field. Therefore, the original connectivity function of the impermeable field

$$A = f\left(\frac{P}{DSC}\right) \quad (2.8)$$

can be converted to describe the connectivity development with infiltration by a simple translation of the argument:

$$A = f\left(\frac{P-I}{DSC}\right) \quad (2.9)$$

in which A is the fraction of the field that contributes to runoff [-], P is the cumulative precipitation [L^3], I is the cumulative infiltration [L^3] and DSC is the depression storage capacity [L^3]. As Eq. 2.9 depends on the cumulative infiltration and precipitation, it follows that infiltration scenarios that have the same cumulative infiltration at a particular cumulative precipitation will also have the same development of connectivity. The relation between these cumulatives is maintained when the ratios K_v/p and K_v/S^2

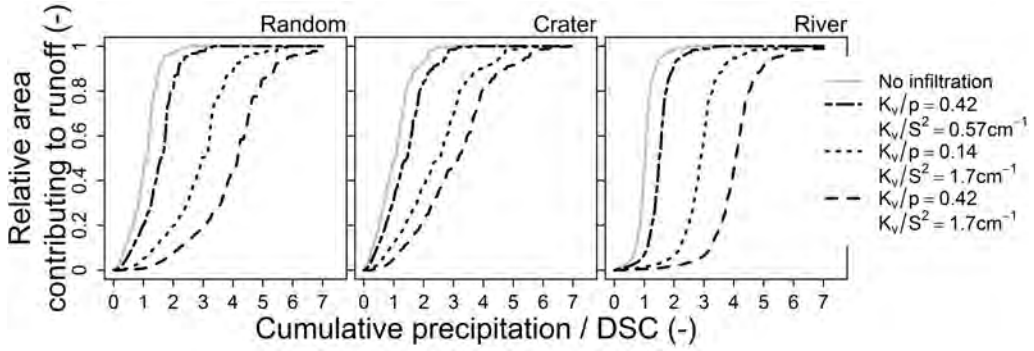


Figure 2.10: Normalized surface runoff rates (with uniform infiltration) as a function of normalized cumulative precipitation for three infiltration scenarios, characterized by the ratios between saturated conductivity and precipitation rate K_v/p and saturated conductivity and sorptivity K_v/S^2 , for the three topography types.

are kept constant. In a simulation for each soil type, fields with a larger ratio σ/l display a bigger shift to the right, as the value of sorptivity S was adjusted to account for the actual surface area of the topography. However, as this adjustment is made for each cell of the topography, the translation of the connectivity function can be applied.

The infiltration process causes a net decrease of water available for ponding, redistribution and runoff. Therefore, the new simplified hydrographs display a vertical as well as a horizontal shift (Fig. 2.10). The final value of the normalized runoff rate no longer equals 1, but approaches $1 - \frac{i}{p}$. Since the infiltration rate depends on the cumulative infiltration, we can again use the function that describes the original curve of the simplified hydrograph

$$R = A = f\left(\frac{P}{DSC}\right) \quad (2.10)$$

to obtain the new simplified hydrograph of the field with a particular infiltration scenario

$$R = \left(1 - \frac{i}{p}\right) f\left(\frac{P-I}{DSC}\right) \quad (2.11)$$

in which R is the normalized runoff rate [-], p is the precipitation rate [$L^3 T^{-1}$], and i is the infiltration rate [$L^3 T^{-1}$]. Again, infiltration scenarios that have the same values for the ratios K_v/p and K_v/S^2 will result in identical simplified hydrographs. This derivation of a new connectivity curve for a certain combination of infiltration characteristics can be done for all types of topography.

Non-uniform infiltration

When the infiltration parameters are no longer uniform in the field, but are characterized by a designated autocovariance function, the connectivity development does not necessarily change. In fields where the spatial distribution of the infiltration parameters is random or lognormal with an integral scale of the covariance function small compared to that of the elevation distribution, the filling of the depressions acts as a suppressing

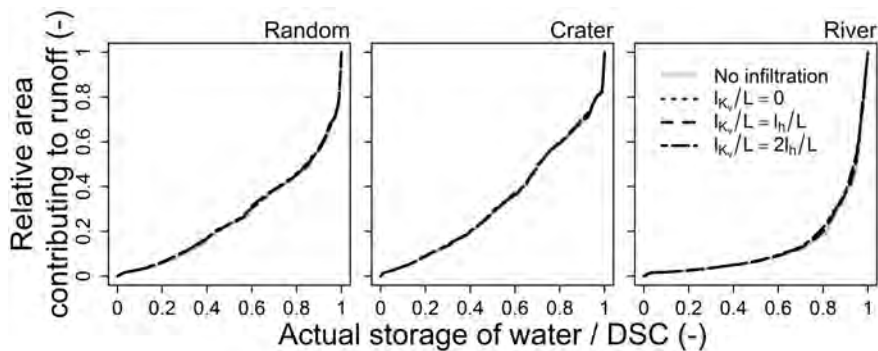


Figure 2.11: Normalized contributing area as a function of normalized actual storage for different normalized integral scales of K_v fields relative to integral scale of the elevation distribution (l_{K_v}/l_h) for the three topography types. This function was termed a scaled relative surface connection function by Antoine et al. (2009).

process. Runoff from a cell that has a shorter ponding time contributes to the infiltration in a downstream cell with a longer ponding time (Eq. 2.3). The depression will only start overflowing at the moment the rate of rainfall and runoff is higher than the infiltration rate in each cell of the depression that is lower than the spillpoint elevation. This is illustrated in Fig. 2.11, where the field fraction contributing to surface runoff as a function of actual storage is plotted for a certain topography and several spatially distributed infiltration scenarios. We call this function a scaled relative surface connection function just as Antoine et al. (2009). Linking the value of parameters K_v and S to the elevation value at a certain position in a field does not influence the connectivity development of the field as a whole. Again, a depression will only overflow when the rate of rainfall and runoff is higher than the infiltration rate in all cells below the spillpoint elevation. As there is no surface gradient underlying the fields, all depressions will have the same range of elevation values lying below the average spillpoint elevation. As a consequence all depressions experience an average delay before ponding and the sequence of spilling and activation of flowpaths in the field remains the same. In these cases, when the depression-averaged infiltration process closely resembles the field-averaged infiltration process, the connectivity development of the field as a whole can still be estimated from the translation described in Eq. 2.11 and the shape of the scaled relative surface connection function (Fig. 2.11) does not change.

When the integral scales of the covariance functions of the infiltration properties are increased, the relation between contributing area and actual storage of fields changes as now depression-averaged infiltration processes vary from the field-averaged infiltration process. Taskinen et al. (2008) mention integral scales from a few meters to a maximum of 20 to 50 m, which correspond on field scale to a ratio of l/L in the range 0.17–0.07. These are large compared to integral scales of the elevation distribution. In this case, depressions do not longer have an buffering effect and Eq. 2.11 can no longer be

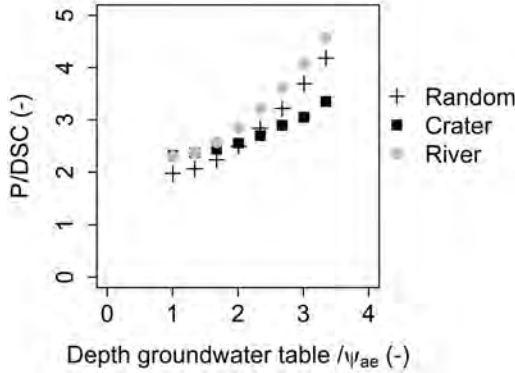


Figure 2.12: Dimensionless volume of water input (cumulative rainfall P / depression storage capacity DSC) needed to achieve full depression storage as a function of ratio of average depth of the groundwater table (with respect to the soil surface) and air entry pressure ψ_{ae} for each topography type. Each point is an average of ten topographies with identical statistics.

used to determine the level of connectivity during a rainfall event. The shape of the scaled relative surface connection function can vary in these situations as the sequence of spilling and therefore the activation of flowpaths within the field will change with respect to the impermeable surface. This may require quite a large difference between integral scales of elevation and K_v . From Fig. 2.11 it can be observed that doubling the integral scales of the covariance function of K_v with respect to that of the elevation causes differences in the River topography, but not yet in the Random and Crater topographies. The reason is that in the River topographies the surface area below the spillpoint elevation is smaller than in the other two topographies.

Limited soil water storage capacity

When we investigate a situation where a groundwater table is present, we expect that ponding will occur faster in cells with a low elevation as 1) the local infiltration rate is low as the sorptivity S is small in these cells and 2) the maximum infiltration in these cells will be reached fast as the available soil moisture storage capacity is smaller than that in cells with a high elevation. In Fig. 2.12 we see that the dimensionless input volume of water required to obtain full depression storage at the surface increases with a deeper groundwater level. Note that the relative increase of dimensionless input volume required, is smaller for the crater topographies than for the random and river topographies. This is due to the fact that in crater topographies the soil water storage capacity is reached before the depression storage capacity (DSC) has been reached. In the period of simulation where the topography is saturated all input water is available for ponding and runoff. In the random and river topographies, the depression storage capacity (DSC) is reached before the soil water storage capacity has been reached. Similar to the scenarios with uniform and non-uniform infiltration, the scaled relative surface connection function retains its original shape as the sequence of spilling and

activation of flowpaths in the field remains the same. It is not hard to imagine that a convex groundwater table, that we typically find in lowland catchments between two ditches, can cause a different sequence of spilling and activation of flowpaths in a field. This is analogous to the changing surface connection response that we find when the integral scales of non-uniformly distributed infiltration parameters is large compared to the integral scale of the elevation.

2.3.4 Field-scale models and experimental studies

The results emphasize the importance of the spatial structure and variability of the microtopography, infiltration parameters and groundwater depth. In the hypothetical situations we investigated, the structure and variability of the microtopography remains the dominant factor in the connectivity development, even when a spatial distribution of other parameters is introduced. The connectivity behaviour can be captured in a scaled relative surface connection function. The function describes the partitioning between depression storage and surface runoff as a function of dimensionless input volume of water, a variable that can be calculated from the actual available volume of water and an estimation of the depression storage capacity. A dynamic determination of this partitioning is obtained as stagnating water at the surface will result in a higher input volume available for partitioning in a subsequent rainfall event.

A scaled relative surface connection function can also be determined for situations in which microtopography is not the dominant factor in connectivity development. Smith et al. (2010) found that in a sloping terrain neither microtopography, nor soil type influenced surface runoff development. In a small watershed where a mesoscale topographic structure was dominant over the microtopography, Mueller et al. (2007) found that surface runoff hydrographs could be modelled correctly only when the model accounted for a spatial distribution of saturated conductivity K_s . At the plot scale Fiedler et al. (2002) found a complex interaction between microtopography and spatial variation of infiltration characteristics with a spatial variation at the size of vegetation patches. When the ponding of water occurs far away from the field boundaries (see Fig. 2.1a), the development of connectivity is a stepwise process instead of a gradual increase. A threshold process instead of a gradual increase of connectivity can be observed when the ponding of water occurs far away from field boundaries (see Fig. 2.1a).

Finding and choosing a scaled relative surface connection function that can represent the connectivity behaviour of (parts of) a field requires insight in the dominant process(es) at a specific location. When investigating the field-scale response itself in more detail, we can use a combination of simplified hydrographs to illustrate the behaviour of different sections of a field.

In this analysis, we ignored the effect of resistance to flow (and its spatial variability), which has been reported to be important for the development of surface runoff (Mueller et al., 2007; Smith et al., 2010). We recognize that we therefore overestimate the connectivity, especially in situations where infiltration rates have a

timescale that is close to that of the surface runoff velocity. However, Smith et al. (2010) also note that conventional equations provide an inadequate description of the surface runoff process at the moment. A relatively simple improvement of our model could be made by accounting for roughness through the introduction of a retardation factor along the flowpaths in the field. Another gap in the current analysis is the fact that we ignore the effect of storm structure and event sequence on the development of connectivity. In the real world, these factors actually determine the dynamics of hydrological connectivity over a longer period of time. As was shown in a study in a semi-arid area, when ponds stagnate in between rainfall events, surface runoff can occur even when the rainfall intensity is lower than the infiltration capacity and before saturation of the subsoil has been achieved (Reaney et al., 2007). In combination with a dynamic groundwater table, rainfall characteristics may easily take over the position as dominant factor in connectivity development in flat areas with microtopography. This is relatively easy to incorporate in the current model structure with some extensions to account for the processes that play an important role in inter-event behaviour, e.g. the infiltration dynamics related to the fluctuations of the groundwater table and evaporation from the ponds.

2.4 Conclusions

The development of surface runoff on a field was investigated with an analysis of the hydrological connectivity. We characterized the connectivity development with a simplified hydrograph consisting of the surface runoff rate, which was normalized by division with the precipitation rate, as a function of the cumulative input of water, which was normalized by the depression storage capacity of the field. The dimensionless analysis provided insight in the generic differences of development of surface runoff behaviour as it enabled the comparison of fields of varying size and varying statistical properties of microtopography of impermeable and infiltrating fields.

The topography of a field is determined either by depressions that have a large area compared to the total field area or the spatial organization of microtopography in craters or microchannels. When large depressions dominate, represented in this analysis by a large ratio l/L , the field response is determined by boundary effects of depressions that immediately drain to surrounding ditches and do not contribute to field depression storage capacity. When the spatial organization of the microtopography dominates, for a sufficiently small l/L , DSC is found to be linearly related to the standard deviation of the elevation distribution, where both the value of the coefficient α and the correlation coefficient of fitting depend on the topography type (Table 2.2). Also, it appears that as DSC is attained, the distance between water level and mean soil surface level is linearly related with σ , with different slopes and correlation coefficients for the three topographies. The ratio σ/DSC and the percentile at which the water level is located in the probability density function of each elevation distribution can be interpreted as a first measure of connectivity, as these are constant for each topographic model, and different

for each considered model.

The relationship for both the normalized area contributing to surface runoff (Eq. 2.8) and the normalized runoff rate (simplified hydrograph, Eq. 2.10) as a function of normalized input of water is unique for each designated topography type and is independent of σ and, provided the ratio is small enough, of l/L . Infiltration has a profound effect on the runoff of water from fields as considered. When the relationship between normalized area contributing to surface runoff as a function of normalized water input has been parameterized, this relationship (Eq. 2.8) can be used to estimate the development of connectivity under circumstances of infiltration as well. By translating the input argument with the field averaged cumulative infiltration a new relationship between normalized area contributing to surface runoff and cumulative input can be determined (Eq. 2.9). By correcting for field average infiltration rate a new simplified hydrograph (Eq. 2.11) can be determined from the original one for a designated topography (Eq. 2.10). However, in terms of the fraction of the field that contributes to runoff as a function of actual storage, the runoff response of a field is unaffected by infiltration, if infiltration parameters are uniform or are spatially distributed at a smaller scale than that of the microtopography. A parameterized scaled relative surface connection function (visualized in Fig. 2.11) can be used to quantify the partitioning between depression storage of water and surface runoff under these circumstances as well as in situations where the soil water storage capacity is limited by a shallow groundwater table.

For field situations the results imply that:

- the average height of ponded water compared to the distribution of microtopographic elevation gives an impression of the connectivity behaviour of a field
- a unique reference scaled relative surface connection function can be defined for each field based on an analysis of the dominant processes contributing to connectivity: it is a result of the unique combination of the spatial distributions of micro- and mesotopography, infiltration parameters, and groundwater levels
- in catchment modelling a translation of these functions based on calculation of precipitation and infiltration volumes can then be used to determine the actual status of connectivity at each field at a certain moment in time.

Acknowledgements

The authors acknowledge Alterra Wageningen UR (project 5232870-06) and the Dutch ministry of Agriculture, Nature, and Food quality (project BO-05-004-KRW) for financing this study. S.E.A.T.M. van der Zee appreciated support of the DFG-NWO funded network NUPUS.

Chapter 3

Observations of surface runoff on flat agricultural fields: interactions between driving mechanisms and surface topography and associated thresholds

Abstract

In flat lowland agricultural catchments in temperate climate zones with highly permeable sandy soils, surface runoff is a rare process with a large impact on the redistribution of sediments and solutes and stream water quality. We examine hydrological data obtained on two field sites in The Netherlands for a period of 1.5 years from several points of view to give an integrated narrative of surface runoff in this type of catchment. In the monitoring period, seven surface runoff events were observed. Four of these events were classified as saturation excess events, due to a shallow water table. Four of the events occurred under precipitation conditions combined with snowmelt. Infiltration excess runoff did not result in surface runoff reaching the field boundaries. During the events with snowmelt, the area contributing to surface runoff was small and located close to the field boundaries. During the saturation excess events, the area contributing to surface runoff was larger and flow paths were relatively long, because the wettest locations within the fields were found at a larger distance from the field boundaries. In the days preceding the events, ponding of water occurred in micro- and mesotopography at these wet locations. In this type of catchment, the formation of surface runoff is a two-stage process with thresholds from storage capacity of the unsaturated zone and the surface topography. In the events we analyzed, up to 10 % of the event precipitation left the fields as surface runoff. This range corresponds to results from other studies in similar catchments at different spatial scales.

3.1 Introduction

Stream water quantity and quality depend on the pathways of water through a catchment. To understand the discharge and water quality characteristics at the catchment outlet, it is important to quantify the relative contributions of the routes over the land surface, through the shallow and the deeper soil and the temporal and spatial variations of these contributions (van der Velde et al., 2009; Rozemeijer, 2010).

Flat lowland agricultural catchments in temperate climate zones have several characteristics that favour flowroutes through the shallow and deep soil above routes over the land surface: 1) rainfall tends to occur at low intensities, 2) the soils consist of highly permeable unconsolidated deposits, 3) soils are intensively artificially drained for optimization of agricultural production, and 4) the topographical gradients are small (Brutsaert, 2005). Surface runoff occurs either when the rainfall rate exceeds the infiltration rate of the soil (infiltration excess or Hortonian runoff) or when the water storage capacity of the soil is exceeded (saturation excess or Dunne runoff).

Though the contribution of surface runoff to the regional water balance in the aforementioned catchments is often small compared to that of other flow routes, the impact of the redistribution of water along the soil surface is significant. Following the structure of microtopography, the redistribution affects vegetation patterns through the formation of a spatially varying soil moisture pattern (Dunne et al., 1991). When ponds on

fields overflow to ditches and streams, surface runoff contributes to peakflow at the catchment outlet (van der Velde et al., 2009). Also, solute and sediment transport associated with surface runoff affect the water quality of ditches and streams in catchments, especially agricultural ones (Bolinder et al., 2000; Langlois and Mehuys, 2003). The focus of most experimental studies regarding surface runoff in temperate lowland catchment lies on the transport of suspended sediment, phosphorus, nitrogen, and pesticides (Withers et al., 2007; Deasy et al., 2008; Kronvang et al., 1997).

In flat agricultural catchments with shallow groundwater, the most natural spatial unit to investigate surface runoff is a field bounded by ditches or streams. Within the field unit, precipitation can be assumed to be spatially uniform. The initiation of surface runoff, however, is variable in space due to 1) heterogeneity of the soil and soil degradation processes such as compaction, sealing, and crust formation affecting the infiltration properties of the soil (Deasy et al., 2009) and 2) saturation levels of the soil due to groundwater fluctuations affecting the subsurface storage capacity (Heathwaite et al., 2005). This spatial heterogeneity combined with temporal dynamics of precipitation create a large intra- and inter-field variability in the extent, volume, rate, and timing of surface runoff events within a catchment (Haygarth et al., 2000).

In hydrology, as in most of the other earth sciences, knowledge needs to be founded in observations, experiments, and measurements (Kirchner, 2006). By gathering abundant empirical data, a hypothesis for the explanation of a certain phenomenon or process can be tested. When it is not possible (either because of missing technology or because it is impossible to reach a certain location) to gather sufficient data on the phenomenon or process, the empirical data may leave room for a wide range of different, even incompatible hypotheses (Kleinhans et al., 2005). Taking surface runoff as an example: to establish its absolute and relative contribution to streamflow discharge, direct measurements of all flow routes would be needed. However, physically separating water from different routes in flat lowland catchments at this scale level is often too laborious and costly to be a viable option (Rozemeijer, 2010). Installing the required equipment with a high spatial density would also change the system under investigation. Considering the practical difficulties, it is not surprising that surface runoff experiments in the field have been restricted to subareas of catchments (Augeard et al., 2005; Deasy et al., 2009; Puustinen et al., 2010) or small first order watersheds (Vellidis et al., 2003). Working with a less extensive measurement installation will most probably result in insufficient evidence to choose between alternative explanations; a situation referred to as weak (or practical) underdetermination. Weak underdetermination prevents the construction of conclusive causal explanations, but leaves open the possibility of constructing narrative explanations (Kleinhans et al., 2005). In this context, addressing qualitative “why” type of questions may even lead to more useful insights than quantitative questions per se (McDonnell et al., 2007).

Whereas we recognize that surface runoff is an important process, it is also clear that such events are quite scarce and poorly predictable in temperate, flat, lowland

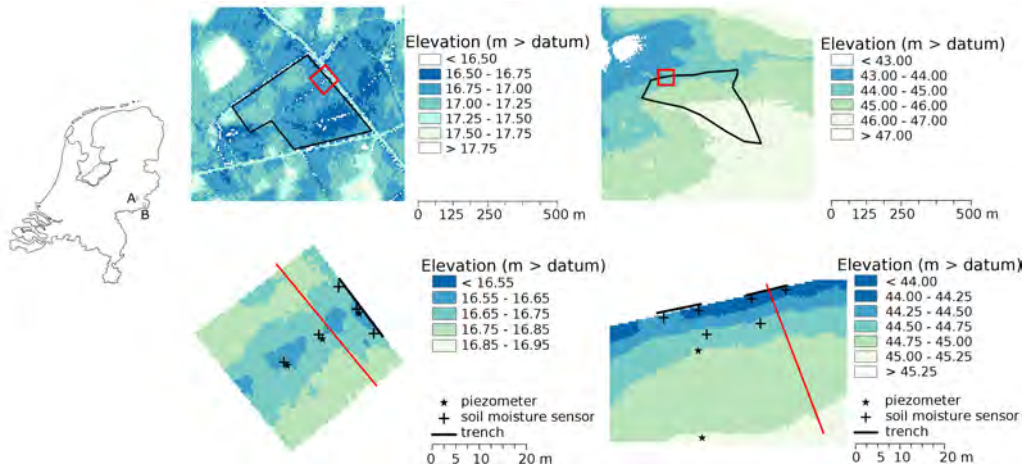


Figure 3.1: Location of field sites in The Netherlands and surface elevation (m) of site A (left) and B (right). Black lines indicate the position of ditches surrounding the fields. Position of measurement devices at field site A (a) and B (b). At site B, a third piezometer was installed some 50 m further South, outside the scope of this map.

catchments. This has resulted in that driving mechanisms and structures have not yet been brought in perspective. Our aim is to use various monitoring and auxiliary information to give an integrated narrative of surface runoff for two field sites in flat, lowland catchments in the sandy part of The Netherlands. We address relevant qualitative questions, such as: What are the main driving mechanisms of surface runoff in these catchments? What rainfall conditions prevail during surface runoff events? How do flow paths develop during surface runoff events? We analyze the characteristics of the surface runoff events by looking at them from the perspective of three generating mechanisms: infiltration excess, saturation excess, and snowmelt. Then we quantify the depression storage and routing features of the soil surface of the sites. And finally, we discuss scale issues that arise when comparing surface runoff measurements between plots and fields.

3.2 Material and methods

3.2.1 Study area

The data were obtained at two fields in the province of Gelderland, eastern part of The Netherlands. Both sites are agricultural sites surrounded by ditches (see Fig. 3.1). Site no. A is located in Beltrum, (52.082°N, 6.538°E). The field has an area of 4 ha. The soil consists of a thick deposit of Pleistocene Coversand. The upper 25–30 cm consist of loamy fine sand with an organic matter content of 5 %. The lower part of the profile is poor in organic matter and consists of the same loamy fine sand to a depth of at least 12 m. The groundwater level increases from the ditches surrounding the field towards its centre. During the year the average groundwater depth fluctuates between 0.5 and 1.5 m below

the soil surface. The ditches surrounding the field run dry in summer. The site has been used for agriculture over the last centuries. During the experimental period maize was grown on the site. The surface elevation ranges from 16.7–17.2 m above Ordnance Datum. Site no. B is located in Winterswijk, (51.915°N, 6.723°E, at some 25 km southeast of site A). The field has an area of 2.7 ha. The soil consists of a fine loamy sand with some gravel underlain by a thick layer of Tertiary heavy clay. The level of the top of this layer varies throughout the field from 40–120 cm below the surface. The groundwater level mainly follows the macrotopography. The average groundwater depth fluctuates throughout the year between 0.25 and 2.0 m below the soil surface and is therefore located in the clay layer during the summer. The ditches surrounding the field run dry in summer. Land use includes a rotation of growing maize and pasture. During the experimental period, the land use was grassland with cows grazing. The surface elevation ranges from 42–45 m above Ordnance Datum. The site slopes with a gentle 2 % down to the ditch north of the field. The eastern part of the Netherlands has a semi-humid sea climate with 750–800 mm annual rainfall. The annual evaporation is 525–540 mm resulting in an annual recharge of 210–275 mm.

3.2.2 Hydrological data

At both sites, measurement equipment was installed to measure groundwater level, soil moisture content, matric potential, and surface runoff fluxes. The sensors and measurement trenches did not cover the whole spatial extent of the fields. They were positioned in the areas that were expected to be most active in surface runoff generation based on previous observations and a survey and analysis of the soil surface topography, using the model of Appels et al. (2011).

At site A a 24 m long trench was installed along the ditch at the northeastern field boundary, which is the lowest field boundary. The trench drained into a wooden container ($0.5 \times 0.5 \times 0.6 \text{ m}^3$) that in turn drained into the ditch via a 28.5° V-notch weir. The water level inside the container was measured with a pressure transducer. A level-discharge relation for the V-notch weir was established in the laboratory. Within the catchment area of the trench, five locations were selected for the measurement of soil moisture and matric potential. At each location, TDR probes and tensiometers were inserted at depths of 15, 40, and 80 cm below the soil surface. Three pressure transducers were installed perpendicular to the trench at distances of 1, 11, 21 m of the ditch to measure the groundwater levels. From March 2009 through September 2010, soil moisture content, matric potential, groundwater levels, and level in the container with the V-notch weir were measured every 30 minutes.

At site B two 12 m long trenches were installed along the ditch at the northern field boundary, again the lowest field boundary. Both trenches drain to a 1.1 l tipping bucket attached to the sides of two large wooden reservoirs. Within the catchment area of each trench, three locations were selected for the measurement of soil moisture and matric potential. At each location, TDR probes and tensiometers were installed at depths

of 15, 40, and 80 cm below the soil surface. From January 2009 through September 2010, soil moisture content and matric potential were measured every 30 minutes. Groundwater levels were measured weekly along a transect perpendicular to the ditch at 2, 5, 44, and 75 m from the ditch.

From each site, soil samples were obtained at ten randomly chosen locations for laboratory analysis of saturated hydraulic conductivity, porosity, and retention characteristics.

Situations in which surface runoff occurred, but did not reach the trenches, could not be recognized from the automatically monitored data. For this reason, we defined surface runoff events as those rainfall events during which the volume of water that was discharged from the trenches towards the ditch was larger than the volume of water that precipitated on the trenches according to the measured rainfall rates during the rainfall events.

3.2.3 Auxiliary data

For the analysis of the field topography, we combined three datasets of macro-, meso-, and microtopography for each site. The macrotopography was obtained from the national Dutch Digital Elevation database (AHN) as a digital elevation model (DEM) with a grid cell size of 5 m. The mesotopography data were collected using Real Time Kinematic GPS equipment (RTK-GPS, Leica GPS 1200+). The RTK-GPS equipment is able to measure a point in space with a horizontal and vertical accuracy of 1–2 cm. The average spatial density of points collected at the sites was 1.5 points per m^2 . The point measurements were interpolated with Inverse Distance Weighing to a grid with a cell size of 0.5 m. At both sites, six 1 m^2 pinmeter measurements were performed to characterize the microtopography with a density of 400 measurement points per m^2 . We superposed the pinmeter measurements on the interpolated GPS datasets, to create an estimate of the field sites with topographical features at macro-, meso- and microscale.

In addition to the field measurements, we analyzed the rainfall intensities that occurred during the surface runoff events at a smaller time interval. We used a downscaled rainfall radar product with a resolution of 1 km^2 and a 5 min interval. The original data were obtained from the Royal Dutch Meteorological Institute (KNMI) and processed into a rainfall series for each field site with the downscaling method described by Overeem et al. (2009a,b).

Several weather stations of the KNMI are located in the immediate surroundings of the study sites. Where needed, we used records from station 283 (Hupsel) for hourly data on temperature, wind speed, solar radiation, and humidity. This station is located at a distance of 8 km from site A and 25 km from site B.

Table 3.1: Characteristics of surface runoff events recorded in 2009 en 2010 at field sites in Beltrum (A) and Winterswijk (B). Cumulative precipitation, ΣP (mm), average rainfall rate, $\langle P \rangle$ (mm h^{-1}), average distance from groundwater level to the soil surface, H (m below soil surface), and amount of surface runoff per site, ΣQ (l).

Date	Event code	ΣP	$\langle P \rangle$	H	ΣQ
28-03-2009	B1	7.2	1.44	0.10	164.76
10-12-2009	B2	21.2	2.2	0.35	72.34
25-12-2009	A1	6.0	0.5	0.20	165.85
25-12-2009	B3	6.0	0.5	0.40	24.64
02-02-2010	A2	12.2	0.72	0.55	261.5
04-02-2010	B4	2.4	0.117	0.60	9.78
28-02-2010	A3	9.8	0.65	0.10	974.95

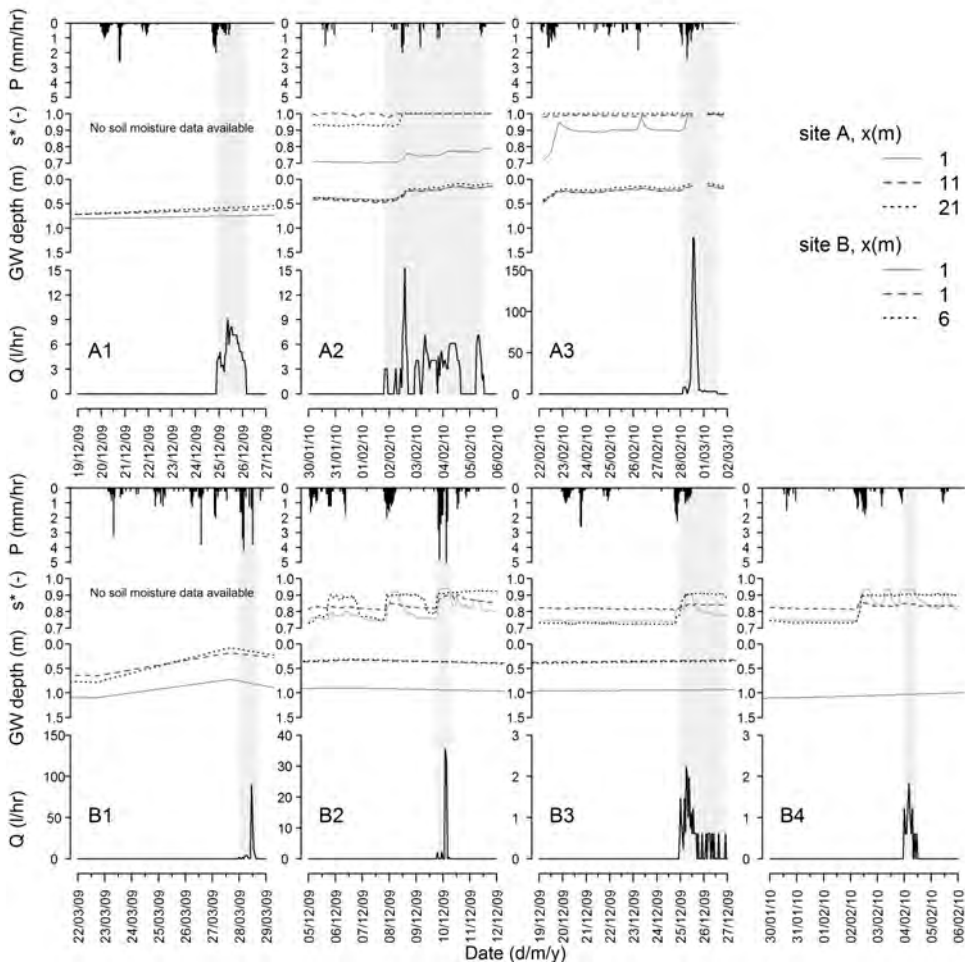


Figure 3.2: Time series of rainfall rate (P), relative saturation at 15 cm under the soil surface (s^*), groundwater depth below the soil surface (GW depth), and surface runoff discharge (Q) in the trenches during a week preceding the surface runoff events.

3.3 Results and Discussion

3.3.1 Event characteristics

During the monitoring period in 2009–2010, surface runoff events were observed three times at site A and four times at site B (Table 3.1). All events were recorded during winter and early spring. The total rainfall volume during the events varied with a factor ten, whereas the total volume of surface runoff differed by a factor hundred between the locations. The average rainfall intensities during the events were small, as were the peak rainfall intensities (see Sec. 3.3.2 for a more in-depth discussion of infiltration excess runoff). The average depth of the groundwater during the events was small: close to the winter average (0.5 m below the soil surface) during events A2, B3, and B4, and closer to

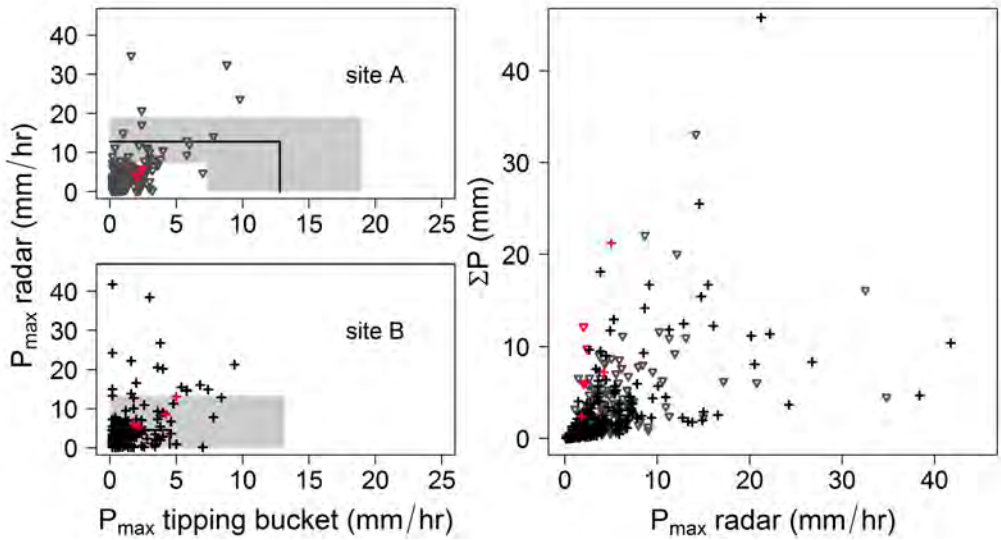


Figure 3.3: Maximum rainfall rate of rainfall events obtained from five-minute rainfall radar series plotted against maximum rainfall rate of the same rainfall events measured with tipping buckets at hourly intervals. The red symbols indicate the maximum rainfall rate during the surface runoff events (Table 3.1). The shaded polygons show the 25–75 percentile values of saturated conductivity at the field sites. In the large figure the cumulative precipitation amount from every rainfall event is plotted against the maximum rainfall rate of the event.

the soil surface during the other events. Considering the scales of the surface runoff events in Fig. 3.2, we observe that the duration of events varied between 6 and 72 hours and the peak discharge varied between 1.8 to 190 l h^{-1} . During surface runoff events A1, A2, B3, and B4, rainfall coincided with melting of a snow cover. On the days before these events, precipitation did not generate an increase in saturation level of the topsoil (Fig. 3.2). The surface runoff events that occurred during snowmelt periods had a longer duration than the ones without snowmelt, but also a lower peak discharge rate and lower total discharge volume. The impact of snowmelt on runoff generation and calculation of the melt rate will be discussed in Sec. 3.3.2.

3.3.2 Event driving mechanisms

Infiltration excess runoff

In Fig. 3.3 the maximum rainfall rate of every rainfall event in the years 2009 and 2010 of the rainfall radar images are compared to the measurements at the field sites, including an indication of the saturated conductivity of both sites. As is expected when sampling at a smaller time interval, the maximum rates obtained from the five-minute rainfall series are higher than those of the hourly rainfall series. The average saturated conductivity, that we measured from ten soil samples of each site in the laboratory, was used as a proxy for the maximum infiltration rate of the soils. The average K_s of site A

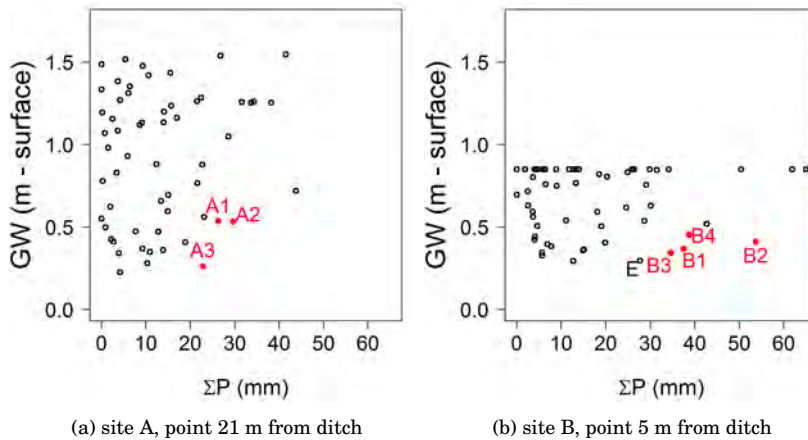


Figure 3.4: Initial groundwater levels of every week in field site operation period plotted versus weekly rainfall sums for the field sites. Weeks during which the surface runoff events occurred are indicated in red.

(fine sand) was larger than that of site B (sandy loam) (Fig. 3.3). The maximum rainfall intensities measured at the field sites during the events were fairly low, see Fig. 3.3 and Table 3.1. During the surface runoff events at site A, neither the hourly interval rainfall intensity nor the five-minute interval rainfall intensity exceeded the median saturated conductivity of the soil. During the surface runoff events at site B, the five-minute interval rainfall intensities exceeded the median saturated conductivity of the soil. Infiltration excess may have been a driver during event B1, because the precipitation intensity was high with respect to the saturated conductivity and the cumulative precipitation was high and could have filled a significant part of the surface storage capacity. It is, however, not very likely that infiltration excess was the main driver during the other surface runoff events, because the higher intensities occurred for a short period of time: the accompanying hourly interval rainfall intensities were much lower than the median of the soil saturated conductivity and the event cumulative precipitation during the events was relatively small.

In the lower depressions of site A water remained present at the soil surface for almost the whole month of February 2010. After the water had receded, the soil surface was sealed with a thin layer of green-black algal and soil material of 1–2 mm thickness. Infiltration experiments with a single-ring infiltrometer indicated that the sealed soil surface had a somewhat smaller infiltration rate than the unsealed surface. However, the final infiltration rates were all contained within the distribution of saturated conductivity that was measured in the laboratory. Also, the lifetime of the deposited layer was short, as it was destroyed at the first round of soil cultivation in spring.

Saturation excess

In five out of the seven events, the groundwater level was within 0.4 m of the soil surface, the only exception being events A2 and B3 during which a groundwater level deeper than 0.5 m below the soil surface was measured at both locations (Fig. 3.2). The soil moisture content at 0.15 m depth, plotted in Fig. 3.2 as a fraction of the total porosity, shows that the topsoil was close to saturation during the actual occurrence of surface runoff. The events that featured snowmelt (A1, A2, B3, and B4), show a steady level of saturation, until an increase occurs due to the temperature increase and accompanying infiltration of melt water.

In the week before event A3, two of the three points show a continuous saturated topsoil. At these measurement locations ponding of water occurred in the mesotopography of the soil surface. The third measurement location was very wet too with an average saturation of 90 %. Before event B2, the soil was initially drier and apparent soil moisture responses to the rainfall events are found at the three measurement points. During event B1, the soil moisture equipment was not yet operational, but groundwater level measurements suggest that large parts of the field site were close to saturation before the surface runoff event. During event A1, the soil moisture equipment was dysfunctional, and groundwater level measurements suggest that the soil was not saturated at the surface. During surface runoff events, only a small part of precipitation can infiltrate, since the soil is close to saturation. As the rainfall quantities during the surface runoff events are not so high (Table 3.1), the filling of the surface depression storage capacity and the cumulative surface runoff discharge cannot be attributed to event precipitation only.

The explanatory capacity of groundwater level (as a proxy of the degree of saturation of the topsoil) and rainfall sums over a period longer than event duration is explored in Fig. 3.4. In this figure, each week of the monitoring period is characterized by the initial distance of the groundwater table to the soil surface (y-axis) and the precipitation volumes at the end of each week (x-axis).

At site B, the groundwater level is situated in the clay layer in parts of the summer. We were not able to accurately measure the levels in the clay layer, due to the very small hydraulic conductivity of that layer. Hence, groundwater depth is assigned a value of 0.85 m for that part of summer, which is clearly visible in Fig. 3.4b. The events are located at the outskirts of the point cloud in the figure. In the plot of site A, the event points are located closer to the point cloud than in the plot of site B. However, the exact position of the points depends also on the somewhat arbitrary choice of the starting point of the weekly periods that were defined for the determination of the precipitation sums and the initial groundwater depths. The events occurred at different moments during the chosen weekly periods and therefore it is not possible to quantify differences between the sites from these figures. The most remarkable point in Fig. 3.4b is labeled “E”. In view of the initial groundwater depth and the cumulative precipitation in the week, surface runoff would have been expected (the timing corresponds to event A3). However, no

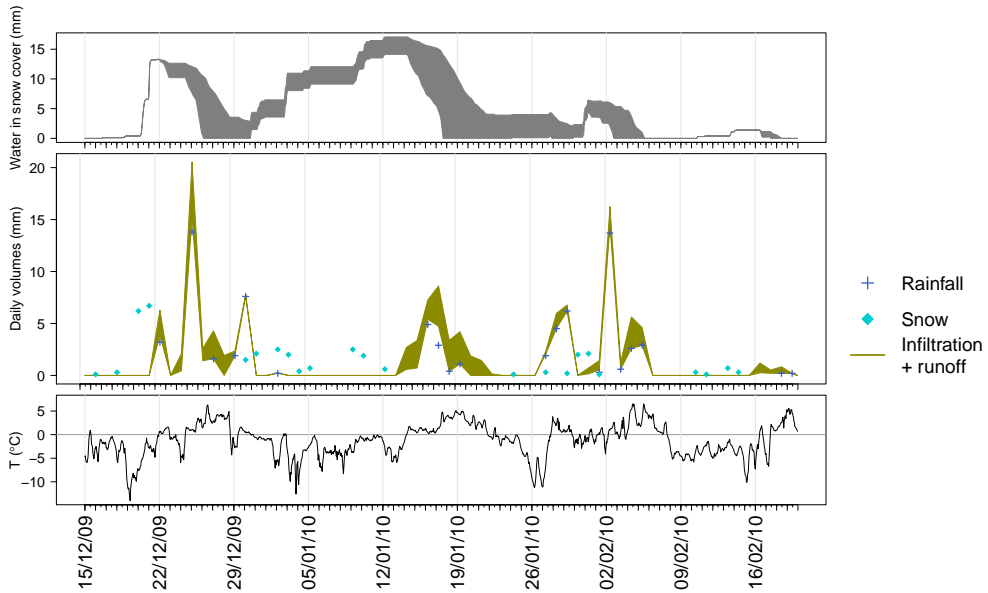


Figure 3.5: From top to bottom: water storage in snow cover, daily volumes of rain, snow and excess water (a combination of melted snow and fresh rain), and temperature time series for the 2009–2010 snowfall period. The bandwidth of the water storage in the snow cover and the daily volumes of excess water result from the uncertainty in the snowmelt calculation due to α of 0.75 to $3.5 \text{ mm } ^\circ\text{C}^{-1}\text{d}^{-1}$.

surface runoff was measured in the trenches. The observations clearly point to saturation excess as the most probable driving mechanism of surface runoff during the measurement period.

Snowmelt

We used hourly temperature recordings from the closest KNMI weather station for a reconstruction of snowfall and snowmelt that is presented in Fig. 3.5. At the weather station precipitation is measured in heated gauges, so we did not need to take into account the relation between volume of precipitation and thickness of the snow cover. The melting of snow and the related amount of water available for infiltration and surface runoff was estimated with the degree-day method (Rango and Martinec, 1995).

$$S = \alpha(T_a - T_s) \quad (3.1)$$

in which T_s ($^\circ\text{C}$) is the minimum temperature at which snow starts to melt, T_a ($^\circ\text{C}$) is the actual average temperature, α is the degree-day coefficient ($\text{mm } ^\circ\text{C}^{-1}\text{d}^{-1}$), and S is the resulting melt rate of snow (mm d^{-1}). The bandwidth in Fig. 3.5 results from analysing the snowmelt development for values of α of 0.75 to $3.5 \text{ mm } ^\circ\text{C}^{-1}\text{d}^{-1}$ (Martinec and Rango, 1986; Rango and Martinec, 1995). The hourly temperature development will not be exactly the same for the location of the weather station and the field sites, but the estimation of bandwidth of available water and daily effects are comparable.

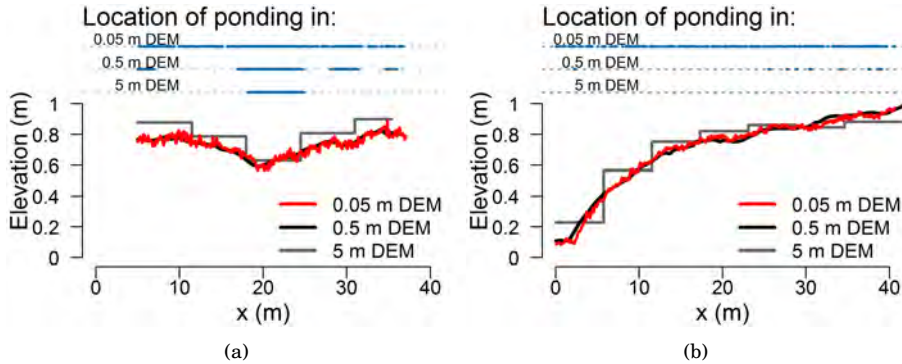


Figure 3.6: Cross section of field site A (left) and B (right) based on three DEMs with three different spatial resolutions. Above the cross sections, lines indicate the location of ponding for each of the DEMs as obtained from simulations with the flow routing event. For position of cross section see Fig. 3.1.

Events A1, A2, B3, and B4 were preceded by a period of snowfall. At the event days, the temperature increased above 0°C and the precipitation of these days occurred as rainfall. The melting of snow close to the trenches in combination with the fresh precipitation caused surface runoff in the trenches.

The melting of snow alone, e.g. as on 16–18 January 2010, did not trigger a surface runoff event. Combined snowmelt and fresh precipitation resulted in a daily cumulative of available water that was able to reach the trenches. The rate of release did not seem to be the determining parameter: maximum release rates estimated to occur during the surface runoff events was around $2.0\text{--}2.5\text{ mm h}^{-1}$, which is the same order of magnitude that also occurred during rainy days 29–30 December and 27–29 January, and melting days 16–17 January.

The snowfall in the winter period of 2009–2010 was higher than average. At the weather station, the winter counted 40 days with a snow cover, where as 13 days is the longterm yearly average.

Estimates of the total released amount of water can be used to make an updated estimate of the contributing area of the surface runoff events (numbers presented in Table 3.1 and discussed in Section 3.3.3).

3.3.3 Surface topography

The surface topography determines the threshold for water storage and the direction of water flow at the fields. We analysed the surface topography of the sites from digital elevation models (DEMs) at three spatial resolutions. In Fig. 3.6, a cross section of the sites based on the three DEMs is presented. The characteristics of the catchment areas of the measurement trenches are presented in Table 3.2.

At site A, the most dominant mesorelief feature is the series of depressions that is located in the middle of the northeastern side of the field, perpendicular to the ditch. At

this location, a ditch was filled up years before, which after compaction became a permanent low spot in the field. The tillage direction of the maize that was grown at this site was southeast to northwest, parallel to the northeastern ditch, cutting through the remains of the former ditch. Most of the field is surrounded by a permanent ridge of about 10 cm that is not cultivated. This ridge provides a permanent barrier to surface runoff reaching the ditch, in theory allowing a DSC of 100 mm. However, this is also the driest and least disturbed part of the field, and therefore the most popular location for macrofauna like moles, mice and rats to burrow. By their burrowing they create a network of preferential flowpaths locally disrupting the threshold effect of the ridge. Observations during the winter of 2009–2010 pointed out that most spillpoints from agricultural fields to the ditches actually follow one or more of these burrows. At site B, two topographically distinct areas can be distinguished. From the northern ditch, where the measurement trenches were located, to approximately 55 m south, the field has a mild slope of 2 %. Further south, the field is flat until it reaches a small secondary ditch (Fig. 3.1). As both ditches are dug perpendicular to the field slope, surface runoff can enter the ditches quite evenly. During the surface runoff events at this site, we observed water entering the trenches at several points and surface runoff contributing to inflow in the ditch at several other locations along the ditch.

Table 3.2: Characteristics of surface topography at field sites in Beltrum (A) and Winterswijk (B) obtained from DEMs with a varying grid cell size. Depression Storage Capacity, DSC (mm), volume of precipitation needed to reach full DSC , P_{DSC} (mm), ponded area under DSC conditions, A_p (m²), maximum area contributing to runoff, CA_{max} (m²). For each surface runoff event the calculated contributing area is presented, CA_{act} (m²), in brackets the resulting area when the snowmelt rate is added to the event rainfall rate.

Site	DEM cell size	DSC	P_{DSC}	A_p	CA_{max}	Event	CA_{act}
A	5.0	14.4	50.0	1600	13375	A1	18.3 (14.3)
	0.5	6.31	24.5	289.8	992.75	A2	21.3 (12.7)
	0.05	9.33	29.5	489.6	1006.3	A3	290.3
B	5.0	2.53	6.0	50.0	1975	B1	62.2
	0.5	0.39	4.0	70.5	1040.3	B2	16.1
	0.05	2.55	12.0	284.4	843.0	B3	4.45 (3.56)
		B4	15.7 (7.81)				

The 5 m DEM is not suitable to analyse the ponding behaviour. In the DEM, elevation gradients of 50 cm between two adjacent grid cells are found, that do not match field observations. The pixel size is too coarse to capture the structure of the topographic features at the sites. The main difference between sites A and B is the scale of the topographic features in which water is stored. At site A, most of the water can be stored in mesotopographic depressions that can be distinguished in the 0.5 m DEM. At site B, the contribution of microtopographic features is much larger than that of the

mesotopographic features (Fig. 3.6b).

Logically, it follows from this observation that the depression storage capacity of site A is larger than that of site B (Table 3.2). The catchment area of trenches at site A is much larger than that of site B. At site B, the elevation gradient towards the ditch creates a relative homogeneous distribution of catchment size along the ditch (relatively narrow, but elongated along the slope), whereas at site A, there is a series of low patches in the central part of the field, which causes a more heterogeneous catchment area within the field. The position of the trenches at site A were chosen such that they drain these patches. Observing that the soil was very close to saturation before the surface runoff events started (Fig. 3.2) and that ponding of water occurred before the events, we calculated the actual contributing area from the proportionality between average rainfall intensity and peak discharge (cf. simple rainfall-runoff relation (Dooge, 1957)). During rainfall that actually resulted in surface runoff at the field boundaries, infiltration of water into the ground can be neglected, because the flow paths consist of connected areas that contained water before the rainfall event. The contributing area calculated in this way is presented in Table 3.2. A correction for the melt rate of snow was included for the events where a snow cover was present. As in the topographical analysis, the contributing area of site A was larger than that of site B. The actual contributing areas are a factor smaller than the catchment areas calculated from the topographical analysis. This can be attributed to the small differences in available surface and subsurface storage.

In addition to the soil surface, water can be stored as interception in the site vegetation. At site B, this was not a factor as the soil was bare during the surface runoff events in winter. At site A, water may be intercepted (and surface runoff delayed) all year, due to the grass cover.

3.4 Discussion

3.4.1 Hypothesis testing

Before starting the field measurements, we anticipated that there would be a few events occurring during the measurement period, because surface runoff is a rare process in these areas. We expected these events to take place mainly as saturation excess events, because the permeability of the soils at the sites was rather high. At site B, it was more plausible that some infiltration excess surface runoff could reach the trenches because of the lower infiltration capacity of the soil and the presence of a slight slope of the soil surface towards the ditch. We thought it was probable that surface runoff was buffered by some large ponds at site A and that we would find a more spatially random buffering of water at site B. From the surface topography characteristics of the sites, we expected that multiple small flowpaths would develop at site B, whereas at site A one large flowpath was more likely.

Indeed, the number of events during which surface runoff actually reached the trenches was small: during 4 out of 283 rainfall events at site A and 3 out of 275 rainfall

events at site B. In 4 out of 7 events, the groundwater level was very close to the soil surface, so these can be classified as saturation excess events. Infiltration excess surface runoff may have occurred at a smaller scale during some rainfall events, but it didn't result in surface runoff reaching the trenches at either site. At site A, water collected in large ponds in the depressions visible on the map of Fig. 3.1. During event A3, a single outlet drained this wet area. At site B, ponding occurred (contrary to expectation) mainly further away from ditches, upslope in larger features. These being full, finally overflowed towards trenches, following multiple flowpaths.

A driver mechanism that we had not foreseen to be so important was snowmelt in combination with fresh rain.

3.4.2 Interpretation of results

The maximum precipitation rates that occurred during the events were not exceptionally high. Where they may have contributed to some within-field displacement of water, it is not very likely that infiltration excess runoff was the major driving mechanism for surface runoff that reached the ditches that surround the field sites. On the occasions where precipitation rates exceeded the saturated hydraulic conductivity of the field sites (see Fig. 3.3), excess water was stored in either micro- and mesotopography. Most likely, the cumulative water during the events that featured these high precipitation rates, was not enough to overcome the depression storage capacity and create continuous flow paths towards the surrounding ditches. This may also explain why we did not find any indication of infiltration excess surface runoff events at site B, where it would have been more probable than for site A.

At both sites, the size of the contributing area was smaller for the events with snowmelt than for those without snowmelt. This was unexpected at site A, where the ridge surrounding the field provided a barrier that could only be overcome when all mesotopographic depressions (Fig. 3.1) had been filled and the contributing area was large. The estimated contributing area during the snowmelt events was larger (12 to 15 m²) than the area of the ridge bordering the trenches (6 m²). A tentative explanation for the intermediate value of contributing area is that the fresh rain and melted snow ran off over the snow cover instead of filling the micro- and mesotopography of the surface.

Event A3, as expected, features a large contributing area. Pondered area had increased in the days preceding the event. When the depression storage capacity was filled, one flow path drained the connected pondered areas over the ridge towards the trenches. At site B, the development of surface runoff flowpaths was similar, with water accumulating in ponds further away from the ditches. When the depression storage capacity was filled, several flow paths drained the pondered areas towards the trenches. The surface topography of site B would have allowed a more gradual increase of contributing area as well. Since there was no ridge surrounding the field and the surface was sloping towards the ditches, flow paths could have been formed from connected ponds close to the trenches expanding to areas further away. This type of flow path development

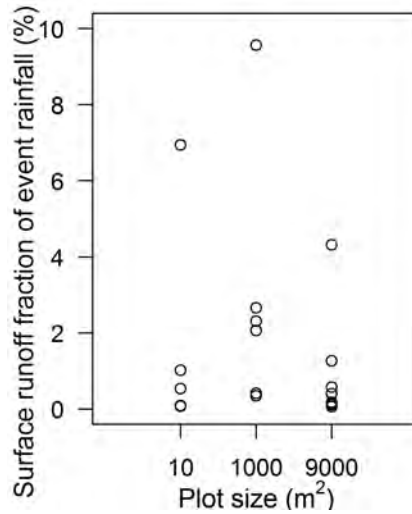


Figure 3.7: Comparison of three surface runoff studies: 10 m² = Augeard et al. (2005), 1000 m² = this study, 9000 m² = Deasy et al. (2009).

has been described from laboratory and synthetic experiments for infiltration excess runoff (Darboux et al., 2001; Moore and Larson, 1979; Antoine et al., 2009). We did not find this type of development because the main driving mechanism was saturation excess. The ponding of water started far away from the ditches and hence the contributing area during surface runoff events was relatively large. When the time lag between rainfall events is short and cumulative rainfall is high, the ponded water will not re-infiltrate between the rainfall events. Under these conditions low-intensity rainfall events can generate surface runoff and form continuous flow paths from ponded areas to ditches and streams.

Given the dominance of saturation excess over infiltration excess as a driving mechanism, the formation of surface runoff flow paths towards streams and ditches is a two-stage process. The storage capacity of the unsaturated zone and surface topography are both thresholds that need to be exceeded to form a continuous flow path over the soil surface. The filling of the surface topography (i.e. overcoming the second threshold) starts when the rainfall rate exceeds the groundwater flux, which determines the infiltration rate under saturated conditions. This type of surface runoff initiation could also be characterized as a hybrid mechanism that contains both aspects from saturation and infiltration excess runoff, for which the term “Dunton” overland flow was coined (Loague et al., 2010).

3.4.3 Scale issues

Comparing surface runoff rates and volumes between locations is hindered by scale issues. In Fig. 3.7 we compare our findings to two studies that we know of, in which surface runoff was measured at field sites. We selected these studies because the

circumstances were similar to those of our sites: agricultural fields in temperate climate regions of Europe, artificially drained, with a small surface slope ($< 2\%$) on which surface runoff was observed mainly caused by saturation excess, with relatively permeable soils. The difference between the studies (Fig. 3.7) is the size of the catchment area of the surface runoff measurement devices: plot size (Augeard et al., 2005), part of field size (this study), and complete field (Deasy et al., 2009). In the figure, the percentage of rainfall that left the catchment area as surface runoff during each event of the study is plotted.

Interestingly, the range of percentages of the three sites, representing three areal orders of magnitude, does not differ significantly (tested with a Kruskal-Wallis test). At spatial scales equal to or smaller than field size, a maximum of 10 % of event precipitation is transported to the field boundaries as surface runoff. At the catchment scale this fraction will be lower, because not all the fields of the catchment feature connected surface runoff flow paths during the rainfall event (Deasy et al., 2009). Obviously, this is a rather small exploration of scale differences that might be worthwhile to get a practical grip on such infrequently occurring phenomena.

3.5 Conclusions and recommendations

Field observations of surface runoff at two sites in The Netherlands resulted in seven monitored events in a measuring period of approximately 1.5 years. Four out of the seven events were associated with saturation excess as a driving mechanism, none with infiltration excess, and three with a possible hybrid mechanism. Four out of the seven events had water input from a melting snow cover in addition to the rainfall occurring during the event.

The number of events presented in this study was small, as surface runoff does not occur under ‘average’ rainfall and hydrological conditions in the climate and geomorphological setting of these field sites. The results presented here, however, show that under the rare conditions required to generate a surface runoff flux to the open water system, up to 10 % of the event precipitation can leave the field as surface runoff, both for loamy and sandy soils and easily overcoming storage thresholds from mesotopography features on the soil surface. Ponding started where the groundwater table was closest to the soil surface. In the well-drained catchments where our sites were located, this means that ponding started far away from the surrounding streams and ditches. Therefore, large contributing areas were observed during the surface runoff events, with multiple spillpoints towards streams and ditches. Snowmelt surface runoff events were of smaller size and impact than saturation excess surface runoff events. Their spatial extent was smaller and there was only temporary saturation of the soil surface: ponding was not persistent after the snow cover had melted.

Further strengthening the narrative on surface runoff in flat, temperate agricultural catchments can be done by conducting studies in which the soil surface topography and ponding of water therein is monitored during events. Also, we emphasize

the use of a wide network of shallow sensors and a dense groundwater sensing network to quantify hybrid driving mechanisms of surface runoff generation. This could also improve the quantification of spatial variation of surface runoff occurrence.

Acknowledgements

This study was financed by Alterra (project 5232870-06) and the Dutch ministry of Agriculture, Nature, and Food Quality (project BO-05-004-KRW). Partial funding by the Dutch Knowledge for Climate Programme is appreciated. The authors thank Han te Beest, Jan van Kleef, Antonie van der Toorn (Alterra), Pieter Hazenberg (Wageningen University) for their help at acquiring the data and Aart Overeem (KNMI/Wageningen University) for downscaling the rainfall radar data.

Chapter 4

Effects of microtopography and shallow groundwater dynamics on ponding and surface runoff in flat areas

Abstract

In relatively flat fields, ponding and surface runoff, and therefore all other components of the water balance, are strongly affected by micro- and mesotopographies. Mathematical modelling of saturation excess surface runoff in this type of field is difficult and requires the balancing of complexity of the equations to be solved versus the heterogeneity of the system one wants to model. We developed a model of reduced complexity, that incorporates processes and feedbacks that are important when considering surface runoff generation under saturation excess conditions, to investigate the generation of ponding and surface runoff in temperate lowland areas, with different types of microtopography, soil types and precipitation forcing. The first storage threshold for the start of ponding and surface runoff is the storage capacity of the unsaturated zone, that is here controlled by the depth of the groundwater table. Microtopography affects surface runoff development under saturation excess conditions by providing a second storage threshold. The timing of surface runoff reaching the ditches under these conditions depends on initial storage capacity of soil and topography and the spatial variation thereof. Mesotopography affects surface runoff development under saturation excess conditions by actually rerouting ponding water over longer distances. The infiltration of water in mesotopographic depressions decreased the gradient of the groundwater table over a large part of each field, thereby decreasing groundwater flow. The presence of mesodepressions effectively results in a nested hydrological system where smaller water bodies are activated when storage of water in the system is large. Because of the nested activation, the effect of the specific structure of rainfall series is large and can lead to differences in total volume of surface runoff generated per season of one order of magnitude for statistically identical rainfall timeseries.

4.1 Introduction

Surface runoff is a relevant process as it 1) is a fast flow path for water and for transport of sediment, solutes, and substances sorbed to the upper soil, 2) affects spatial variation in groundwater recharge, 3) affects spatial variation of vegetation site factors, and 4) causes erosion and soil sealing.

Surface runoff develops when the rainfall intensity exceeds the infiltration capacity of the soil or when the soil is saturated. Also, hybrid mechanisms exist where infiltration is hampered by slow vertical or lateral percolation of water through the soil, even though the rainfall intensity is smaller than the saturated conductivity (Loague et al., 2010). In flat lowland catchments with sandy soils in temperate climates, surface runoff does not occur very often (Church and Woo, 1999). Typically, precipitation occurs in rainfall events with a long duration and low intensity. The high permeability of the soil and small surface slopes provide plenty of infiltration capacity, therefore flow occurs mainly through soil and groundwater (Hendriks, 2010). The natural ecosystems of these regions are mostly characterized by shallow groundwater tables and frequent saturation

excess surface runoff. In agricultural areas, artificial drainage is usually aimed at the prevention of water logging during wet periods. With analytical solutions for groundwater flow and design rainfall events, optimal drain or ditch spacing is determined (Hooghoudt, 1940; Ernst, 1956). However, both ponding and surface runoff are still observed frequently in these areas, mainly in winter.

In relatively flat fields, ponding and surface runoff, and therefore all other components of the water balance, are strongly affected by micro- and mesotopographies (Darboux et al., 2001). Amongst these are features that can be characterized statistically, e.g. resulting from tillage or vegetation structure, and erratic ones such as macrofauna burrows. A large part of the abundant studies on the effect of microtopography on surface runoff are embedded in erosion research (Helming et al., 1998; Romkens et al., 2002; Alvarez-Mozos et al., 2011). These tend to focus on sloping sites and infiltration excess events because of the erosive potential involved. In semi-arid areas, spatial variability in surface runoff generation occurs due to the presence of vegetation tussocks and the associated variability in infiltration characteristics (HilleRisLambers et al., 2001; Rietkerk et al., 2002; Ludwig et al., 2005; Mueller et al., 2007). In waterlogged ecosystems, the spatial distribution of vegetation enhances hysteretic aspects of the rise and fall of the groundwater table. In soils with shallow groundwater, both the infiltration capacity and storage capacity depend on the groundwater depth, increasing with deeper groundwater levels and decreasing with shallower groundwater levels (Nachabe, 2002; Sumner, 2007).

Mathematical modelling of saturation excess surface runoff is quite a challenge, as it involves a coupled system of ephemeral free flow and flow through a variably saturated porous medium. In heterogeneous, partly submerged topographies the direction of flow routing can change rapidly in the process of filling, overflowing, and merging of small ponds (Antoine et al., 2009; Darboux et al., 2001). Moreover, in soils close to saturation, small changes in water volume result in large changes of the groundwater gradient. Therefore, the system is prone to numerical instabilities and usually requires long convergence and computation times.

Coupled models for surface and subsurface are abundant, for example ParFlow (Kollet and Maxwell, 2006), CATHY (Paniconi and Wood, 1993; Orlandini et al., 1996; Camporese et al., 2010), tRIBS (Ivanov et al., 2004), and HydroGeoSphere (Therrien et al., 2008). However, even for the models that are able to deal with heterogeneous flat surfaces, solving the equations involved is not trivial because of the aforementioned instabilities and computation times (Frei et al., 2010). Therefore, there is a continuing need for robust and parsimonious models when investigating the feedbacks of a shallow groundwater table, ponding, and surface runoff under a range of conditions, in order to achieve an optimal balance between computation speed and included process complexity. This leads to spatially distributed models that contain both conceptual and process elements, tailor-made for the precise topic of investigation (Camporese et al., 2010).

We want to understand triggers and thresholds of surface runoff in temperate

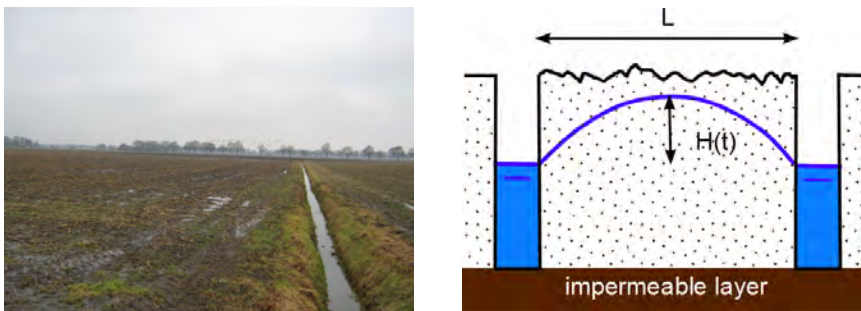


Figure 4.1: Impression of a microtopographic agricultural field with ponding, surface runoff, and groundwater flow between two ditches.

lowland areas, with different types of microtopography, soil types and precipitation forcing. To this end, we investigate the generation of ponding and surface runoff for fields with designated micro- and mesotopography. We developed a model that incorporates processes and feedbacks that are important when considering surface runoff generation under saturation excess conditions, but conceptualized in such a way that the computation times are kept as small as possible. We address the following research questions: 1) how is surface runoff development affected by the presence of a shallow groundwater table?, 2) how does microtopography affect surface runoff development under saturation excess conditions?, and 3) how does mesotopography affect surface runoff development under saturation excess conditions?

4.2 System schematization

An example and a schematic representation of the systems that we investigate are presented in Fig 4.1. The system consists of a field in between two ditches or streams. The soil is relatively deep (order of magnitude is 5–10 m) and homogeneous. The surface between the ditches is relatively flat, but features various types of meso- and microtopography, e.g. resulting from tillage. The maximum elevation of the groundwater mound, i.e. the **convexity** of the water table, depends on the combination of transmissivity and precipitation. The distance between soil surface and water table is therefore determined by the, often regulated, water level in the ditch or stream and the specific convexity. This system is a classic agricultural drainage problem that has been described analytically for steady state and transient conditions by a.o. Hooghoudt (1940); Ernst (1956); de Zeeuw and Hellinga (1958); Kraijenhoff van de Leur (1958); Glover and Dumm (1960). The considerations on feedbacks and processes that underlaid the setup of our FAST-Runoff model (Fast Areal Simulator with Topography for Runoff) are the following.

At the soil surface, we prioritize the filling and spilling of basins within the field over an accurate estimate of the surface runoff flow velocities. The filling and spilling

algorithm allows flow directions of surface runoff to change during the ponding and redistribution process. To solve for flow within a reasonable computation time, we assume surface flow within and between the basins to be instantaneous instead of solving appropriate equations such as those of St. Venant. At the end of every timestep, we have a steady state situation. In a field that contains many small depressions, the transfer of water is controlled by the duration needed to fill the depressions, hence, the time required by water to move from one depression to the other can be neglected and the assumption of instantaneous water transfer is justified.

The infiltration of precipitation or ponded water into the soil depends on the soil water storage capacity of the unsaturated zone and on the vertical saturated hydraulic conductivity of the soil and the soil moisture content at the soil surface. To enable a fast determination of these variables, we made a second significant assumption, namely the presence of a hydrostatic equilibrium in the unsaturated zone at all timesteps. By doing this, we can calculate the amount of water in the unsaturated zone easily by integrating the soil moisture profile over the thickness of the unsaturated zone. We ignore the shape of a downward travelling moisture front, by assuming that the unsaturated zone reaches this steady state condition at the end of every timestep. Since wet situations with much precipitation and shallow groundwater tables have our interest, the assumption of the hydrostatic equilibrium profile, which is a rather wet one, can be justified. The approach will be less suitable for drier summer conditions.

In the saturated zone, the main direction of flow is oriented towards the ditches. We neglect vertical groundwater flow (Dupuit assumption) and assume the ditches to be fully penetrating to the bottom of the soil, thereby neglecting radial flow towards the ditches or regional flow underneath them. The assumption of hydrostatic equilibrium in the unsaturated zone means that we have a unique relation between the groundwater level and the volume of water stored in the soil at every point in the field in space and time. Besides using this relation to determine the infiltration characteristics dynamically, we can also use this relation to incorporate a dynamic relation between water volume change and groundwater table change into the model. This relation, known as specific yield, phreatic storage coefficient, or drainable porosity, is important under shallow groundwater conditions. The addition of a small amount of water into the soil can result in a large increase of the groundwater table, an effect that is enhanced when the groundwater level is close to the soil surface. Groundwater flow is therefore affected by the extent of saturation throughout the field. As we consider the volume of water integrally in both the unsaturated and the saturated zone, we do not have to calculate a flux between these zones, relieving us from a potential source of numerical instability. While using the groundwater head as the driving force of groundwater flow, we can express the groundwater equations as a function of water volume, thereby keeping a close watch on the water balance. These simplifications are acceptable in coarse-textured soils without cracks or macropores in shallow groundwater conditions and therefore suitable for the system that we investigate here.

4.3 Model description

4.3.1 Ponding and surface runoff

The digital elevation model (DEM) of each field is analyzed and a database of microdepressions is created. These microdepressions are characterized by their area, storage capacity, and spill points to neighbouring depressions. In case of excess water at the surface during a timestep of the simulation, a water balance is calculated for all depressions in the database under the assumption of instantaneous water transfer. When the amount of rainfall in a certain depression exceeds the capacity of the depression, water spills over the lowest spillpoint to a neighbouring depression. Depressions can merge into larger depressions with spillpoints at higher elevations, or simply pass on water in a chain-like manner. In the system of the simulations excess water is allowed to infiltrate from the lowest points of the catchments, i.e. either in the depressions, or (when excess water is generated outside the area bounded by the depressions) in the ditches. A detailed description of the algorithm can be found in Appels et al. (2011).

4.3.2 Infiltration scheme

Incoming precipitation is partitioned between infiltration and excess water based on the soil water storage capacity availability of the unsaturated zone and the infiltration capacity of the soil. For the calculation of the infiltration capacity we chose Philip's infiltration equation (Philip, 1957b), because it contains parameters with a physical meaning and a simple form can be used to express both the infiltration capacity and cumulative infiltration as a function of time and sorptivity. Philip's infiltration equation is an infinite-series solution to the Richards equation, of which usually only the first two terms are used:

$$i = \frac{S}{2\sqrt{t}} + K_v \quad (4.1)$$

in which i is the infiltration rate [$L T^{-1}$], S is the sorptivity [$L T^{-1/2}$], t is time [T], and K_v is the hydraulic conductivity [$L T^{-1}$]. Sorptivity S is a measure of the capacity of the soil to infiltrate water by capillarity and depends on the hydraulic properties of the soil and on its initial saturation. The reduction of hydraulic gradient when the soil gets wetter is reflected by the decreasing influence of sorptivity with time. Mathematical solutions for the value of the sorptivity can be found by solving the Richards equation. Another simpler, but approximate, approach is to express the sorptivity as an integral functional of the diffusivity. With this approach, approximate expressions for the sorptivity as a function of soil hydraulic parameters of characteristic functions such as Brooks-Corey or Van Genuchten can be obtained. In compliance with the description of the hydrostatic equilibrium with the Van Genuchten function, we use the following approximate expression with Van Genuchten soil hydraulic parameters to calculate the sorptivity (Zimmerman and Bodvarsson, 1995):

$$S = \sqrt{\frac{2(1 - 1/n)^{4/3} K_v (\theta_s - \theta_i)}{\alpha}} \quad (4.2)$$

in which α [L^{-1}], and n [-] are shape parameters of the Van Genuchten water retention model, θ_s [-] is the saturated soil moisture content, θ_r [-] is the residual soil moisture content, and θ_i [-] is the initial soil moisture content at the soil surface. Due to our assumption of hydrostatic equilibrium in the unsaturated zone, θ_i is directly linked to the depth of the water table at a certain location, providing a feedback between depth of the groundwater and infiltration capacity.

Originally designed for a ponding boundary condition, Eq. 4.1 can be extended to a rainfall boundary condition by correcting the cumulative infiltration. When the precipitation rate is lower than the initial infiltration capacity, a correction is applied for the cumulative infiltration. The time compression approximation (Salvucci and Entekhabi, 1994; Sivapalan and Milly, 1989) provides a two-step correction effectively substituting time in Eq. 4.1 for cumulative precipitation. In the first step, a correction time t_c is calculated at which the potential infiltration rate i is equal to the effective precipitation rate p_e [$L T^{-1}$].

$$t_c = \frac{S^2}{4(p_e - K_v)^2} \quad (4.3)$$

In the second step, the ponding time t_p is calculated from the cumulative infiltration at t_c divided by the precipitation rate:

$$t_p = \frac{S\sqrt{t_c} + K_v t_c}{p_e} \quad (4.4)$$

The final expression for infiltration during a rainfall event then becomes:

$$i(t) = \begin{cases} p_e & \text{for } t < t_p \\ \frac{S}{2\sqrt{t - (t_p - t_c)}} + K_v & \text{for } t \geq t_p \end{cases} \quad (4.5)$$

In the case of spatially non-uniform infiltration, excess water from a certain cell can form runoff for a cell downslope that did not reach its ponding time yet. Hence, for each cell, precipitation rate, runoff rate, and the local value of $i(t)$ are combined in a water balance. The effective precipitation rate p_e in Eqs. 4.3, 4.4, and 4.5 is the local sum of precipitation rate and runoff rate.

When microtopographic variation is large, the actual surface area of a landscape is significantly larger than the horizontal extent of the DEM and the absorptive area of the soil is increased. In situations like this, a compensation factor should be applied to the sorptivity (Thompson et al., 2010). In our topographies, the ratio between actual surface area and DEM surface area was close to one, and therefore we did not bother to apply such a compensation factor.

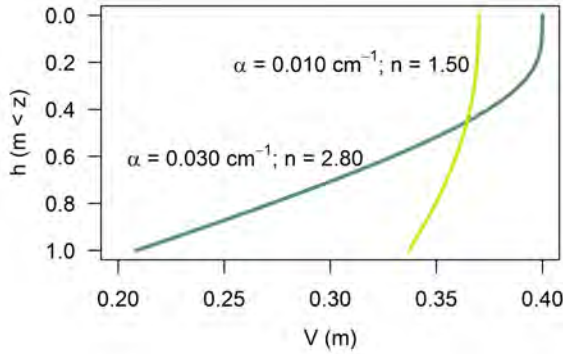


Figure 4.2: Groundwater depth below the soil surface as a function of volume of water stored in a soil column for two soils. Note the strong non-linearity when approaching complete saturation.

4.3.3 Water flow in the soil

The schematic field of Fig. 4.1 is composed of a set of vertical soil columns, one for each cell of the DEM. In these columns, the matric potential, ψ [L], is a function of water table depth, h [L], and vertical position in the unsaturated zone, z [L], (Eq. 4.6).

$$\psi = h - z \quad (4.6)$$

We used the Van Genuchten water retention function (van Genuchten, 1980), given by

$$\theta(z) = \theta_r + (\theta_s - \theta_r) \left(\frac{1}{1 + (\alpha(h - z))^n} \right)^{1-1/n}. \quad (4.7)$$

Our integral consideration of the water volume in each soil column requires a unique solution for θ along the entire length of the unsaturated zone and the capillary fringe, therefore simpler functions, such as the Brooks-Corey function, cannot be used in this approach. Eq. 4.7 can be integrated over the length of the unsaturated zone and added to the water storage in the saturated zone to obtain the total volume of water stored in the soil column.

$$V(h) = \begin{cases} h\theta_s & \text{for } z \leq h \\ h\theta_s + \theta_r(z - h) + (\theta_s - \theta_r)(z - h) {}_2F_1\left(\frac{1}{n}, \frac{n-1}{n}; 1 + \frac{1}{n}; -(\alpha(z - h))^n\right) & \text{for } z > h \end{cases} \quad (4.8)$$

where ${}_2F_1$ is the hypergeometric function (NIST, 2010). In this way, we have a unique relationship between water volume in a soil column and elevation of the groundwater table at each timestep for every set of soil hydraulic parameters.

Disregarding vertical groundwater flow rates and evapotranspiration, the 2-dimensional mass balance equations are given by

$$Q_x + Q_y = \frac{\partial V}{\partial t} - R(x, y, t)\Delta x\Delta y, \quad (4.9)$$

in which Q_x and Q_y [$L^3 T^{-1}$] are the fluxes in, respectively, the horizontal x- and the y-directions, R is the rainfall rate [$L T^{-1}$], Δx and Δy [L] are the cell length and width, and

V [L^3] is the volume of water stored in the soil column. When we substitute Q with the Darcy equation and apply the chain rule to keep V as our state variable, Eq. 4.9 becomes

$$K_s D \Delta y \frac{dh}{dV} \frac{\partial V}{\partial x} + K_s D \Delta x \frac{dh}{dV} \frac{\partial V}{\partial y} = \frac{\partial V}{\partial t} - R \Delta x \Delta y, \quad (4.10)$$

in which K_s is the horizontal saturated hydraulic conductivity [$L T^{-1}$], D is the aquifer height [L], and b is the width of cell [L]. The numerical solution of Eq. 4.10 requires the possibility to obtain h as a function of V . Unfortunately, Eq. 4.8 cannot be inverted. Therefore, we built a table of h -values and their corresponding V -values. The system of equations is then solved explicitly at very small timesteps. The size of the timesteps is determined according to Eq. 4.11,

$$\frac{\Delta t K_s D}{S_y \Delta x \Delta y} \leq 0.1 \quad (4.11)$$

where S_y is the specific yield, or the first order derivative of V with respect to h . It depends on the depth of the water table below the soil surface and changes rapidly when that depth is small. It can be expressed analytically as the derivative of Eq. 4.8 to water table depth, or

$$S_y(h) = (\theta_s - \theta_r) \frac{(\alpha(z-h))^n - ((\alpha(z-h))^n + 1)^{\frac{1}{n}} + 1}{(\alpha(z-h))^n + 1}. \quad (4.12)$$

In the groundwater equations 4.9 and 4.10, the specific yield is not explicitly defined, but its inverse is included in the $\frac{dh}{dV}$ term of the equations.

4.4 Numerical experiments

The equations described in the previous section were solved numerically on idealized domains with a configuration such as that in Fig. 4.1. The domain is a 2 dimensional slice of a larger field between two ditches, with a fixed-head boundary condition where these ditches are located and no-flux boundary conditions at the other two sides. Soil types were characterized by parameters α and n for the Van Genuchten retention curve, and conductivity parameters K_v and K_s for the saturated hydraulic conductivity in the vertical and horizontal direction. To account for anisotropy of many soils, K_v was related to K_s as $K_s = 4K_{vs}$. For surface microtopographies, we generated Gaussian fields for various combinations of standard deviation σ and correlation length l . We transformed these fields with a transform developed by Zinn and Harvey (2003) to obtain microtopographies that have identical statistical properties, but different spatial configurations that affect their hydrological connectivity (Antoine et al., 2009; Appels et al., 2011). In a random topography, i.e. the original synthetic Gaussian microtopography, the values around the mean of the distribution are connected, whereas the Zinn-Harvey transformation results in microtopographies where the lowest values (channel topography) or the highest values are connected (depression topography). Mesotopography was simulated deterministically, with depressions positioned at three locations in the field (Fig. 4.3). The depression storage capacity (DSC) of these

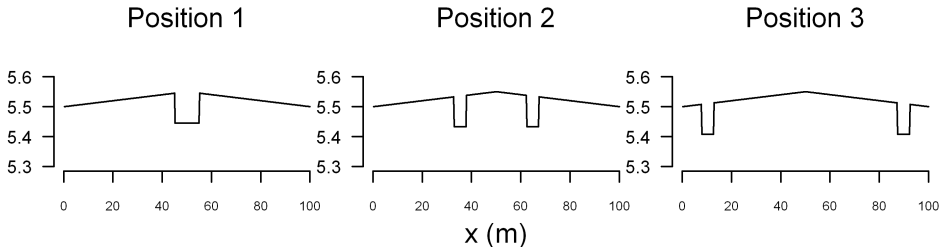


Figure 4.3: Schematized design of three positions of mesorelief depressions. The elevation range is the distance to the impermeable layer under the aquifer.

depressions was varied by changing their width D_w in order to keep the volumes equal throughout the three positions. Choosing four DSC-values resulted in twelve unique surface topographies. These topographies did not feature any extra microtopography. The initial conditions were determined by the depth of the water table at the domain boundaries below the soil surface, h_0 , and the maximum elevation of groundwater mound with respect to boundary condition, i.e. the convexity m_0 . The variables and their ranges for the numerical experiments are summarized in Table 4.1.

We performed a sensitivity analysis in three pieces. A flat cross section of a field (1 m wide) the model was simulated under varying conditions of parameters α , n , K_s , P , T_p , h_0 , and m_0 . The soil hydraulic parameters α and n were varied in pairs, the other parameters independently. This analysis therefore consisted of 15000 simulations. On a 30 m wide field cross section, simulations were performed with microtopographical patterns.

Table 4.1: Variable ranges for numerical experiments

Variable			Min	Max
σ	(m)	standard deviation of microtopography	0.005	0.025
l	(m)	correlation length of microtopography	0.5	0.5
L	(m)	distance between the ditches	100	100
$\Delta x, \Delta y$	(m)	cell size of the DEM	0.1	0.25
α	(cm^{-1})	Van Genuchten parameter	0.005	0.05
n	(-)	Van Genuchten parameter	1.1	2.5
K_s	(m d^{-1})	saturated hydraulic conductivity	1.0	15.0
h_0	(m)	groundwater depth boundary condition	0.6	1.0
m_0	(m)	convexity ^a	0.1	0.5
P	(mm d^{-1})	precipitation rate	2	10
T_p	(hr)	amount of precipitation hours per day	6	24
D_w	(m)	width of depressions in mesotopography	1	10

^a maximum elevation of groundwater mound with respect to boundary condition

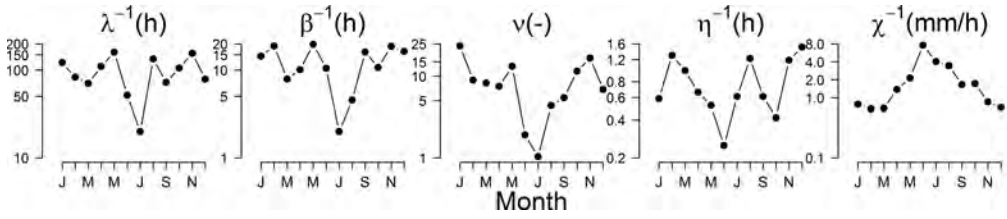


Figure 4.4: Monthly values for the five RainSim parameters obtained from analyzing 10-year hourly precipitation data from KNMI station “Hupsel” with RainSim software. The hourly precipitation time series generated with these parameter values were used as atmospheric forcing of the simulations of surface runoff in the mesotopographies.

Varying parameter values of α , n , σ , h_0 , and m_0 in combination with 10 realizations of each type of microtopography resulted in 6750 simulations. The analysis of the field cross sections with a schematic mesotopography consisted of 1080 simulations in which parameters α , n , and K_s were varied under ten realizations of statistically generated rainfall timeseries.

We considered two cases of atmospheric forcing. The first one consisted of a period of 10 days with daily rainfall in events with designated length T_p and precipitation rate P , aimed at systematically scanning effects of cumulative precipitation and precipitation intensity (with intensities lower than the saturated hydraulic conductivity). The second one consisted of a period of six months with a randomly generated precipitation pattern with statistical characteristics from rainfall in the winter months in The Netherlands. We analyzed 10-year hourly precipitation data from KNMI station “Hupsel” with RainSim software (Burton et al., 2008). The software assumes that rainfall patterns consist of storms that contain multiple rainfall cells. A rainfall pattern is characterized by five parameters: λ^{-1} [T], the mean waiting time between adjacent storm origins, β^{-1} [T], the mean waiting time for raincell origins after storm origin, ν [-], the mean number of raincells per storm, η^{-1} [T], the mean duration of raincell and χ^{-1} [L T⁻¹], the mean intensity of a raincell. The fitted parameter values that were obtained from the 10-year precipitation data (Fig.4.4) were then used to generate an hourly precipitation time series with a length of ten years with RainSim. The simulations were performed for the period of October–March, i.e. ten realizations with identical characteristics of winter rainfall at an hourly timestep with RainSim.

The hydrological system of a field between two streams has several analytical solutions that describe the elevation of the groundwater H in the cross section of such a field. We compare our numerical results with one of these equations to investigate how shallow groundwater dynamics affect surface runoff generation compared to ignoring these dynamics. For this purpose we use the transient solution of Kraijenhoff van de Leur (Kraijenhoff van de Leur, 1958).

$$H(x, t) = \frac{4Rj}{\pi S_y} \sum_{n=1,3,5..}^{\infty} \frac{1}{n^3} (1 - e^{-\frac{n^2 t}{j}}) \sin \frac{n\pi x}{L} \quad (4.13)$$

in which t [T] is time, x [L] is the distance from the stream ($0 < x < L$), R [$L T^{-1}$] is groundwater recharge, L [L] is the distance between the streams, and j [T] is the reservoir coefficient, that characterizes the speed of response of the system to groundwater recharge and discharge, i.e.

$$j = \frac{S_y L^2}{\pi^2 K_s D} \quad (4.14)$$

$$q_0(t) = -\frac{4RL}{\pi^2} \sum_{n=1,3,5..}^{\infty} \frac{1}{n^2} (1 - e^{-\frac{n^2 t}{j}}) \quad (4.15)$$

A small reservoir coefficient indicates a system where the groundwater level responds quickly to recharge, either due to its small dimensions or its high transmissivity. Equation (4.13) is applicable for scenarios of continuous rainfall on a system with an initially flat groundwater table. Because Eq. (4.13) is linear, superposition is allowed and the rise and recession of a groundwater table under a fluctuating rainfall regime can be calculated. As surface runoff under saturation excess conditions starts at the wettest point, it suffices here to look into the behaviour of H at the water divide $x = 0.5L$, as this is the place where the convexity will reach its maximum value in our domain, in other words, the place where ponding and surface runoff start. In that case, Eq. (4.13) reduces to

$$H_{x=0.5L}(t) = \frac{\pi^2 R j}{8 S_y} \left(1 - \frac{32}{\pi^3} \sum_{n=1,-3,5..}^{\infty} \frac{1}{n^3} e^{-\frac{n^2 t}{j}} \right). \quad (4.16)$$

4.5 Results and discussion

The two well-known bottle necks in the process of surface runoff generation are the vertical infiltration capacity and storage capacity of the unsaturated zone. Focussing on the latter, as infiltration excess runoff is rare in temperate lowland areas, we find that the soil water storage capacity is dynamic, also under wet conditions. Because the areas are well-drained, there is always a lateral groundwater flux. The ratio between the rainfall rate and this lateral flux determines when and how long surface runoff occurs. In order for the soil to fill up, this ratio needs to be pretty high, or the rainfall event needs to be very long. When the soil water storage capacity and depression storage capacity of (part of) the field have been exceeded, surface runoff can reach the ditches, e.g. events of day 35 and 127 in Fig. 4.5. After a rainfall event, relocated water infiltrates in the ponds. This infiltration of water initiates spatial variations in groundwater recharge. In subsequent rainfall events, the filling and spilling pattern of the surface depressions may be different than during the previous one, because of the altered spatial pattern of soil water storage capacity and changes in groundwater flow. This could be the case in the events between days 35 to 53 in Fig. 4.5, when the groundwater level fluctuated in the upper part of the soil and the dry periods between the rainfall events were short.

We explore the characteristics of the ponding and redistribution process in the next sections by quantifying the amount of surface runoff and the start of surface runoff

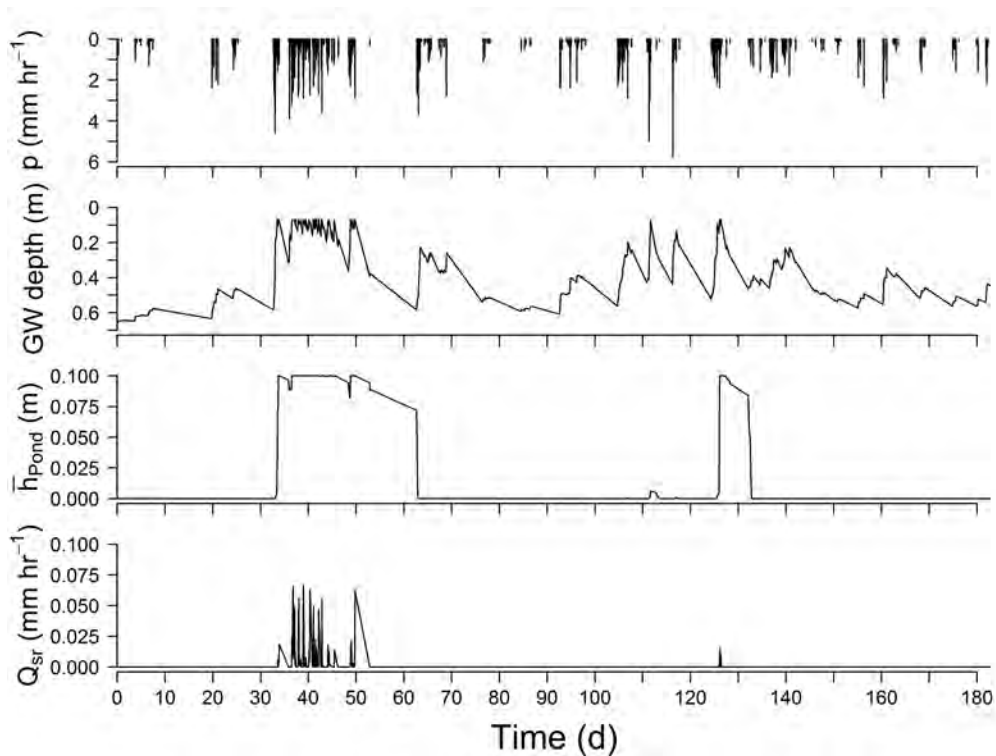


Figure 4.5: Time series of FAST-Runoff model on mesotopography type 2: precipitation realization time series (top), groundwater level below soil surface, water level in meso-depression, surface runoff rate

events. The results of the numerical experiments are organized around the three research questions posed in the introduction: 1) how is surface runoff development affected by the presence of a shallow groundwater table?, 2) how does microtopography affect surface runoff development under saturation excess conditions?, and 3) how does mesotopography affect surface runoff development under saturation excess conditions?

4.5.1 How is surface runoff development affected by the presence of a shallow groundwater table?

The effect of adding a thin unsaturated zone in hydrostatic equilibrium to a simple groundwater problem is illustrated in Fig. 4.6, in which the lateral groundwater flow towards the ditches is plotted as a function of the convexity of the water table for four cases, combining two sets of Van Genuchten parameters and two values of saturated hydraulic conductivity. These numerical solutions can be compared to the analytical solutions of Kraijenhoff van de Leur for the ditch discharge and groundwater level in the middle of the field (Eq. 4.15 and Eq. 4.16) with both K_s values. The rainfall in Fig. 4.6 is applied in pulses of 2 h during each day, such that the groundwater level rises during rainfall events and decreases in the dry time inbetween. In flat groundwater dominated

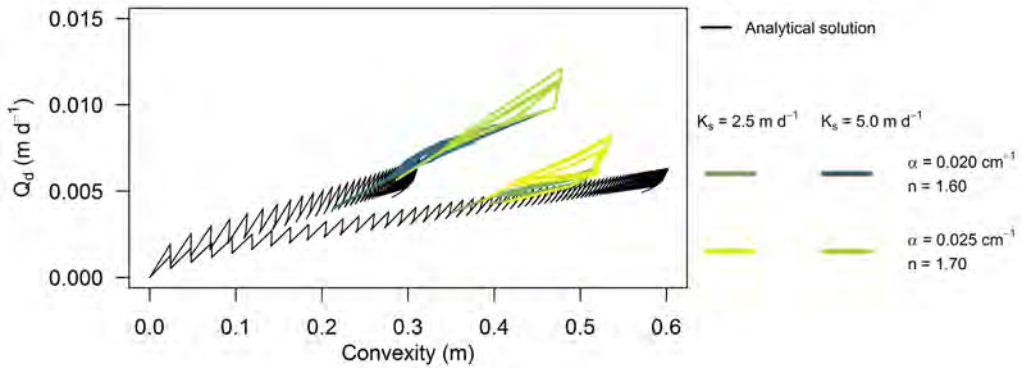


Figure 4.6: Discharge of field to ditch as a function of convexity of the groundwater level in the middle of the field. In black, the result of the analytical solution for discharge of Eq. (4.15) and convexity of Eq. (4.16). The rainfall is applied in pulse of 2 h during each day of the simulation.

areas, the shape of the groundwater mound is distinctly different during recharge than during recession (Kraijenhoff van de Leur, 1958; van der Ploeg et al., 2012). Both the numerical solution and the analytical equation account for this difference. Therefore, in Fig. 4.6, the value for Q_d for a designated value of the convexity is higher during recharge than during drainage of the groundwater.

Accounting for the storage of water in the unsaturated zone results in a slower recession of the groundwater compared to an analytical solution and in a steeper increase of the groundwater level during a rainfall event. The more curved the $h(V)$ function of the soil is (see Fig. 4.2, i.e. when α and n increase), the steeper the increase and the slower the recession are, i.e. the shape of the Q_d -convexity loop changes. If the convexity of the groundwater level in Fig. 4.6 is more than 0.45 m, surface runoff is usually generated.

The differences between our numerical solution and the analytic solution of Eq. 4.16 can be understood from the fact that in our numerical simulations the values of specific yield S_y and the groundwater recharge rate R become functions of the elevation of the groundwater level, because precipitation is added to the total volume of water in the soil column and the partitioning between unsaturated and saturated zone is based on function $h(V)$. As such, both the elevation and the shape of the groundwater mound change with respect to the shape that results from the analytical Kraijenhoff van de Leur solution (Eq. 4.16). As a result, the analytical solution underestimates the amount of surface runoff generated during the precipitation events.

In Fig. 4.7 the fraction of rainfall that leaves the field as surface runoff is plotted for the four designated combinations of soil characteristics of Fig. 4.6 for pulse precipitation events of varying magnitude and duration. The ratio between rainfall intensity per day and saturated hydraulic conductivity is the main cause of difference in the surface runoff generation process. Subtle differences are caused by the fact that the two retention profiles have different soil water storage capacities at the beginning of the

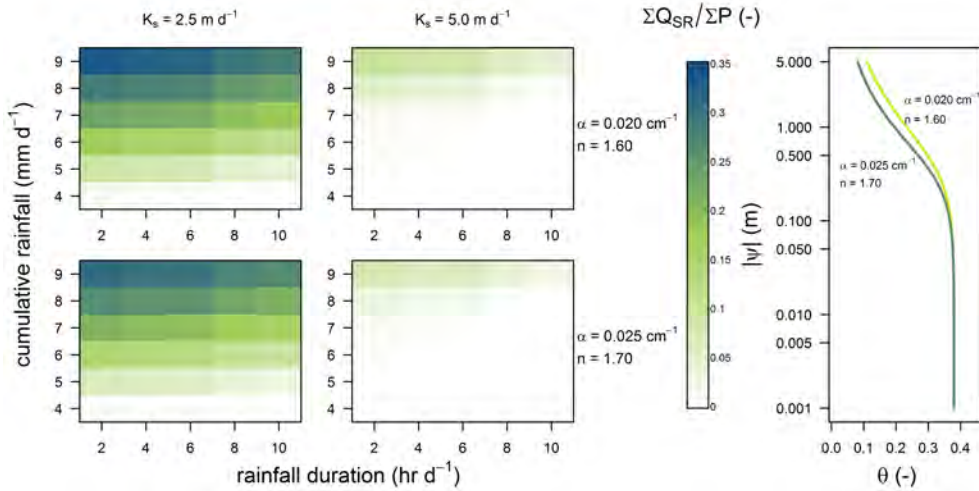


Figure 4.7: Fraction of input precipitation ΣP that is converted into surface runoff ΣQ_{SR} in a schematized flat field during a ten day period with daily rainfall (a). Each panel shows results for varying cumulative rainfall (y-axis) and rainfall duration (x-axis) for four combinations of saturated conductivity (K_s) and soil hydraulic parameters (α and n). The soil moisture profiles associated with these soil hydraulic parameters are illustrated in (b).

simulations. The shape of the groundwater mound, and therefore the lateral groundwater flux, is affected by the unsaturated zone parameters, but with the application of large cumulative amounts of rainfall in regular time intervals, this results in just a small spatial difference of the saturated area. Even under these wet circumstances a higher hourly rainfall intensity leads to higher volumes of surface runoff: the area of saturated surface remains the same, but because the difference between rainfall intensity and lateral groundwater flux is larger, more water runs off from these saturated areas.

4.5.2 How does microtopography affect surface runoff development under saturation excess conditions?

For various scenarios of surface microtopography and soil hydraulic parameters (Table 4.1), we analyzed the arrival of surface runoff at the ditches surrounding the fields. We consider a period of 10 days with continuous rainfall, filling up the soil and the surface from a certain initial condition. Because of the continuous rainfall, the infiltration rate is much higher than the lateral groundwater flux, and we assume the latter to be insignificant in comparison.

Looking at the surface runoff curve differences of the topographies under impermeable conditions (the dotted lines in Fig. 4.8), the difference between topographies is that the microchannel structures have a very fast and steep increase of runoff rate as hydrological connectivity is established rather quickly throughout the field. The depression structure has a longer startup phase as well as a less steep increase of surface

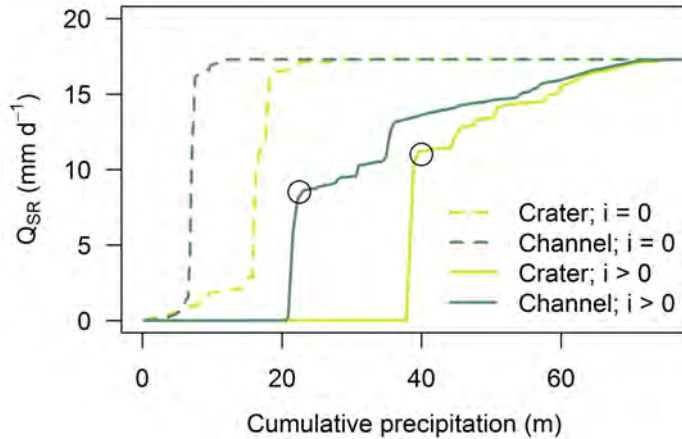


Figure 4.8: Surface runoff rates as a function of cumulative precipitation for two different microtopography structures with infiltration rate $i > 0$. For illustration purposes the curves that result from simulating surface runoff on an impermeable surface ($i = 0$) are plotted as well.

runoff rate afterwards. Alternatively, when surface runoff develops after a part of the field has been saturated, the arrival of surface runoff at the ditches is delayed by infiltration of water and storage in the surface topography. Again, both topography types have a very steep first part of the surface runoff rate, but the second part of the curves is stretched and extended. Since runoff is generated first at the water divide of the field, the relative contributing area of spillpoints discharging water to the ditch is immediately large.

In the realizations presented here, the second part of the runoff curve of the channel topography is longer than that of the depression topography. This seems somewhat counter-intuitive as one would expect a channel topography to conduct water faster to the field boundaries than a topography containing deeper depressions. However, the distances over which water is transported over the soil surface are determined by the correlation length of the distribution used for simulating the microtopographies. These distances are therefore similar for both the channel and the depression topography and rather short when compared to the distances over which the depth of the groundwater mound changes. This means that the saturation of the soil is more important than the routing of water over the field. Therefore, the surface runoff curves will reach their maximum value more or less at the same moment for fields that have similar initial soil water storage capacity and depression storage capacity.

The curves have a clear breakpoint between the aforementioned first and second part, where the slope of the surface runoff curve changes from large to small gradient. This **locus** is defined by the critical precipitation amount needed to establish a complete flow path from saturated area towards the ditch and the surface runoff rate associated with it. When the lateral groundwater flux is very small compared to the vertical

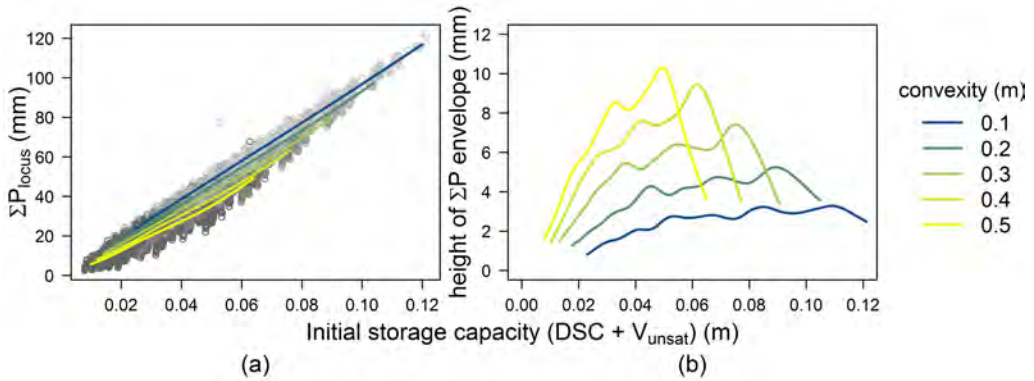


Figure 4.9: Responses defining locus of surface runoff curves of microtopographies with 1) varying statistics, 2) spatial organisation, 3) soil type and 4) initial groundwater conditions. In the left panel the cumulative precipitation of the locus plotted as a function of the initial water storage capacity of soil and microtopography. The lines are fitted LOESS curves through the sets of points with the same initial convexity of the water table. In the right panel the height of the envelope surrounding each of these sets of datapoints is plotted as a function of initial water storage capacity of soil and microtopography.

infiltration flux, the surface runoff rate is linearly related to the size of the saturated area generating surface runoff. Therefore, the locus represents a critical threshold in the process of surface runoff generation and we will use it to quantify the effect of initial conditions and microtopography on surface runoff generation.

In Fig. 4.9a the cumulative precipitation amount associated with the loci is plotted as function of the initial soil and surface water storage capacity of the domain. The amount of precipitation of the locus is directly and linearly related to the initial storage capacity of both the soil and the surface and therefore increases when initially the groundwater is located deeper below the soil surface, when the hydrostatic equilibrium soil moisture profile has a larger soil water storage capacity, and when the depression storage capacity (DSC) of the microrelief is larger. The variability of points in Fig. 4.9a can be explained by the convexity of the initial groundwater level. The larger the convexity, the larger the spatial variation of soil water storage is. Thus, the initiation of ponding has a larger spatial variation as it depends on the erratic presence of lower parts of depressions at the locations with the shallowest groundwater. Accordingly, the height of the envelope surrounding each of set of datapoints sharing the same initial convexity increases with a larger convexity (Fig. 4.9b).

In Fig. 4.10 the initial depth of the groundwater table in the middle of the field is used for the grouping of points, because it has more explanatory power than the convexity alone for the variability of Q_{SR} of the loci. When a surface runoff flow route is established towards the ditch or stream, the associated surface runoff rate is determined by the extent of the saturated area in the field. The sooner saturation is reached in a certain part of the field, the faster ponding water will start to contribute to the filling of

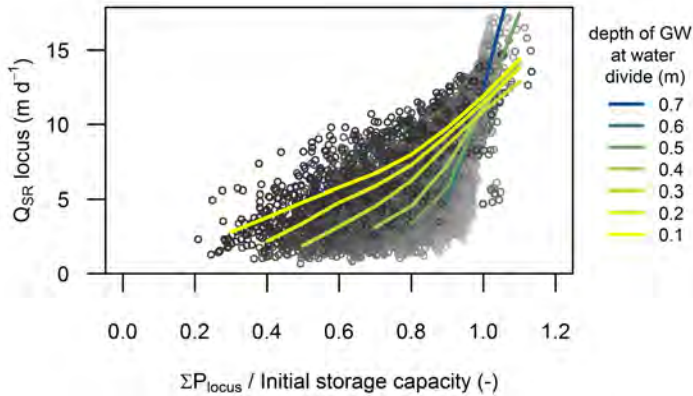


Figure 4.10: Surface runoff rate of the locus plotted as a function of the ratio between cumulative precipitation defining the locus and the initial water storage capacity of soil and microtopography. The lines are fitted LOESS curves through the sets of points with the same initial depth of the water table in the middle of the field.

the unsaturated zone under adjacent depressions and the larger the contributing area will be when a full flow route is established. A smaller initial depth of the groundwater table in the middle of the field therefore results in a large Q_{SR} when the average initial storage capacity is the same.

Under these circumstances of saturation excess, Gaussian microtopography, regardless of the spatial organization, has its main effect in providing extra depression storage capacity. For a topography with the same standard deviation, this will be lower in a channel topography than in a random or a crater topography.

4.5.3 How does mesotopography affect surface runoff development under saturation excess conditions?

Of the 1080 simulations that were performed on field cross sections with mesotopographic elements (Fig. 4.3), 23 % of the simulations resulted in surface runoff reaching the ditches during ponding conditions. In addition, another 17 % of the simulations experienced ponding conditions, but without the depressions spilling water towards the ditches. The majority of these events, 60 % of the ponding events, occurred on the fields with the lowest saturated conductivity value of 2.5 m d^{-1} .

Similar to the field observations (chapter 2 and 4), the stochastic forcing of our simulations resulted in a limited number of surface runoff events per season, most of which occurred in the months of November, January, and February, respectively days 32–62 and 117–148 of the simulations as in the timeseries of Fig. 4.5. The number of surface runoff events per season is related to the cumulative amount of precipitation (not shown). The more surface runoff events, the higher the cumulative amount of surface runoff. However, there is quite some variation around this trend (Fig. 4.11). The largest

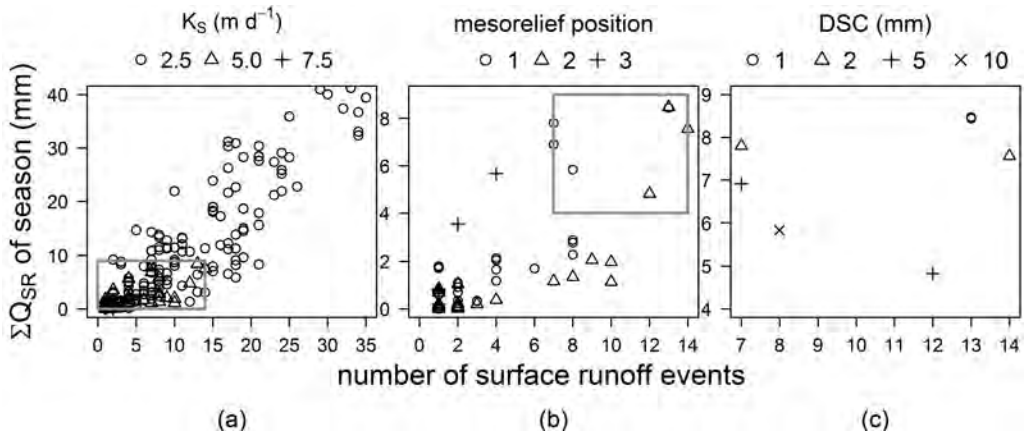





Figure 4.11: Cumulative amount of surface runoff per season vs number of surface runoff events per season. Symbols indicating saturated conductivity (left panel), position of depression (middle panel), and depression storage capacity (right panel).

number of surface runoff events occurs of course on fields with the smallest saturated hydraulic conductivity (Fig. 4.11a). However, within a set of fields with the same soil type, the position of the depressions is responsible for the varying number of events (Fig. 4.11b), whereas the area of the depressions (i.e. the resulting depression storage capacity) determines the amount of surface runoff (Fig. 4.11c).

In Fig. 4.12 the development of cumulative precipitation of two RainSim simulations, with identical statistical structure, is plotted with the cumulative surface runoff of the twelve mesorelief types (with the same soil type and initial conditions). The total cumulative amount of surface runoff during the simulated seasons was always largest for fields with depressions located in the center of the field and always lowest for fields with depressions located at the most outward position (position 3). Ponding and surface runoff are generated in the centre of the fields, over an area that can be larger than the area of the ponds. The capacity of the field to intercept all generated surface

Table 4.2: Cumulative surface runoff during simulated season (precipitation realizations 5 and 6) for every type and size of mesorelief

DSC						
	PR 5	PR 6	PR 5	PR 6	PR 5	PR 6
1 mm	9.64	31.2	8.35	30.4	5.14	26.3
2 mm	9.12	30.3	5.90	28.3	3.14	21.7
5 mm	8.24	27.4	3.12	23.9	0.00	11.6
10 mm	7.06	22.8	1.37	19.0	0.00	1.34

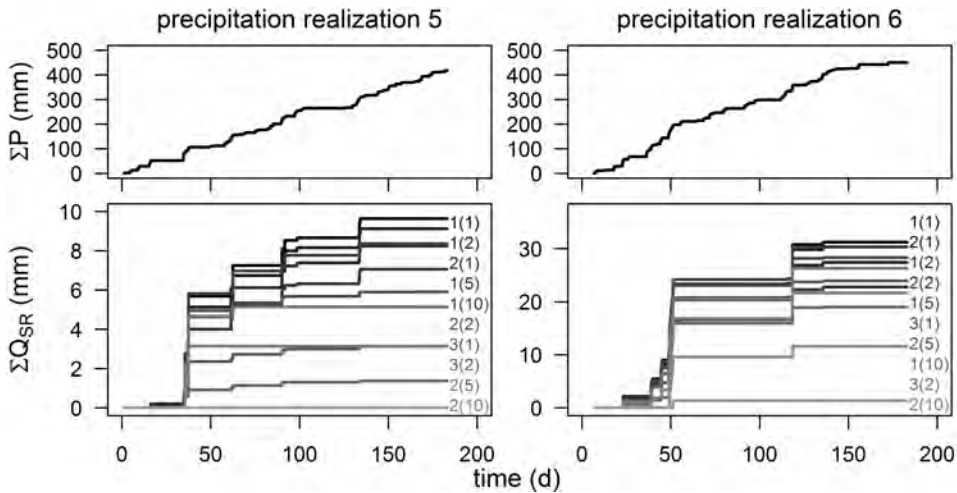


Figure 4.12: Cumulative precipitation and cumulative surface runoff development for two rainfall realizations. The colors of the lower panel indicate the surface runoff responses of the 12 mesotopographies. The seasonal cumulative amounts are presented in Table 4.2.

runoff and allow it to re-infiltrate after a rainfall event increases when ponds are located closer to the ditches. Therefore, surface runoff volumes of the fields with depressions located at position 3 differ more for the four designated depression sizes than the volumes of the fields with depressions located at position 1. When the depressions are located at the intermediate position 2, the buffering capacity will be completely used, but surface runoff may also be generated outside the area contributing to the depressions when rainfall events have short lag times and high totals. Therefore, the ranking of the total volumes changes per rainfall realization (Fig. 4.12 and Table 4.2).

The groundwater levels during a wet period generating surface runoff are plotted in Fig. 4.13 for one realization of each of the mesotopography positions. Groundwater elevation and the associated groundwater gradient are plotted for five timesteps of three simulations.

In all simulations, the groundwater depth in the middle of the field is very small, though it actually only touches the soil surface when the depression is located in the middle of the field (position 1, upper row of Fig. 4.13). As expected from theory, the gradient of the groundwater table is smallest in the middle of the field and increases towards the ditches. When the groundwater touches the soil surface of the depressions, the gradient can be subject to very sharp peaks, because of the very small values of specific yield under these circumstances. The model performance remained stable, though, and these fluctuations did not propagate or lead to large numerical errors. The presence of mesodepressions decreases the gradient of the groundwater table between them during the rainfall events. The change in gradient of the phreatic surface effectively causes a temporary reduction of groundwater flow towards the ditches during and shortly after long rainfall events. The profiles of the gradient of the phreatic surface

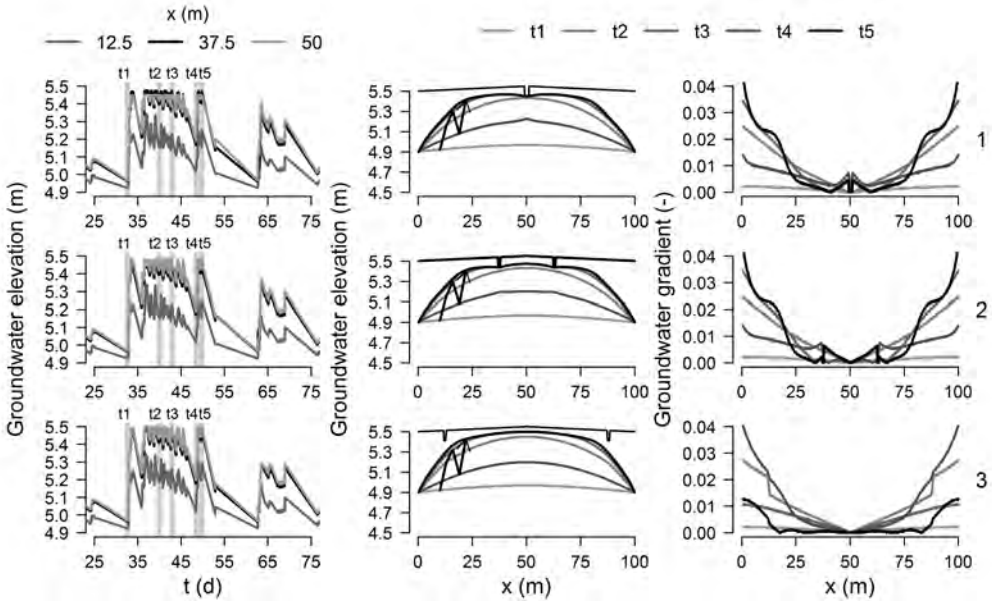


Figure 4.13: Groundwater level characteristics of three cross sections with different position of mesotopography. The selected time period is the 50 days from precipitation realization 2 (Fig. 4.5) where surface runoff occurred. Time series of simulated groundwater levels at three positions in the cross sections (left column). Groundwater profile in the cross sections at the five designated timesteps (middle column). The arrow indicates the time sequence of the five profiles. Absolute gradient of the phreatic surface in the cross sections at the five designated timesteps (right column). The panels are ordered by position of the depressions (rows).

in Fig. 4.13 of t3 and t5 show that this effect is stronger when the depressions are located closer to the ditches and the depressions have a larger area (i.e. have a higher DSC). We did not observe strong effects of delayed infiltration of ponded water on subsequent ponding or enhancing of surface runoff events over periods larger than a couple of days. Even with the lowest value for saturated conductivity (2.5 m/d), the groundwater level would drop back to its initial level during drier weeks and the build-up of surface runoff had to start all over again.

4.6 General discussion and concluding remarks

The two decisive factors in the surface runoff process are infiltration capacity and storage capacity. These factors each have characteristic and different time scales that determine whether a designated rainfall intensity as well as duration will generate redistribution of water at the soil surface will occur. Infiltration capacity has a time scale similar to that of rainfall events: ponding and surface runoff occur when the infiltration capacity is exceeded. Storage capacity has a much larger time scale: filling up can occur along the timespan of several rainfall events, especially when groundwater drainage is slow.

The FAST-Runoff model employed in this study contains crucial characteristics

and feedbacks of the surface runoff process in shallow groundwater systems with a heterogeneous soil surface. The hydrostatic equilibrium condition of the unsaturated zone allows for an analytical relationship between groundwater depth and total water stored in the soil and soil moisture content at the soil surface and hence provides feedbacks through sorptivity and specific yield under shallow groundwater table conditions. The sorptivity feedback did not affect the results of the analyses presented in this study, because the rainfall intensities in the simulations were not higher than the infiltration capacity. The specific yield feedback was well visible in the increased non-linearity of the groundwater table increase and decrease (Fig. 4.6).

The first storage threshold for the start of ponding and surface runoff is the storage capacity of the unsaturated zone. Because of the assumption of hydrostatic equilibrium, it is controlled by the depth of the groundwater table and soil characteristics in the analyses presented here. Microtopography affected surface runoff development under saturation excess conditions by providing a second threshold, namely the depression storage capacity. The spatial structure of the microtopography only affected surface runoff generation by altering the depression storage capacity of a furthermore statistically identical surface. There was no effect of faster routing of water towards the ditches. The timing of surface runoff reaching the ditches under these conditions depended on initial storage capacity of soil and topography and the spatial variation of both. This spatial variation was mainly explained by the initial convexity of the groundwater mound. The magnitude of the surface runoff rate that occurred when a flow route towards the ditches was established, was determined by the saturated area. The rate was therefore largest when the initial groundwater level in some part of the field was so shallow that saturation was reached quickly and the microtopography could transport water to unsaturated parts of the field early in the simulations.

Mesotopography affects surface runoff development under saturation excess conditions, by actually rerouting ponding water over longer distances. Excess water is rerouted to a location in the field that is not necessarily as close to saturation as the location where it originated from. The re-infiltration of water in mesotopographic depressions decreased the gradient of the groundwater table over a large part of each field, thereby decreasing groundwater flow. This effect increased when the mesotopographic depressions were located closer to the ditches, because the area over which the groundwater table was levelled increased.

The difference can be explained by looking at the hydrology of nested systems. When a nested system wets up, the amount of water stored in the catchment increases, the elevated groundwater level activates lower order streams and the drainage efficiency of the catchment increases (de Vries, 1994, 1995). When considering a single agricultural field, the rise of the groundwater level activates the spatially distributed network of rills and mesodepressions. The drainage efficiency increases, provided that there is a connected pathway between the small water body and the catchment outlet (van der Ploeg et al., 2012). In our fields, the surface runoff drainage efficiency increased most

when the mesodepressions were present in the middle of the field. The schematic setup of the cross sections allowed extra surface runoff to flow directly towards the ditches. The gradient of the groundwater table was hardly affected. Mesodepressions that were located closer to the ditches disconnected the pathway between area of surface runoff generation and outlet (the ditches) and therefore the drainage efficiency increased less. This in turn resulted in a wetter system. The gradient of the groundwater table was reduced over a larger area.

Because of the nested activation, the effect of the specific structure of rainfall series, in the sense of the size of events and the lag time between the arrival of storms and raincells, was large. It led to differences in total volume of surface runoff generated per season of one order of magnitude for statistically identical rainfall timeseries, which is in agreement with the general variable occurrence of surface runoff events in flat, well-drained, wet catchments.

Acknowledgements

The authors acknowledge Alterra Wageningen UR (Project 5232870-06) and the Dutch ministry of Agriculture, Nature, and Food quality (Project BO-05-004-KRW) for financing this study. SvdZ appreciated support of the DFG-NWO funded network NUPUS.

Chapter 5

Spatiotemporal variability of saturation excess surface runoff in flat fields due to interactions between meso- and microtopography

Abstract

Surface runoff is the fastest route from field to stream and the main transport route for sediment and adsorbed contaminants, and as such an important cause of surface water contamination in agricultural areas. The goals of the study were to explain differences in measured surface runoff volumes and nutrient loads of surface runoff between fields on the basis of characteristics of their meso- and microtopography, and to investigate the representativeness of plot scale measurements for the surface runoff behaviour of the whole field. The surface runoff measurements were performed at grassland, an arable field and a horticultural field. We combined these measurements with detailed topographic data at meso- and microscale. The nutrient concentrations measured in the surface runoff were high, especially on the grassland. The differences in nutrient loads were caused both by differences in surface runoff volume and in nutrient concentrations in the soils of the fields. However, the overall estimated yearly nutrient load from surface runoff was lower than expected from similar studies. The effect that microtopography has on flow route shapes in flat fields can be quantified with metrics from surface runoff curves. We performed simulations with the FAST-Runoff model for coupled instantaneous redistribution of water over a heterogeneous surface and infiltration and 2D groundwater flow. The simulations showed that ponding evolved unevenly throughout the fields, suggesting different times of activation of the flow routes within the fields. Unfortunately, this spatial variability could not be linked to the full meso- and microtopographies of the fields, because the non-linearities introduced by the dynamic specific yield, could only be treated at very small timesteps resulting in very long computation times.

5.1 Introduction

Quantification of the various routes that water and contaminants follow through a catchment is the basis for understanding dynamics in discharge and stream water quality (Hendriks, 2010; van der Velde et al., 2012). Surface runoff is the fastest route from field to stream and the main transport route for sediment and adsorbed contaminants, such as pesticides and phosphorus (Turtola and Jaakkola, 1995; Pärn et al., 2012). As such, it is an important cause of surface water contamination in rural areas, and a major concern for compliance with water quality regulations such as those incorporated in the EU Water Framework Directive. As slope angle and heavy rainfall are the driving factors of infiltration excess surface runoff, its impact is obviously less in flat lowlands and temperate climate zones. When such lowlands are also dominated by permeable soils with good natural or artificial drainage, saturation excess surface runoff is relatively rare. Only during wet winter periods drainage is not sufficient and saturation excess surface runoff is generated (Church and Woo, 1999). Both shallow groundwater tables and perched groundwater tables cause stagnation of water at the soil surface (Loague et al., 2010). The agricultural areas in The Netherlands most vulnerable to surface runoff are peat grasslands, where groundwater levels are kept close to the

surface (less than 60 cm below soil surface), riverine heavy clay grasslands with low permeability and drainage by superficial trenches (less than 40 cm below soil surface), and sandy or clay soils with topsoil or subsoil compaction caused by treading, overstress due to large wheel loads of agricultural machinery, and tillage (van den Akker, 2004). Although the frequency of surface runoff incidents is low in flat lowlands, it is still an important nutrient source to lowland streams, due to high nutrient concentrations. van Beek et al. (2009) estimated yearly surface runoff nutrient loads from grazed grassland in The Netherlands between 2.25 and 10.95 kg ha⁻¹ total nitrogen (N) and between 0.75 and 1.76 kg ha⁻¹ total phosphorus (P). The variation in these values depends mainly on the denitrification capacity of the soil for N and on the sorption characteristics of the soil for P, but also on the importance of various hydrological pathways (i.e. the ratios between surface runoff, artificial drainage, shallow groundwater flow, and deep groundwater flows) (van Beek et al., 2009). These loads are comparable to the median ranges of 1.5 to 15 kg ha⁻¹ for nitrogen and 0.3 to 1.9 kg ha⁻¹ for phosphorus measured in catchments around the world (Pärn et al., 2012). Incidental surface runoff can have a severe impact on surface water quality (Withers et al., 2003). van der Salm et al. (2012) measured up to 56 % of yearly P loss in one event. The large variation in reported surface runoff nutrient loads can be explained by the horizontal and vertical spatial variation of nutrients in the top soil, and by the incidental and spatially variable nature of surface runoff in temperate lowland catchments.

Its incidental and spatially variable nature makes measuring surface runoff a challenging task. Surface runoff to streams in a temperate lowland catchment is always measured at shorter lengths of water courses, and usually at locations where surface runoff is known to occur, thus leading to biased results. Therefore, such measurements cannot be used directly for estimating the contribution of surface runoff to the water balance of a catchment, and additional characterization of differences in surface runoff generation within and between fields is required. Also, modelling studies that quantify nutrient loads for larger scales (e.g. Wolf et al. (2003); Oenema et al. (2005)) tend to overlook the dynamics and heterogeneity of surface runoff within and between fields. Information on these dynamics and heterogeneity is not only needed for a better calculation of the contribution of surface runoff to the water balance, but also for the selection of measures to mitigate nutrient loads to surface waters. The exact location and timing of surface runoff spilling to the ditches or streams determine the positioning, length of application, and thereby the costs of these measures. In flat fields with saturation excess surface runoff, groundwater flow and the routing of water through small-scale field topography are determinant factors causing spatial and temporal variability of surface runoff. This study therefore focuses on surface runoff dynamics and location related to field surface topography and groundwater flow.

The goals of the study are 1) to explain differences in measured surface runoff volumes and nutrient loads of surface runoff between fields by characteristics of their meso- and microtopography, and 2) to investigate whether the plot scale measurements

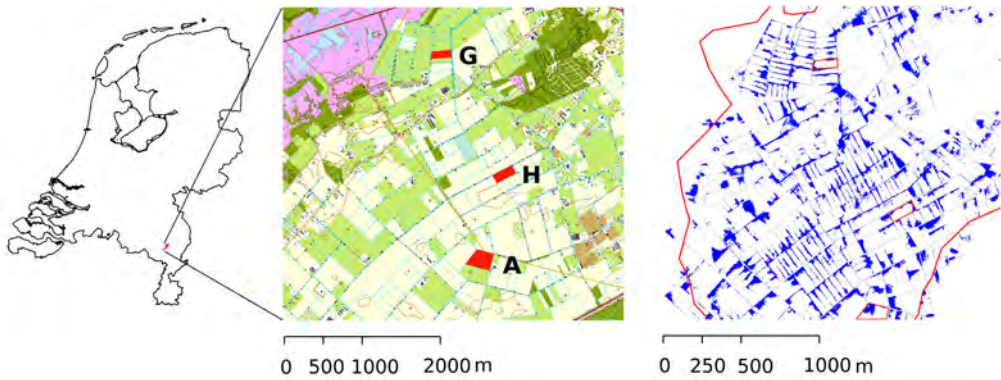


Figure 5.1: Location of the P-pilot area in The Netherlands (left), the experimental fields A, G, and H (middle), and spatial distribution of the elevation values below the 15th percentile within these fields (right). Weather data were obtained from a station 12 km south of field A, outside scope of middle panel.

we performed are representative for the surface runoff behaviour of the whole field, with simulations. In this study we present measured data of surface runoff volumes and concentrations, and surface topography of three flat agricultural fields. To analyze ponding, subsequent water redistribution and surface runoff at these fields, we use a model that simulates groundwater flow, infiltration and water flow over a heterogeneous surface. We investigate the key factors controlling the different surface runoff responses of the fields and assess the representativeness of the surface runoff measurement locations for the surface runoff response of the entire fields.

5.2 Material and methods

5.2.1 Field sites: selection and description

The measurements were carried out in a region with sandy soils in the south eastern part of The Netherlands (Fig. 5.1). The intensive agriculture in this region is a source of phosphate pollution of surface waters and water quality standards are not met. Phosphate loads will not decrease in the near future, because the large past and smaller present manure surplus have resulted in a high P concentration of the soil. The implementation of stricter regulation alone is not enough to improve surface water quality and other measures are required. A “P-pilot” area was designated in 2005 to identify the various diffuse sources of phosphate and to evaluate the effect of practical mitigation measures (Noij et al., 2007, 2009).

As discussed previously, the local surface topography is an important driver in surface runoff development in flat areas. Ponding of water is likely to occur in patches of a field that are low compared to the average elevation of the field. The potential of surface runoff to actually reach a ditch or stream increases when these low patches are located at small distances from the ditches and streams. In order to assess the potential

for surface runoff we analyzed the local topography of all agricultural fields in the pilot area. We overlaid a digital elevation model (DEM) with grid cell size 5 m from the Dutch national digital elevation database (AHN) with a map featuring all water courses (ditches and trenches) in the area. For every field within the pilot area the surface elevation distribution was determined and the location of patches with an elevation below the 15th percentile value was determined (right panel in Fig. 5.1). We estimated surface runoff risk R_f (-), by calculating the fraction of the lowest 15 % that was located within 5 m from the ditches and trenches bordering the field (eq. (5.1)):

$$R_f = A_B/A_T \quad (5.1)$$

where A_B is the area of low patches located within 5 m distance from ditch or water course (m²), and A_T is the total area of patches in the field (m²), i.e. being part of the lowest 15 % of the field area. We estimated the cumulative surface runoff impact for the whole field R_I (m²) by accounting for field size (eq. (5.2)):

$$R_I = R_f \times A_F \quad (5.2)$$

where A_F is the total field area (m²).

The three fields for the surface runoff measurements ranked in the highest 20 % with regard to surface runoff impact R_I and featured different land uses, as this affects the microtopography of the field surface (Massop et al., 2012). We installed the measurement gutters at the lower patches close to the ditches, where surface runoff was expected (red lines in Fig. 5.2). Such patches could be distinguished from the field DEMs with a resolution of 5×5 m, even though the elevation ranges were small.

Field A is an arable field on a sandy soil, gleyic podzol in the FAO classification (FAO, 2008). Some thin compacted layers were found in the soil profile at 0.35 to 0.5 m depth. On the field, maize was grown during the monitoring period, except for 2008, when chicory was grown. The field was always harvested in the beginning of autumn and left with an compulsory winter crop until March or April when tillage activities for the maize started. Field G is a grassland on a peat soil with a sandy toplayer, terric histosol in the FAO classification. The upper part of the soil (0–0.35 m) has been leveled up with sand. Field H is a horticultural field on a sandy soil, umbric gleysol in the FAO classification system. Some thin compacted layers were observed in the soil profile from

Table 5.1: Estimated surface runoff risk and impact of experimental fields within the pilot area. Low ranking value indicates large surface runoff risk in the total pilot area of 857 fields.

Field	Land use	Area (ha)	R_f (-)	Ranking	R_I (m ²)	Ranking
A	arable rotation	4.7	0.20	377	937	60
G	grassland	1.9	0.37	203	687	129
H	open field horticulture	2.4	0.32	246	769	94

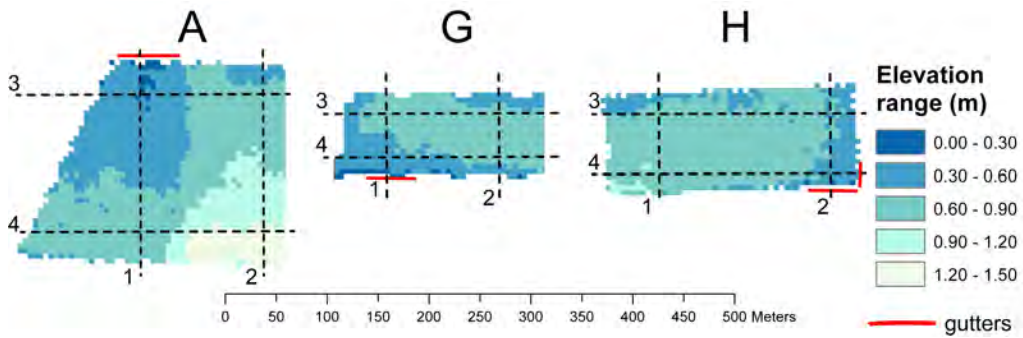


Figure 5.2: Digital elevation models for the mesotopography of the three fields A obtained from the Dutch Digital Elevation database (AHN). The grid cell size is 5 m. Red bars indicate the location where the gutters and measurement devices were installed. Dotted lines indicate the position of the cross sections used in the model simulations of Sec. 5.3.3. All fields were surrounded by ditches.

0.6 m depth down. The field was under crop rotation from 2007 to 2011 with maize, French bean, carrot, winter wheat, and sugar beet. The field was harvested between August (winter wheat) and November (sugar beet), depending on the crop. After harvest, the field was left bare in winter until main tillage activities for the next season in March or April, except in the winter of 2009–2010, when winter wheat was grown. At all fields, ground water levels in winter may reach the upper 0.2 m of the soil. The water level in the ditches surrounding the fields was maintained by the water board in winter. The pursued ditch levels were 0.8 m below the average soil surface around fields A and H, and 0.5 m below soil surface around field G. At site G, the ditch flooded the field a couple of times during wet periods.

Hourly precipitation data were obtained from the Royal Dutch Meteorological Institute (KNMI). The nearest weather station, no 377 at Ell, is located 12 km south of field A (Fig. 5.1).

5.2.2 Data acquisition

Surface topography

Digital Elevation Models of the fields were constructed by interpolation of point data from the Dutch Digital Elevation database (AHN) with Inverse Distance Weighing to a grid with a cell size of 0.5 m (Fig.5.6). At the three sites, six 1 m² pinmeter measurements characterized the microtopography with a density of 400 measurement points per m². The measurements were performed in January 2009, at least three months after harvest at sites H and A. At the time of measuring both the arable and horticultural field were bare, while site G was covered with grass.

Surface runoff measurements

At each field, two 10 m PVC rain gutters were installed in the top soil with the rim at soil surface level (Fig. 5.3). In order to prevent surface runoff by-passing below the gutter the

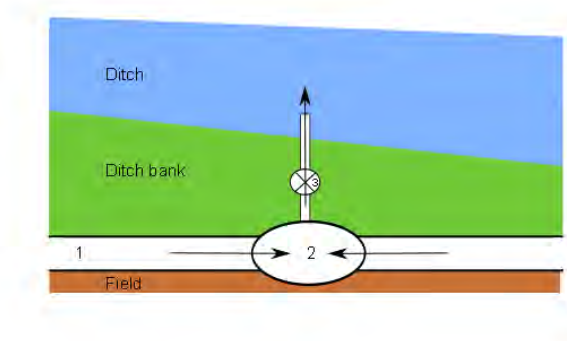


Figure 5.3: Ground plan of the installation to measure surface runoff. Water from the field is collected in the gutter (1) and transported towards the reservoir (2). It passes a flow meter (3) before discharging into the ditch.

gap between rim and soil surface was filled with bentonite clay. Between the two gutters a 1 m³ plastic tank was dug into the soil. The tank had a lid with two holes to provide access for measuring the water level and for stirring, sampling and pumping. A small ridge between field and tank forced surface runoff to discharge towards one of the gutters. The gutters were filled with coarse gravel to minimize water storage, and connected to the tank with a pipe. A second pipe provided a spillpoint from the tank to the ditch. The discharge volumes were measured with a discharge meter that was installed between the pipe outlet and the tank. A water pressure sensor was installed at the bottom of the tank and connected to a mobile phone to send a warning in case of a surface runoff incident. In winter, the sites were visited weekly. In case a surface runoff event had occurred, the tank was stirred by pumping and a water sample was taken for laboratory analysis. At each visit, the volumes of the discharge meters were read and the water level in the tanks was determined, after which the water was pumped out of the tanks.

Water and soil quality measurements

The effect of soil P content on runoff P concentration and loads is often assessed with P indices based on soil P measurements (e.g. Sharpley et al. (2003); Hart and Cornish (2012); Ouyang et al. (2012); Poethig et al. (2010)). To date, P surface runoff risk has not been quantified in The Netherlands. In terms of groundwater loads, P load risk from fields to surface waters is generally quantified in terms of the P saturation degree, PSD (-). The PSD concept has been developed by van der Zee et al. (1990), to quantify the loading of soil with phosphate. It is indicative of the amount of inorganic P in soil that may readily leach. Expressed as a percentage, the P saturation degree is calculated according to

$$PSD = \frac{P_{ox}}{0.5(Al_{ox} + Fe_{ox})} 100\% \quad (5.3)$$

Where P_{ox} , Al_{ox} and Fe_{ox} are the amounts of phosphorus, aluminum and iron extracted from dry soil with acid ammonium oxalate (in mol kg⁻¹). According to Poethig et al. (2010), PSD has a strong correlation with water soluble P for a wide range of different soils and is therefore a quite uniform indicator for water soluble P loss risks. As sediment transport hardly occurred in our study, we can also use this indicator for establishing the effect of top soil P content on surface P load risks in our study. Two concentric strata within the potential catchments of the gutters were selected to take soil samples of the topsoil. Within each zone three mixed samples of 10 random borings, taken at 10 cm (field G) and 30 cm (field A and H) below the soil surface, were analyzed for the N and P content of the topsoil. Sampling dates were 25-3-2010 at H and A, before fertilizer application, and 22-11-2010 at G, after the growing season. Soil samples were dried (40 °C), sieved (2 mm) and extracted with acid ammonium oxalate to determine aluminium (Al_{ox}), iron (Fe_{ox}) and phosphorus (P_{ox} , all in mol kg⁻¹) with ICP-AES (Novozamsky et al., 1986). The degree of phosphorus saturation (PSD) was computed according to Eq. (5.3).

Current soil fertility indices are based on selective extractability of P. The extractability of P from our fields was characterized using 2 methods denoted as P_w (mg P₂O₅ l⁻¹ dry soil) (fields A, H) and P-Al (mg P₂O₅ 100 g⁻¹ dry soil) (field G). The first procedure is a mild extraction (water) commonly used in agriculture in The Netherlands to determine the content of readily available P in soil samples (Sissingh, 1971). The second procedure involves the extraction of P with ammonium lactate at pH 3.75 (Egner et al., 1960). P_w and P-Al were measured with a segmented flow analyzer (SFA, ISO/TS-14256-1: 2003). Mineral nitrogen, N_{min} (NH₄-N + NO₃-N + NO₂-N in mg kg⁻¹ dry soil), was determined with SFA in a 1M KCl extract ($s/l = 1 : 2.5$). Water samples were mixed thoroughly and then split into three subsamples. The first unfiltered subsample was analyzed for total N (N_t) and P (P_t) with the SFA after persulphate-borate destruction (NEMI I-4650-03 and I-2650-03; www.nemi.gov). The second subsample was analyzed in the same way, but after filtering over 0.45 μm (Whatman RC55 regenerated cellulose membrane), to measure total soluble N (N_{ts}) and P (P_{ts}). The third subsample was filtered in the same manner and analyzed for NO₃-N, NO₂-N, NH₄-N and PO₄-P in 0.01M CaCl₂ with the SFA. Nutrient loads per event i , L_i (g m⁻³), were estimated according to:

$$L_i = V_i C_i \quad (5.4)$$

Where V_i is the surface runoff volume of event i (m³) and C_i is the nutrient concentration measured in the collection tank just after event i (g m⁻³). For each site, the cumulative surface runoff volume, V_C (m³), and cumulative nutrient load, L_C (g) were calculated according to

$$V_C = \sum_{i=1}^n V_i \quad (5.5)$$

and

$$L_C = \sum_{i=1}^n L_i \quad (5.6)$$

Where n is the number of events per field for the entire duration of the experiment. The yearly average number of events, \bar{i} (y^{-1}), surface runoff volume, \bar{V} ($m^3 y^{-1}$), nutrient loads, \bar{L} ($g y^{-1}$) and average concentration, \bar{C} ($g m^{-3}$) were calculated per site by dividing the cumulative by the duration of the experiment of 4 years.

5.2.3 Modelling setup

The surface runoff measurements were performed at a short section of the field boundaries. Hence, there was no information available on where the surface runoff water originated from or where ponding was present at the fields. However, we had detailed topographical data available. We analyzed this data with the modelling approach described in the following sections to analyze ponding, subsequent water redistribution and surface runoff at the fields.

Numerical model

The numerical model used to analyze surface runoff development on the three fields consists of two parts. Water flow over the soil surface is simulated with a fill and spill algorithm that takes a detailed DEM of the surface as input. The algorithm identifies the catchments within a flat field and makes a database of storage capacities and overflow points of these catchments. During simulation of a rainfall event, the catchments fill up and spill excess water to their neighbours, thus merging to form larger catchments during the process. A detailed description of this algorithm can be found in Appels et al. (2011). Water flow in the soil is simulated in 2D with a finite-volume solution of the Darcy equation for groundwater flow. The unsaturated zone is assumed to be in hydrostatic equilibrium with the groundwater table at all times. Therefore, a unique relationship exists between the volume of water in a soil column and the elevation of the water table, the shape of which is determined by the soil hydraulic parameters. This model setup incorporates some of the important feedbacks of shallow groundwater (decreasing sorptivity of the soil, decreased soil water storage capacity, decreasing specific yield), while providing flexibility due to the absence of the need to explicitly calculate fluxes from the unsaturated to the saturated zone. For a detailed description of the FAST-Runoff model (Fast Areal Simulator with Topography for Runoff) and equations, the reader is referred to Chapter 4.

Surface topography: meso- and microtopography

We considered several surface topographies. For each field A, G, and H, their own mesotopography was considered. The pinmeter measurements performed at the sites were used to characterize the microtopographies of each field. These characteristics were used to simulate microtopographies over the entire extent of the three fields. In fields A and H the microtopography consisted of a regular pattern, resulting from ploughing (tillage) and a random component, whereas the measured microtopography of field G could be characterized by the random component alone. The plots of field A had a regular sine pattern with wavelength 50 cm and amplitude 3 cm. Field G revealed a random microtopography, with exponential covariance function for soil surface height (variance

1.25 cm²; correlation length 50 cm). Field H again featured a sine pattern with wavelength 50 cm and amplitude 6 cm. Though the main component of the microtopography of fields A and H was the sine pattern, both fields showed some extra variation (caused by soil clods and redistribution of sediment) that could be characterized by a random microtopography with exponential covariance function (variance 4.0 cm²; correlation length 50 cm).

The following five microtopographies were simulated with these statistics: random microtopography (RA) without ploughing rills, only the exponential covariance function with variance 1.25 cm² and correlation length 50 cm; small horizontal (SH) with ploughing rills parallel to the longest side of the field and sine amplitude 3 cm; large horizontal (LH) with ploughing rills parallel to the longest side of the field and sine amplitude 6 cm; small vertical (SV) with ploughing rills parallel to the shortest side of the field and sine amplitude 3 cm; and large vertical (LV) with ploughing rills parallel to the shortest side of the field and sine amplitude 6 cm. The simulated microtopographies were created with the RandomFields package of R and superposed on the interpolated DEMs of Fig. 5.6. The interpolated DEMs without microtopography served as a zero case (M0) to compare the effect of microtopography on surface runoff generation to the underlying mesotopography. All simulated microtopographies are presented in Appendix 1.

Numerical experiments

We applied the stand-alone redistribution algorithm of the FAST-Runoff model to the field surfaces to determine the composition of flow routes in the fields caused by the mesotopography and the five simulated microtopographies. For different cross sections through the fields, the interactions between ponding and surface runoff and groundwater flow were characterized. Despite the compromise with regard to model complexity, such as adopting a fill-and-spill approach for the water flow at the soil surface and approximating the redistribution of water in the unsaturated zone, the computational demand of the FAST-Runoff model remained large when simulating rainfall on the full extent of the fields with microtopography. The main reason is that due to the highly nonlinear behaviour of the specific yield function when the soil is close to complete

Table 5.2: Parameter ranges used in the model simulations.

Parameter	Unit	Range of values
α shape parameter Van Genuchten equation	(cm ⁻¹)	0.025–0.035
n shape parameter Van Genuchten equation	(-)	1.5–1.7
K_s saturated hydraulic conductivity	(m d ⁻¹)	0.5–2.5
H_i boundary condition	(m below mean soil surface)	0.8–0.6
m_0 initial maximum elevation of groundwater mound above ditch level	(m above H_i)	0–0.1

saturation (Chapter 4), extremely small time steps are required for a stable model simulation (i.e. 10^{-7} d). With the number of grid cells required to properly characterize the microtopographies of the fields, computation times were equal to or larger than simulated times.

For the numerical simulations we used the rainfall time series of January 2008, during which surface runoff events were recorded at the three fields. For the parameterization of the model, we used several combinations of soil hydraulic parameters and a range of initial conditions (Table 5.2). We did not have enough (detailed) data supporting a model calibration and validation cycle, but carefully examined the plausibility of model results. Values for these parameters were obtained from the Staring Series for the soil types identified in the fields (Wösten et al., 2001).

5.3 Results

5.3.1 Runoff quantity and quality measurements

With approximately 25 events occurring in each field during a 50 month period, it is clear that experimental quantification requires automated measurement designs. Probably for this reason, little comparison material on surface runoff quantities is available for similar conditions. Between December 2007 and April 2010, a total of 80 surface runoff events were recorded (Fig. 5.4). Most events occurred in the grassland field G (35), fewer in horticultural field H (26) and the least in arable field A (19). The total volume of surface runoff measured in the fields followed the same sequence, though the yearly surface runoff volumes of fields G and H are comparable. In 2010, one surface runoff event was missed in field H, because the installation was flooded with silt from the field. The gutter had to be cleaned and reinstalled afterwards to continue the measurements. During the same incident, also the surface runoff volumes from field A were largely underestimated, because the trenches were drowned and surface runoff was only partially captured in the tank. Looking at the precipitation and groundwater level time series we can observe that surface runoff occurred exclusively in winter periods (November through April) when the groundwater level was close to the soil surface (less than 50 cm below the surface) and was not necessarily linked to large daily volumes of precipitation. The only exception was an event in October 2009, where surface runoff was generated in field G during an intense rainfall event, even though the groundwater level was deeper than 50 cm below the soil surface. The amount of events and cumulative volume per year varied throughout the measurement period, the winter of 2008–2009 experiencing the smallest number of events and the winter of 2010–2011 the largest number. The inter-field differences regarding number of events and their volumes varied throughout the measurement period, where the winter season of 2010–2011 was the most homogeneous season.

The nutrient concentrations measured in surface runoff (Fig. 5.5) were high, especially for total phosphorus (P_t) on grassland (G), with a median value larger than $5 \text{ mg l}^{-1} \text{ P}$, and a maximum of $9 \text{ mg l}^{-1} \text{ P}$, almost a hundred times the commonly used limit of $0.1 \text{ mg l}^{-1} \text{ P}$ for good surface water quality. Although the P concentration in

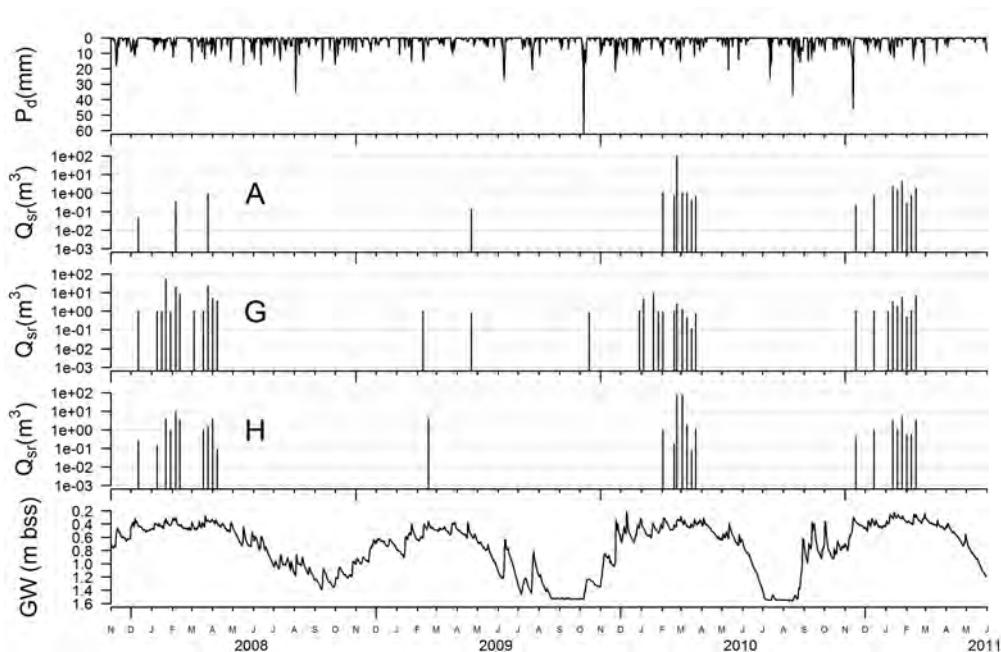


Figure 5.4: Daily precipitation time series from the KNMI station close to the field sites (top row). Weekly surface runoff volumes (m^3) measured in the three fields (row 2, 3, and 4). Groundwater level time series from TNO-NITG (2012) in the pilot area (bottom).

runoff from the arable sites was much lower, all measured values were above the mentioned P limit. Measured P was largely soluble inorganic phosphate. Most total nitrogen (N_t) concentrations were well above the commonly used limit of 2 mg l^{-1} . Most average concentrations for N_t and P_t (Table 5.3) were higher than median values, which suggests that relatively high N_t and P_t concentrations coincided with higher surface runoff volumes.

Though median surface runoff volumes were comparable for the three sites, the average values were quite different due to the different magnitudes of the large events. Both surface runoff volumes and nutrient concentrations at field G were clearly higher than those measured at fields A and H. Differences in nutrient loads were mainly caused by different surface runoff volumes. Seeing the large differences between the mean and median surface runoff values, it is however quite likely that the underestimation of one large surface runoff event at both field A and field H has resulted in an underestimation of the nutrient loads from these fields. The higher P concentration in surface runoff at H compared to A could be explained by a very high P saturation degree of the top soil in field H: PSD 89 % and P_w $93 \text{ mg P}_2\text{O}_5 \text{ l}^{-1}$ in field H, compared to PSD 57 % and P_w $65 \text{ mg P}_2\text{O}_5 \text{ l}^{-1}$ in field A. The relatively high load from G compared to H and A could be explained for N by a higher N_{\min} content of the soil: 5.2 mg kg^{-1} in field G, compared to 0.9 mg kg^{-1} in field H and 2.7 mg kg^{-1} in field A; but not for P, because the P saturation degree of the grassland top soil was, at a value of 68 %, in between that of H and A.

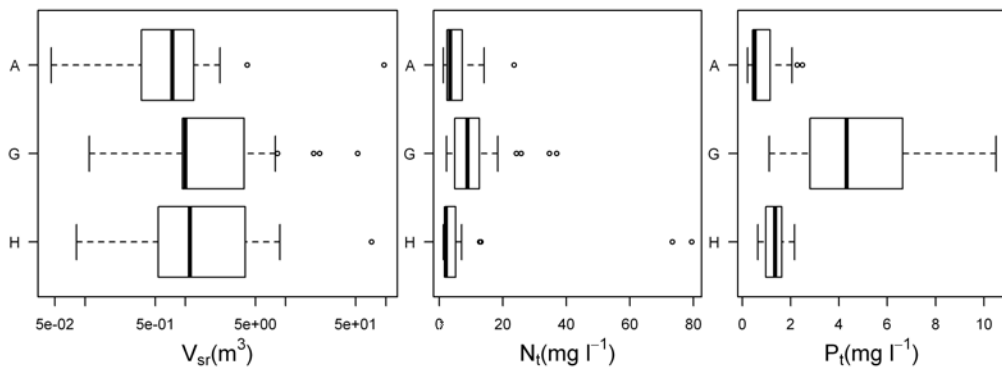


Figure 5.5: Boxplots of measured surface runoff volumes (left) and concentrations N_t (middle) and P_t (right)

However, field G was the only field where a clear difference in top soil PSD was measured between the sampling points close to the gutters and those further away from them.

Close to the gutters, the PSD was 60 % and P-Al was 32 mg P_2O_5 100 g^{-1} , whereas PSD was 76 % and P-Al 23 mg P_2O_5 100 g^{-1} further away from the gutters. The cattle grazing the field entered and left through a gate located some 5 m from the gutters. A higher rate of animal droppings in this part of the field could explain the higher P saturation degree of the topsoil.

5.3.2 Effects of micro- and mesotopography on properties of surface runoff flow routes in the fields

With the FAST-Runoff model, it is relatively simple to map the different basins in the fields. Such a map provides a rapid intuitive impression of the organisation of surface runoff in a field. Also, they can give an impression of the complexity of flow routes for surface runoff, defined as the collection of basins that share the same spillpoint to the ditch or stream. In Fig. 5.6, an impression of the flow routes in the three fields is given

Table 5.3: Average number of events \bar{i} , median number of events i_{50} , average surface runoff volume \bar{V} , median surface runoff volume V_{50} , average concentration \bar{C} , median concentration C_{50} and average loads \bar{L} of both phosphorus and nitrogen for each field.

	Events		Surface runoff volumes		Phosphorus, P_t			Nitrogen, N_t		
	\bar{i} (y^{-1})	i_{50} (y^{-1})	\bar{V} ($m^3\ y^{-1}$)	V_{50} ($m^3\ y^{-1}$)	\bar{C} ($g\ m^{-3}$)	C_{50} ($g\ m^{-3}$)	\bar{L} ($g\ y^{-1}$)	\bar{C} ($g\ m^{-3}$)	C_{50} ($g\ m^{-3}$)	\bar{L} ($g\ y^{-1}$)
A	4.8	5.0	4.72	0.74	0.6	0.5	2.7	4.8	3.4	20.4
G	8.8	10.5	39.9	1.0	7.2	6.6	273	9.0	9.2	341
H	6.5	7.5	12.3	1.0	1.4	1.4	14.7	3.0	2.2	30.7

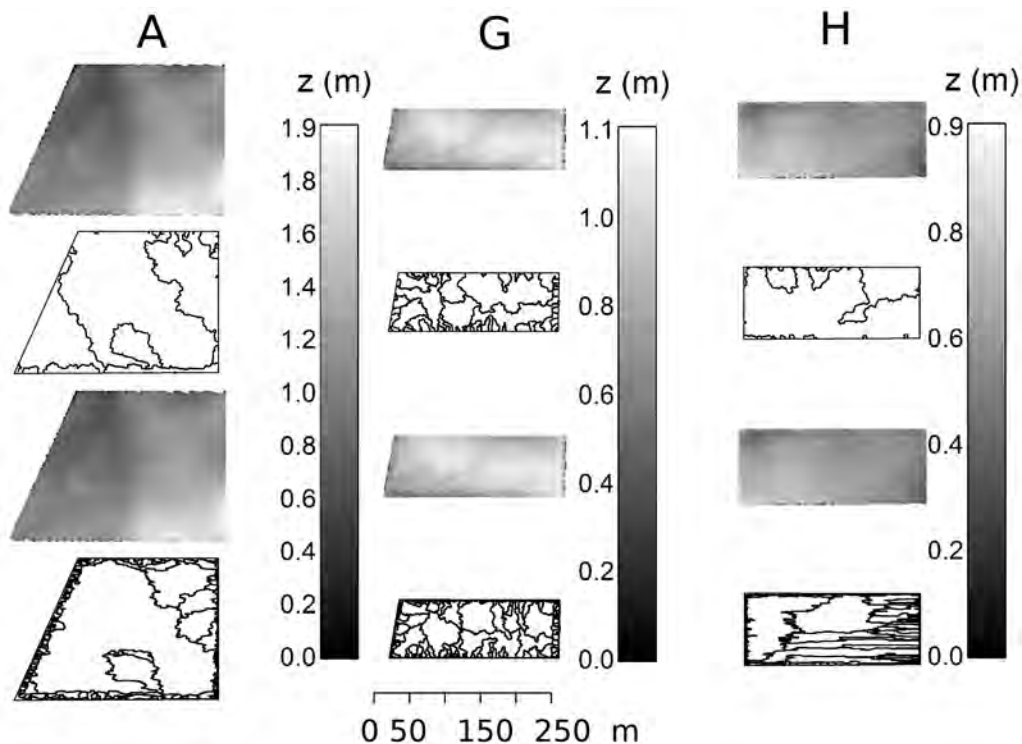


Figure 5.6: DEMs of the fields at meso scale (upper row), grid cell size 0.5 m, and micro scale (third row), grid cell size 0.1 m. In the second and fourth row, the flow route maps of the fields, obtained from the analysis with the FAST-Runoff model. Each flow route consists of a collection of basins that share the same spillpoint to the ditch. The microtopography realisations used in this figure are small horizontal (SH) for field A, random (RA) for field G, and large horizontal (LH) for field H.

when considering only mesotopography features and when considering the microtopography that is most representative for the actual microtopography during the measurement period. Particularly, the differences between the mesotopographies of the three fields are well reflected in the flow route map (second row of Fig. 5.6). In field A, the map is dominated by one large flow route that discharges at the northern boundary of the field, where the gutters were located. In field G, the presence of a small (less than 2%), yet well-defined slope with a water divide along the central axis of the field is reflected in the presence of flow routes with a similar size and orientation at both long sides. Field H contains flow routes to all sides of the field, with a medium range of variation.

In field A, the addition of microtopography results in a larger part of the field discharging at the north field boundary. In field G, the areas of flow routes change, but the shapes and overall composition of these routes in the field are rather similar to those present in the M0 case (i.e. mesotopography only). In field H, the effect of the horizontal ploughing rills on flow route shape and size is most visible in the lower right corner, where the gutters were located. In general, flow routes in this field with microtopography

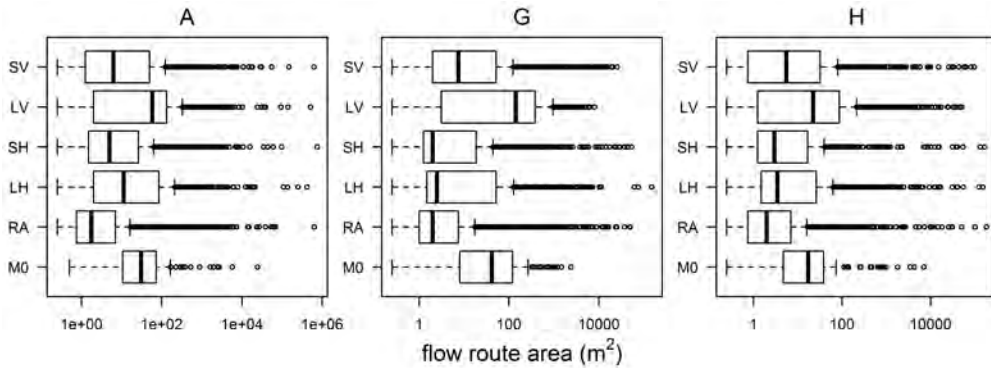


Figure 5.7: Boxplots of flow route area of each field (panels). From top to bottom the five microtopography realizations (small vertical, SV, large vertical, LV, small horizontal, SH, large horizontal, LH, random, RA, and mesotopography only, M0).

are more horizontally stretched than those determined from the mesotopography alone. If we compare the median area of the flow routes of a field with microtopography to that of the zero case with only mesotopography (Fig. 5.7), adding a microtopography always leads to a smaller median for each of the fields A, G, H. However, there is one notable exception: in case of a large rill amplitude in the vertical direction (LV microtopography in Appendix 1, Fig. A.4), the median flow route size is larger than that of the zero case and much larger than that of the other microtopographies.

These results are a bit counter-intuitive, e.g. when comparing the flow routes through mesotopography and microtopography of field H in Fig. 5.6 one would assume that the addition of microtopography leads to a larger size of the flow routes. However, the addition of microtopography leads to the presence of a large number of very small (area < 1 m²) flow routes towards the ditches at the field boundaries. These small flow routes dominate the distribution of flow route area. Only in the LV microtopography case, the direction of the larger flow routes is such that they encompass all small basins at the field boundaries.

Though numerous, it is not the presence of small flow routes that is characteristic in the potential changes of surface runoff routing through the microtopography of a field. We therefore focus on the upper outliers of the distribution of the flow route area under the various types of microtopography. To this end, we plotted the minimum number of flow routes required to cover a certain fraction of each field (Fig. 5.8). The large rill amplitude in the vertical direction (LV microtopography) can be clearly distinguished from the other realizations and the zero case, but the other microtopography realizations differ only to a small extent from the zero case and each other. This static analysis therefore reveals that to understand the surface runoff behaviour in fields as considered, also a dynamic approach is needed.

The dynamic analysis (plotting the surface runoff behaviour obtained from the FAST-Runoff model) shows some differences. The simplest case of surface runoff

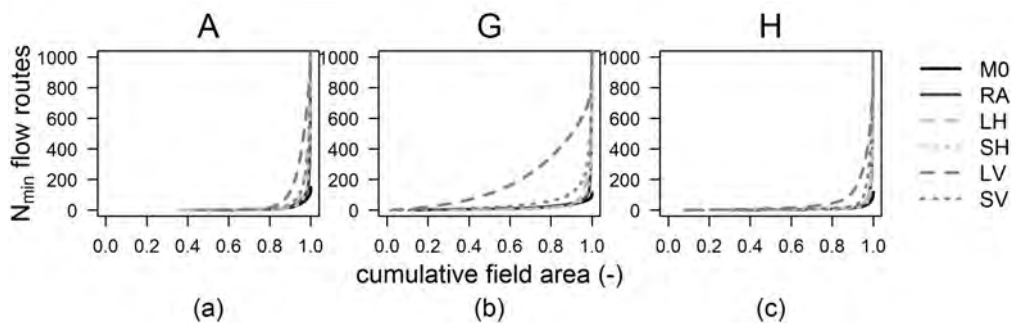


Figure 5.8: Minimum number of flow routes needed to cover the cumulative field area of the three sites.

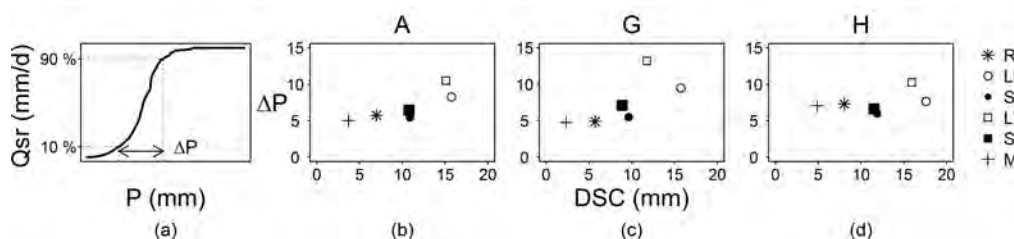


Figure 5.9: Example of surface runoff curve (panel left). Metric ΔP plotted as function of DSC of the meso- and microtopographies for the three fields.

behaviour is given by simulation of a continuous rainfall event on a field with minimal infiltration. The field fills up and basins spill and form continuous flow routes as a function of cumulative precipitation with a maximum surface runoff rate that is equal to the precipitation rate (first panel of Fig. 5.9). The slope of this curve is large when shallow basins with a large surface area spilling water to small ponding areas connect quickly or small when the ponding area is larger and the ponds connect more slowly.

Therefore, the surface runoff curve can be used as a representation of hydrological connectivity of the surface (Antoine et al., 2009; Appels et al., 2011; Peñuela et al., 2013). First, we determined surface runoff curves for every microtopography realization and the zero case of the three fields. Then we quantified the difference in connectivity behaviour by determining the amount of precipitation required for the increase of the surface runoff rate from 10 % to 90 % of its maximum value (Fig. 5.9 panel 1). We plotted the amount of precipitation, ΔP , versus the depression storage capacity of the microtopography realization (Fig. 5.9 panel 2, 3, and 4).

On the mesoscale (M0), the depression storage capacity of the fields is smallest in field G (2.34 mm), has an intermediate value in field A (3.03 mm), and is largest in field H (4.81 mm). The ΔP metric varies accordingly from field G (4.75 mm), to field A (5.00 mm), and field H (7.05 mm). The addition of a microtopography always results in a larger DSC, as more topographical detail is included. The ΔP metric could decrease due to the

addition of a microtopography, when its structure is such that it enhances the connectivity characteristics of the mesotopography more than the extra amount of rainfall that is required to fill the increased DSC. This is the case for the SV and SH microtopographies when superposed on the mesotopography of field H. When adding microtopographies with higher amplitude to this field, there is no such connectivity increase anymore and the ΔP metric increases with increasing DSC. In the fields A and G, the ΔP metric increases with increasing DSC immediately, with a stronger slope in field G. In view of the very small (non-significant) decrease of ΔP of the SV and SH microtopographies of field H, it is probably more appropriate to say that the ΔP increase of this field occurs later and at a slower rate than that of the other two fields. This can be attributed to the fact that in field G, the present mesotopography slope dominates the connectivity behaviour and microtopography mainly influences the storage thresholds, whereas in field H, the connectivity behaviour will be more influenced by the microtopography too.

5.3.3 Effect of saturation excess locations on ponding and surface runoff

The soil water storage capacity at the beginning of a rainfall event is the major factor that determines whether or not ponding and surface runoff will occur. This (initial) storage capacity is non-uniformly distributed within each field. To illustrate the effect of this distribution with a full 3D simulation of microtopography is highly demanding with regard to computation time, as mentioned before. However, some of the time and space dependence of ponding and surface runoff can be illustrated with 2D transects, using the simulated realizations of microtopography. For each field, two vertical and two horizontal transects were simulated (Fig. 5.10, position in fields indicated in Fig. 5.2). In Fig. 5.10, ponding is shown for each of these transects, as a function of time. In this figure, we recognize two dominant ways of how ponding develops as a function of time. For some transects, the ponding starts midway of the field, i.e. at some distance from the ditches that are found at the outer ends of each transect. The groundwater mound has its highest elevation with respect to the ditch level at this exact location when mesotopography is virtually absent or when the surface slope changes gradually. An example is field G, where the water divide of the surface is located in the middle of the field. The other possibility is that ponding starts closer to the ditch induced by a particular mesotopography pattern. In those cases, the groundwater mound is still at its highest elevation with respect to the ditch level right between the ditches, but due to the abrupt decline in soil surface height towards the ditch, the soil water storage capacity of the unsaturated zone is smallest here. This is the case in field A, where ponded areas actually grow from the outer ends of the field inward over time. The simulations therefore illustrate that the onset of both ponding and surface runoff depends on the gradual increase of groundwater level if one moves away from the ditches and the simultaneous change in soil surface level.

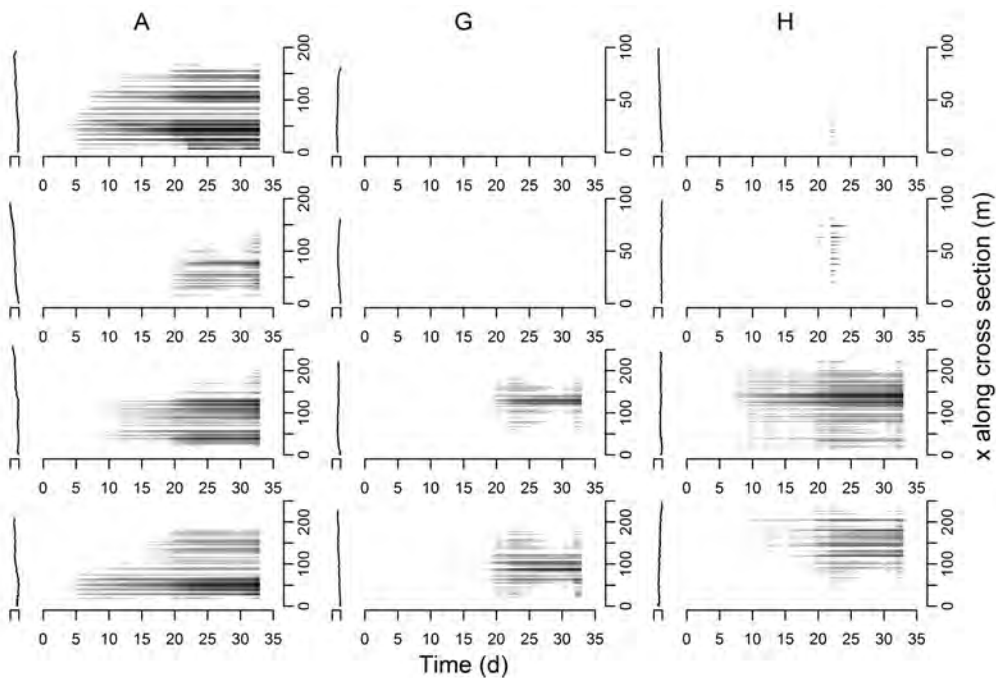


Figure 5.10: Ponding evolution map with depth of ponding (grayscale intensity) as a function of time (x-axis) and space (y-axis) in the four cross sections of each field (depicted along the y direction) during simulation of rainfall events of January 2008. The upper two cross sections are taken along the vertical axis of the fields, the lower cross sections along the horizontal axis of the fields.

For practical reasons, the surface runoff data of the three fields were only available in the form of week-aggregated quantities. The precise time that runoff occurred and the surface runoff rate as a function of time were both not available. The comparison of model predictions with these data sets for fields A, G, and H, is therefore limited to whether or not surface runoff was predicted in the correct week, and the cumulative volume runoff for each week or for the entire simulation. When evaluating the prediction of surface runoff in a certain week, we define an “overestimation” of incidence when surface runoff was predicted in a week where it was not observed and an “underestimation” of incidence when it was not predicted in a week where it was observed. Accordingly, in weeks where the incidence of events was correctly predicted, we can over- or underestimate the predicted volume of surface runoff with respect to the measured volume. As mentioned in the introduction, one of the major issues with surface runoff measurements is scaling and representativeness of measurements on a limited field stretch of the field for the response of the whole field. Because of the computation limitations we faced, we were not able to use model results to check on the various locations at which surface runoff could have been initiated and determine the initiation of ponding under groundwater saturation excess conditions. However, we scaled the measured and simulated volumes with field area to enable a comparison between measured and simulated surface runoff. In Fig. 5.11

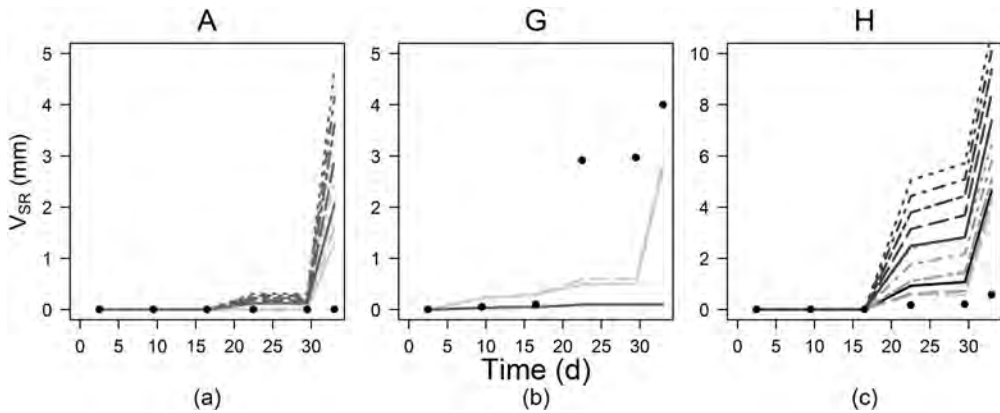


Figure 5.11: Cumulative weekly surface runoff discharge (mm) for the three fields during the simulation period January–February 2008. Successful model simulations depicted with gray lines, the black dots are measured cumulative discharge (mm) scaled to total field area. Gray intensity indicate sets of simulations performed with the same soil type and ditch level, whereas line type indicates variation in the initial elevation of groundwater mound with respect to the ditch level.

the cumulative measured volumes (scaled to mm) of surface runoff is plotted for the period of January–February 2008 combined with the most successful model simulations of the fields. That implies that for field A, the five simulations that predicted all incidents correctly are plotted together with the five simulations that had one overestimated week. Similarly, for field G, the two correct simulations and five simulations with one underestimated week are plotted. For field H, the eleven simulations that contain one over- and/or one underestimation are plotted. The cumulatives of the simulation have a time resolution of one hour. The simulations of field A, even the ones that had the right timing, overestimated the cumulative discharge of surface runoff with respect to the measured amount. The magnitude of overestimation increases with an increasing initial soil water storage capacity. The simulations of field G, where surface runoff started already in week two, overestimated the surface runoff amount for the first three weeks

Table 5.4: Model evaluation of over- and underestimation of surface runoff occurrence during the weeks simulated.

Success rate	Field A	Field G	Field H
all weeks correct	5	2	-
one underestimation	30	5	2 ^a
one overestimation	5	38	10 ^a
>1 underestimation	-	-	9
>1 overestimation	5	-	25

^a One simulation in field H resulted in an overestimation in one week and underestimation in another, therefore the sum of this column is not equal to 45

and then underestimated the final amounts. The underestimation was smallest for the soils with a smaller porosity. The simulations of field H, all resulted in an overestimation of the cumulative surface runoff amount. Overall, the most successful simulations were realized from combinations of ditch levels and unsaturated zone characteristics (porosity and Van Genuchten profile) that resulted in similar initial soil water storage capacity conditions. In the next section, we elaborate on potential explanations for the pattern of over- and underestimation of both surface runoff incidence and cumulative amounts.

5.3.4 Interpretation of results

The goals of the study were 1) to explain differences in measured surface runoff volumes and nutrient loads of surface runoff between fields by characteristics of their meso- and microtopography, and 2) to use model simulations of the fields to investigate whether the plot scale measurements we performed were representative for the surface runoff behaviour of the whole field. As expected from the climate characteristics and soil type in the P-pilot region, surface runoff was observed only in winter periods when groundwater levels were close to the soil surface. In the ranking of surface runoff impact, field G had the highest risk and field A the lowest. The occurrence of surface runoff events corresponded with the order of surface runoff risk: field G experiencing most events and field A the smallest number of events. These findings suggest that the proximity of the lowest patches to the small strip along ditches and streams is a reasonable indicator for surface runoff risk.

The nutrient concentrations measured in the surface runoff were high, especially on field G. The differences in nutrient loads were caused both by differences in surface runoff volume and in nutrient concentrations in the soils of the fields. The high loads of field G were most probably also caused by animal droppings close to the measurement gutter. However, the overall estimated yearly nutrient load from surface runoff was lower than expected from similar studies (Pärn et al., 2012; van Beek et al., 2009). When we assume that the surface runoff we measured was the only surface runoff, (so only one outlet point in each field), resulting ranges are 0.6–140 g ha⁻¹ for P_t and 4–180 g ha⁻¹ for N_t. When we assume that all parts of the field generated surface runoff, we can calculate the yearly loads per hectare based on the size of the areas contributing surface runoff to the gutters from Fig. 5.6. In this case, the ranges are 0.9 g–2.7 kg ha⁻¹ for P_t and 7.0 g–3.4 kg ha⁻¹ for N_t, with the highest values for field G, where high surface runoff volumes and nutrient concentrations coincide with a small contributing area. The actual loads will be found somewhere between the ranges mentioned here, because we know from field observations and model simulations that not all parts of the fields contributed equally to surface runoff generation. The measured load was underestimated because the measurement equipment failed during some of the larger events. This underestimation is not only a result of the volume of water that was not measured, but also with an underestimation of nutrient concentrations during these incidents, as overflow of the gutters coincided with large sediment transport. We certainly missed this part of the

total loads from fields A and H. Also it is possible that some solids were stored in the gutter, and thus not measured. As shown before by van der Salm et al. (2012), an incidental surface runoff event can take a disproportionate share in total surface runoff load (up to 56 % of yearly P loss), and can have a severe impact on surface water quality (Withers et al., 2003).

The mesotopography of each field had a distinctive feature that was determining the surface runoff flow routes at this scale. Field A had a large basin, causing more than 60 % of the field area to drain towards the ditches via only one spillpoint. Field G had a water divide along the centre of the field, causing a pattern of evenly sized parallel basins to spill via individual spillpoints towards the ditches. Like field A, field H had a small surface elevation range, but due to the absence of a single “collection basin”, the resulting flow route pattern is a mix of surface runoff flow routes of various size and spill direction. The superposition of a microtopography pattern to these mesotopography surfaces had several effects on the ponding and surface runoff characteristics of the fields. In field A, where the storage of water at the soil surface was mainly concentrated in one mesotopography basin, the microtopographies increased the buffering effect of this depression, especially when the orientation of the microtopography transported more water in the direction of the basin. In field G, where the role of mesotopography in creating depression storage capacity was limited but important in determining flow directions, the main effect of microtopography was found in providing depression storage capacity in this field. In field H, surface runoff is actually routed towards different spillpoints to the ditches by the microtopography.

The simulations of surface runoff with our redistribution and groundwater flow model illustrate how ponding evolves in the fields. It is not equally distributed throughout the fields and therefore not all surface runoff flow routes within the field will be activated at the same time. To allow a comparison between measured and modelled amounts of surface runoff, we were required to scale the results back to the same field area. This implies ignoring potential other spillpoints in the field boundaries. However, with this assumption we may hypothesize on the differences in flow route activation of the fields from the ponding evolution maps and cumulative surface runoff curves. In field A, the differences between the 5 simulations (Fig. 5.11) are caused by the fact that the initial storage available in the subsoil differs. The rainfall provided in the entire month is more than enough to overcome storage capacity. Ponding starts very early in the month (Fig. 5.10), but the threshold to overcome is quite high. The threshold at the surface is located just in front of the ditches and is present in the cross sections as well as it would be in a 3D field. In field G, it seems that both the threshold and the choice of cross sections are not good. Surface runoff starts too early, but is eventually underestimated, suggesting that the cross sections are drier than the wet patch where we measured surface runoff. In field H we have a good overestimation of amounts, though there is an underestimation of incidences. This could be attributed to the fact that the buffering effect of the microtopography is underestimated here: the long cross sections, in which a

lot of ponding is present, may spill too easily, because more storage of water will take place in the complex microtopography in the corner of the field where the measurement equipment was installed.

In the current setup of the FAST-Runoff model, we cannot test these hypotheses. In order to draw firmer conclusions with respect to representativeness of the measurement locations for the whole field, we need to perform a complete 3D simulation. Especially for the fields where microtopography plays a dominant role in flow route definition (field H), the fine detail of surface topography is needed. Adjustments to the original model scheme should be focussed on reducing the number of calculations to be performed. This reduction can be achieved by increasing the area of the cells of the groundwater part with respect to that of the soil surface cells. Conceptually, such an assumption would be reasonable, because it is very unlikely that the groundwater table shows the same amount of roughness as the soil surface: instead it is much smoother and may be more closely related to a coarse DEM than a fine DEM (Sørensen and Seibert, 2007).

Some aspects of the surface topography that are important for ponding and surface runoff are incorporated in the surface runoff risk definition based on large scale DEM with Eq. 5.1 and 5.2. For field A, the ratio between spillpoint and catchment area is captured in the surface runoff risk. For field G, this fraction is larger, which is also quite correct. This fraction could be linked to the occurrence of events: low fraction, less events, buffering capacity of low patches is probably larger. The impact of individual events could be larger at field A than at field G, because the field is larger. The measurements show that the impact of individual events was generally smaller at field A than that of those at field G, indicating that the maximum contributing area of the gutters was not always contributing during events. Only in the event we missed because of the flooding of the measurement equipment, this contributing area was considerably larger than that at field G. The surface runoff risk definition is more difficult in fields like field H, where the activation of surface runoff flow routes depends largely on microtopography. Using this type of indicator in a larger catchment could yield a first indication of identifying frequency versus impact.

5.4 Conclusions

The effect that microtopography has on flow route shapes in flat fields can be quantified with metrics of surface runoff curves and the rerouting of ponded water along the soil surface. Groundwater dynamics and the depth of the unsaturated zone account for a spatially variable initiation of ponding and surface runoff. In order to improve the quantification of contributing area to spillpoints at the field boundaries, numerical concepts for saturation excess surface runoff on a heterogeneous surface need to be further improved with respect to computation time. The interactions between groundwater and redistribution in microtopography is a determining factor for ponding and contributing areas to surface runoff discharge at field boundaries, that cannot be

sufficiently grasped in current modelling concepts at the required spatial scales.

Acknowledgement

The authors acknowledge Willy de Groot, Jan van Kleef, Antonie van den Toorn, and Philip Wenting for their help in acquiring the data and Patrick Bogaart and Marieke Oosterwoud for suggestions for illustrations and text. This study was financed by Alterra through projects 5232870–06 and 5236185. Part of the project was funded by the Dutch Ministry of Agriculture, Nature, and Food Quality (project BO-05-004-KRW) and by the Innovation programme KRW (KRW08085).

Chapter 6

Microtopography as a driving mechanism for ecohydrological processes in shallow groundwater systems

Abstract

Microtopography can have a large effect on flow processes at the soil surface and the composition of soil water. Microtopography is often represented by a roughness parameter in hydrological models. In areas without a strong topographical gradient, microtopography may be underestimated when accumulated in a single parameter, especially in shallow groundwater systems. This study reviews the intricate relationships between microtopography, surface runoff, and ecohydrology in systems featuring shallow water tables. We specifically focus on relations between microtopography and runoff, impact of microtopography on response times of shallow groundwater ecosystems and microtopography and spatial distribution of groundwater quality parameters and site factors. We advocate the use of microtopography in modelling approaches by examples that feature typical ecosystems with shallow groundwater under influence of microtopography. With a simple modelling approach, we show how microtopography could add flexibility to the acrotelm-catotelm concept in raised bog hydrology. The classic acrotelm-catotelm concept hinders progress in understanding small scale hydrological variations and other ecohydrological relations. Furthermore, we illustrate possible self-organization properties of wetlands. Finally, we show how microtopography and surface runoff affect the mixing of water with different chemical signatures, resulting in variations of the occurrence of plant species.

6.1 Introduction

Surface runoff is the free flow of water over the soil surface, and is an important term in the hydrological cycle (Beven, 2004). Surface runoff occurs as soon as the water supplied to the soil surface cannot infiltrate, either because it exceeds the maximum infiltration rate, or because the capacity of the vadose zone to store additional water is exceeded. The soil water storage capacity is mainly influenced by the depth of the water table, whereas sealing and crust formation at the soil surface, poor wettability of the soil matrix, and subsoil compaction influence the infiltration capacity of the soil. Surface runoff caused by saturation excess and infiltration excess are known as Dunne and Horton runoff, respectively. Surface runoff may also occur when phreatic groundwater seeps up and exfiltrates at the soil surface (Dunne and Black, 1970). It is evident, from the different weather, soil, soil cover, and geohydrological conditions, that many features of surface runoff, such as magnitude, frequency of occurrence, and distance of overland displacement of water is difficult to predict (Sophocleous, 2002). In hilly areas, the large scale topographical gradient is the dominant aspect in determining such surface runoff features, as is apparent from early distributed runoff models (Freeze and Harlan, 1969) and later ones such as SHE (Abbott et al., 1986) and TOPMODEL (Beven et al., 1995). As the topographical gradient influences both the convergence and velocity of flow, a larger slope implies a larger risk of erosion (Hairsine and Rose, 1992). Accounting for microtopography on a hillslope results in an increase of effective infiltration rate with

hillslope length as the downslope increase of overland flow depth and discharge progressively inundate the higher and more permeable parts of microtopography (Dunne et al., 1991; Thompson et al., 2010). In areas with a negligible large scale elevation gradient, microtopography, consisting of (ir)regular topographical features such as soil clods, crop rills, clumps of vegetation or washed on sediments, is the main factor in routing non-infiltrating water. Representing microtopography with a roughness parameter only would misrepresent the importance of retention of water that does not flow, but is stored in depressions to await infiltration or evaporation (Antoine et al., 2009). Surface runoff modelling in flat areas received much less attention than in sloping areas, as is apparent from the common simplification to describe surface runoff as sheet flow of uniform depth over a tilted rough surface in most process-based models (Beven, 2002).

As surface runoff is an ephemeral process and typically comprises only a small fraction of average catchment discharge, neglecting it may be understandable from a quantitative point of view. However, ignoring it is inappropriate. During storm events, surface runoff provides a considerable contribution to peak discharges at the catchment scale and to inundation and ponding at field scale. Moreover, even a limited amount of surface runoff facilitates fast transport of solutes, such as nutrients, pesticides, and other contaminants, and can significantly contribute to surface water loading (Turtola and Jaakkola, 1995; Louchart et al., 2001; Mueller et al., 2007; van der Velde et al., 2009, 2010). Particularly solutes that are strongly sorbed to the top layer of soil can by-pass the (un)saturated zone. The strong link between surface runoff and solute fate makes surface runoff in relatively flat areas an environmentally important hydrological process. For systems with shallow groundwater levels, wetlands that are inundated or saturated at a frequency and duration sufficient to support vegetation adapted for hypoxia, the interaction between surface runoff, groundwater quantity and quality, and ecology is of particular interest (He et al., 2010). Wetlands are often located in the lowlands of deltaic areas (e.g. of Mississippi, Rhine-Meuse, and Nile) and other coastal areas. More inland, shallow groundwater may be found in areas, adjacent to streams and rivers and in areas where groundwater flow is impeded. Raised bogs and fens are types of ecosystems that require wet conditions to form, and are therefore characterized by shallow groundwater (Ingram, 1978; van Wirdum, 1991; Belyea and Clymo, 2001; Belyea and Baird, 2006). A wetland's ecology is not only determined by the frequency and duration of saturation, but also by the local groundwater quality. Groundwater flowing through the subsurface geochemically interacts with the solid matrix. With organic matter as the driving reductant, groundwater chemistry may change due to the dissolution of calcite, denitrification, the dissolution of manganese and iron, and the reduction of sulfate. These biogeochemical processes gradually change the chemical fingerprint of the groundwater from the moment of infiltration until the moment of discharge (van Wirdum, 1991; Mulder et al., 1995; Klijn and Witte, 1999; Kvarner and Klove, 2006). As the chemical signature of groundwater depends on the geochemical characteristics and the exposure time to the soil and bedrock, classifications for different groundwater types have been

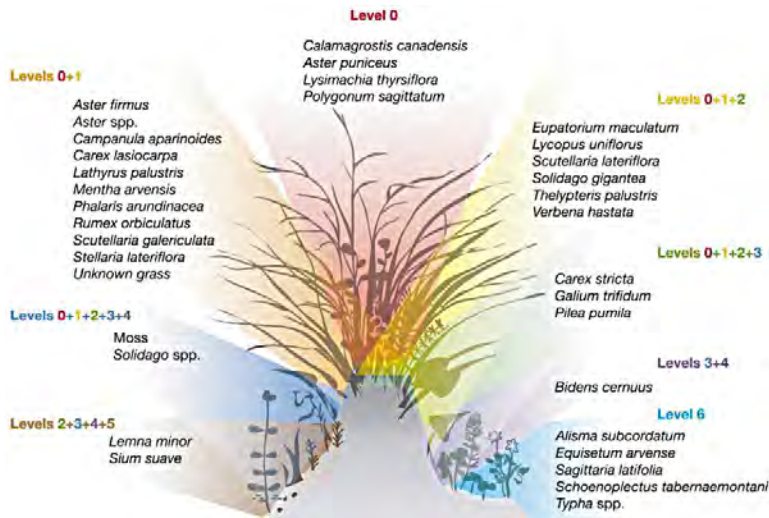


Figure 6.1: Example of species preference driven by microtopography: Tussock micro-habitats (from Peach and Zedler (2006) reproduced with kind permission of the authors). Level 0 indicates the top of the tussock, level 6 the bottom of the tussock; level 1-5 are in between from top to bottom

developed. For instance, van Wirdum (1991) distinguished atmocline (recently infiltrated rain water), lithocline (old ground water), and thalassocline (saline groundwater), based simply on the calciumchloride ratio and EC. More elaborate water quality characterization and classification methods were developed by Stiff (1951), Piper (1953) and Stuyfzand (1986). In systems with shallow groundwater levels, infiltrating water, direct precipitation and groundwater from upward seepage meet close to the soil surface, causing different chemical signatures (atmocline, lithocline) to meet in the rootzone (van Wirdum, 1991; Schot et al., 2004; Cirkel et al., 2010). A transition zone caused by mixing is formed between these two types of water. The resulting chemical gradients may create opportunities for very different plant species and soil organisms (Sterling et al., 1984; Vivian-Smith, 1997; Peach and Zedler, 2006; Moser et al., 2007). An intuitively attractive explanation for the high biodiversity in wetlands with upward seepage is that the proximity of groundwater with different chemical signatures offers opportunities to plant species that differ in ecological demands. Plants find the environment to compete successfully at close distances, owing to different root density profiles and growing seasons (Fig. 6.1, (van Wirdum, 1991; Cirkel et al., 2012)). Vegetation affects surface runoff in several ways. Firstly, plant roots keep soil particles together and intercepting vegetation decreases the impact of rain drops, thereby preventing soil erosion caused by surface runoff (De Baets et al., 2006). Secondly, vegetation stimulates the infiltration capacity of the soil, through preventing sealing of the soil and increasing soil organic matter and macroporosity (Dunne et al., 1991; Abrahams et al., 2003; Weiler and Naef, 2003) leading to a net displacement of surface runoff from bare soil to vegetated patches (HilleRisLambers et al., 2001; Mueller et al., 2007). These vegetated patches are mainly

found in semi-arid areas where plant growth is limited by water availability. The increased infiltration capacity allows the persistence of self-organized vegetation patterns, whereas the plants would die, had they been homogeneously distributed (Rietkerk et al., 2002). Thirdly, stems and other parts of plants contribute to hydraulic resistance to water flow, thereby delaying and impounding the water (Nepf, 1999; Holden et al., 2008). The hydraulic resistance caused by vegetation depends on the size of the plants, their structural properties, plant location in the channel, and the local flow conditions (Green, 2005). This dependency means that approaches for the definition of roughness and resistance formulated for macrophytes with protruding and bending stems found in streams and floodplains (e.g. Lane and Hardy (2002); Luhar et al. (2008) cannot be applied automatically to wetlands, where vegetation has a completely different structure and size relative to flow depth than in vegetated streams and floodplains (Holden et al., 2008). Fourthly, clumps and tussocks of plants create a microtopography of their own (Peach and Zedler, 2006). Some plant species form higher tussocks, because they produce large amounts of litter that is not easily decomposed. In peat bogs, natural differences in peat moss growth create a hollow and ridges pattern within 10-30 years from initiation of peat formation (Pouliot et al., 2011). It is clear that interactions between microtopography, surface runoff, groundwater quantity and quality, and vegetation are intricate and numerous. Here, we focus on the influence of microtopography on mass transfer processes just above and under the surface from an ecohydrological perspective in flat ecosystems. We therefore consider 1) microtopography and runoff, 2) microtopography and response time in shallow groundwater ecosystems, and 3) microtopography and spatial distribution of groundwater quality parameters and site factors. We discuss these topics using published literature and selected examples to illustrate the significance of such interacting processes. We show the ecohydrological importance of considering microtopography for flat areas with shallow groundwater.

6.2 Microtopography and runoff

To call an area flat, instead of sloping, is a qualitative attribute, because a soil surface's elevation varies at different scales. In flat areas, topographic features with dimensions in the range of centimeters and decimeters control storage of water at the soil surface and surface runoff, whereas in sloping areas the global gradient in elevation of the soil surface is dominant (global referring to the system scale, such as an agricultural field or an area with natural vegetation). The demarcation between flat and sloping areas itself, remains a relatively arbitrary subdivision. However, it seems logical that the size of microtopographical features relative to the global gradient is a factor in that demarcation.

In ecosystems in flat areas with shallow groundwater, surface runoff occurs ephemerally as sheet flow and channel flow in micro-channels. We distinguish it from streams, because the underlying soil may be unsaturated (Horton flow) or because the surface runoff occurs incidentally (Dunne flow). As soon as the global gradient of

elevation is sufficiently smaller than the size of local microtopography variations, a fill-and-spill process of depressions becomes important (Darboux et al., 2001). The fill-and-spill process adds complexity to the flow pattern, as ponded depressions may merge through wetting, or separate through drying. In turn, local horizontal flow directions may reverse, even repeatedly, as a function of time during either a wetting or a drying sequence. Moreover, the rate of surface runoff and the quantity and timing of its discharge in the open channel or stream network may be strongly affected by the temporal storage of water in ponds at the soil surface.

Our focus on relatively flat areas has implications for the modelling approach that is taken. A readable account of simplifications and approaches to the conservation of mass and the momentum equations is provided by Lane (1998). In view of the commonly shallow water layer that is involved in surface runoff, the two-dimensional unsteady flow equations known as the Saint Venant equations, which are depth-averaged adaptations of the hydrodynamic Navier-Stokes equations, are suitable (Beven, 2002). Modelling of flow over two-dimensional soil surfaces is challenging, both with regard to parameterization and numerically (Bates et al., 1992, 1997; Fiedler and Ramirez, 2000). For this reason, additional simplifications are often needed to address complex surfaces with both a slope and microtopography (Tayfur and Kavvas, 1998). Mathematical models for surface runoff over an infiltrating surface often use less complex approximations of the Saint Venant equations such as the kinematic wave approximation when microtopography is neglected and the water surface slope equals the topographic slope (Morbidelli et al., 2006; Meng et al., 2008) or the diffusive wave approximation when microtopography is accounted for (Antoine et al., 2009). When simulating water flow in a watershed, these models are computationally demanding. Simpler water transfer approaches can have computational benefits while preserving the main characteristics of the surface runoff process. When the “dead storage” (i.e. water retained at the soil surface in micro-depressions) is large compared to “live storage” (i.e. water that is detained at the soil surface in the layer of flowing water), the development of surface runoff can be simulated well with an instantaneous water transfer algorithms instead of a 2D hydraulic model (Antoine et al., 2009). With these fast models, the effect of size and spatial organization of microtopography on the onset and development of surface runoff can be investigated systematically. Real topographies consist of a complex of features on macro-, meso-, and microscale. Focusing on a peat bog as an example of flat, wet ecosystems, these scales are reflected in the small gradient of a bog from its center towards its outer boundaries, the hollows and ridges pattern that characterize parts of peat bog slopes (Belyea, 2007) and the patterning of different types of vegetation. Simulating fast runoff processes in these ecosystems with a fill-and-spill model (extendable with groundwater module) could therefore lead to more insight in the hydrological response of these ecosystems. In the following paragraph we explore the use of detailed surface topography data and surface runoff concepts to model water flow on a raised bog. It is possible to numerically simulate flow for the heterogeneous coupled

groundwater-vadose zone-surface runoff system we described above to obtain an understanding of the complexities involved. Frei et al. (2010) built a model in the HydroGeoSphere code (Therrien et al., 2008) to explore the feedbacks between groundwater levels, ponding, and surface runoff in a riparian wetland with a (synthetic) heterogeneous microtopography. As was already noted, exploring such a system with a fully coupled physically based computer model, comes at a price. In this case a simulation of one hydrological year could take up to seven weeks of computation time. We illustrate an alternative approach with a simulation of depression filling and surface runoff on a slope of the Männikjärve raised bog in Estonia. We measured an elevation profile from the center to the margin of the raised bog (the bog is surrounded by open water), with a length of 400 m, width 1 m and a vertical elevation drop of 1.5 m (0.4 %). We simulated a microtopography with a spatial structure that visually matches field observations of microtopography (as it was not measured). The random topography was generated in R Statistical Software with the RandomFields package. We used an exponential covariance function for the definition of the semivariogram shape with a standard deviation of 5 cm and correlation length of 30 cm. This microtopography was superposed on the measured elevation profile. We then analyzed how often surface runoff reached the margin of the raised bog subject to a designated rainfall forcing measured at Männikjärve bog during spring, summer, and autumn of 2009. The analysis was performed with an algorithm for ponding and redistribution of water (Appels et al., 2011). For illustrative purposes, the analysis was kept simple and therefore featured no groundwater or Richard's subsurface flow. Infiltration and evaporation losses were assumed to occur at a constant rate throughout the entire slope during rainfall events and under ponded areas during the periods between rainfall events. At the start of the simulation all ponds at the slope were filled with water, originating from melting of snow cover on the bog in winter.

In Fig. 6.2 the rainfall and surface runoff rates are plotted together with the volume of water that is stored in the microtopography. Surface runoff occurs only when more than 80 % of the available depression storage capacity of 50 mm is filled with water. This amount is plausible in the waterlogged ecosystem we investigated. We find several values of surface runoff rate occurring with the same amount of water stored at the surface because of two reasons. The first cause is the variation in rainfall rate; once a flowpath towards the bog margin has been established through ponds filled with water, the surface runoff rate depends on the rainfall rate in the timestep under consideration. Secondly, even though the infiltration rate was fixed at a constant value, the cumulative water losses from pools in periods between rainfall events depend on the pools' dimensions. This, combined with a variation of area contributing excess water to each pool, leads to a change in activation of the flowpaths on the bog over time. The occurrence of surface runoff becomes a function of characteristics of the rainfall sequence as well. The spatial differences are amplified when we consider the whole raised bog, instead of just a thin (semi 2D) profile. The various morphological features of the raised bog have specific relations between amount of water stored at the soil surface and surface runoff

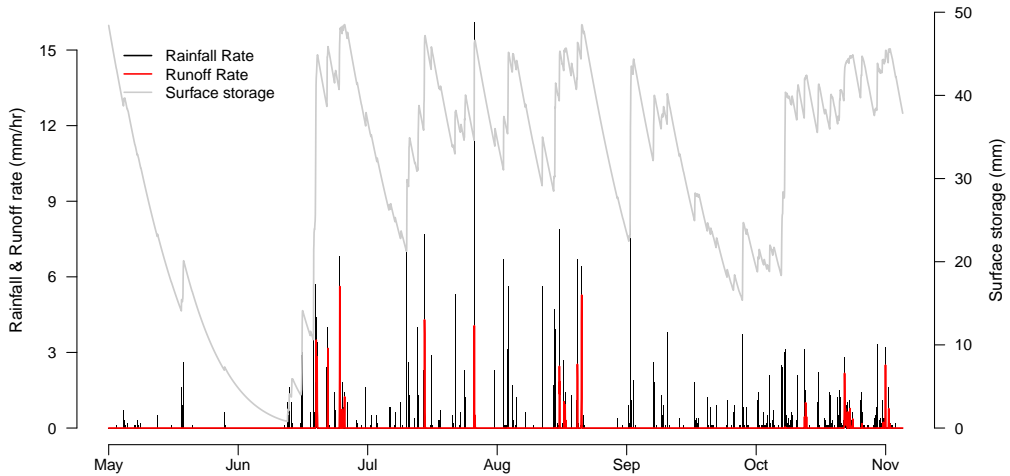


Figure 6.2: Rainfall and surface runoff rate and amount of water stored at the soil surface of a raised bog. The surface topography of the raised bog was based on elevation measurements in Männikjärve bog (Estonia) and a synthetic microtopography. The hourly precipitation data were measured in Männikjärve bog in 2009.

rate at boundaries between morphologies. Therefore, the total surface runoff rate of a bog will reflect the presence of these different morphological features.

6.3 Microtopography and response time in shallow ground-water ecosystems

A typical example of systems with shallow groundwater levels are raised bogs. Raised bogs are dome-shaped and have the groundwater level typically located within a few decimeters below the ground surface (Baird et al., 2008). Raised bogs develop from lakes or flat marshy areas, over mineral substrates. With time, the peat progresses to a level where it is only fed by precipitation and the groundwater develops an atmocline signature. At this point the bog starts to form its dome shape. In NW-Germany, Eggelsmann (1967) found an average dome-height of 5 m for 64 raised bogs with an average diameter of 6 km. These peat bodies drain horizontally by gravity to adjacent areas with lower groundwater levels. The integrity of these bogs is only ascertained when water is stored in the peat body in periods of a precipitation deficit and efficiently removed in wet periods (Tsuboya et al., 2001; Baird et al., 2008). The vegetation that constitutes the raised bogs requires shallow groundwater levels to avoid consolidation and mineralization, but cannot survive prolonged periods of flooding. To maintain a relatively stable water table, the bog's top layer swells in response to precipitation excess, and shrinks under evaporative demand, thereby influencing its hydraulic conductivity, while deeper layers have a much lower hydraulic conductivity as a result of compaction

despite water contents up to 90 % (Rycroft et al., 1975; Rezanezhad et al., 2010).

The surface topography of peatlands (Fig. 6.3 features examples) consists of several morphological features: pools, wet depressions with *Sphagnum* species and sedges (hollows), stretches of *Sphagnum* species (lawns), drier mounds with *Sphagnum* species and vascular plants (hummocks), and higher, drier areas with terrestrial vegetation (ridges) (Wallen et al., 1988; van Breemen, 1995; Belyea and Clymo, 2001). Hummocks and hollows have a characteristic spatial scale of 10–100 m², and reported heights from a few centimeters to over 50 cm. On bogs, the higher ridges can feature smaller scale compositions of lawns and hummocks, whereas on fens the ridges tend to have a more uniform small scale surface topography. In boreal to sub-arctic zones, and sometimes in maritime and alpine parts of the mid-temperate zone, raised bogs are characterized by a surface pattern of pools and ridges (Belyea, 2007). Pools form secondarily on such bogs and the cause of their formation remains an open question. The width of the pools ranges from less than 1 m on sloping sites to over 100 m in flat areas. Once formed, the topographic features are sustained by a positive feedback mechanism, in which hummocks and ridges have a higher growth rate in comparison to hollows and pools and therefore keep their elevated position in the peat bog (Sjors, 1990; Belyea and Clymo, 2001). Ridge-pool patterning mainly orients perpendicular to a bog's slope and has a profound influence on surface runoff by determining the length and orientation of flowpaths. In wet periods, the depression storage capacity of pools may be exceeded, leading to coalescence of pools and rapid drainage by surface flow (Quinton and Roulet, 1998). In addition, microtopography increases species richness in peatlands and other wet ecosystems (Vivian-Smith, 1997; Peach and Zedler, 2006). An increase in species richness can directly influence the routing of surface runoff. It was shown by Holden et al. (2008) that *Sphagnum* provided a greater effective hydraulic roughness than peatland grasses. Variation in hydraulic roughness may have an influence on the convergence or divergence of surface runoff, in turn affecting the amount of water a neighboring patch of vegetation receives. Similar feedbacks are found in semi-arid areas where vegetation patches influence hydraulic conductivity and direction of flowpaths (Bergkamp, 1998; Rietkerk et al., 2002; Mueller et al., 2007).

The structure and the hydraulic properties of raised bogs make a sharp distinction between the surface and the subsurface difficult. In the mid-twentieth century, Russian scientists therefore separated surface and subsurface processes with the acrotelm-catotelm concept to explain peatland functioning. The concept comprises an upper active “acrotelm” layer with a high hydraulic conductivity, storage capacity, and a fluctuating water table and a more inert lower “catotelm” layer that corresponds to the permanently saturated main body of peat (Romanov, 1968; Ivanov, 1981). Outside Russia, the acrotelm-catotelm concept was adopted by Ingram (1978) who considered it a fundamental concept for all understanding of the hydrology, ecology, and pedology of peatlands. The distinction between acrotelm and catotelm is a conceptual one, the layers cannot be separated in the sense of physical or morphometrical properties like soil

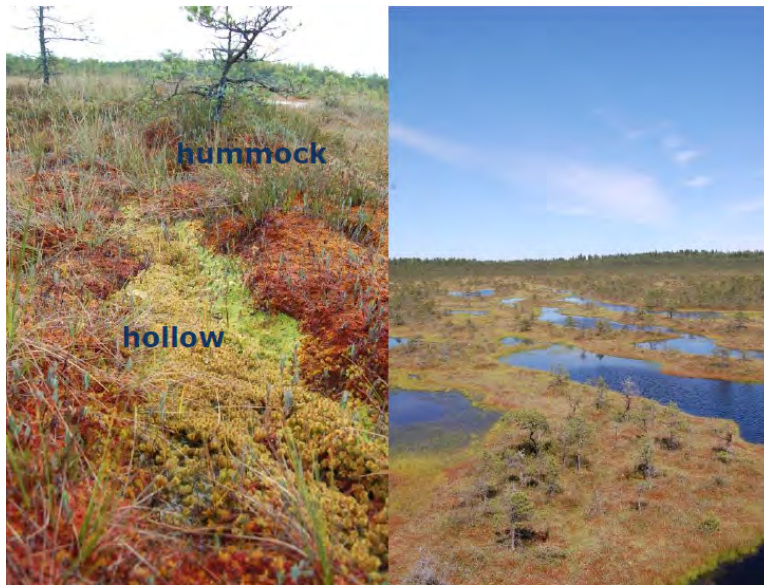


Figure 6.3: Surface topography at two spatial scales on Männikjärve raised bog in Estonia. Left: a hollow surrounded by hummocks, right: secondary formed pools between ridges.

horizons. The concept is mainly based on the position of the lowest groundwater level during a year with drought. Clymo (1984, 1992) defined acrotelm and catotelm differently, by partitioning the oxic and anoxic decomposition of peat. This concept is often used in peatland decomposition and accumulation studies (e.g. Frolking et al. (2001)). Both definitions were then mixed and perceived as linked (Morris et al., 2011), and nowadays they are used regularly in ecohydrology and peat-development modelling.

In the acrotelm-catotelm concept the raised bog is modeled with a groundwater equation based on Darcys law and the equation of the conservation of mass. The acrotelm is treated as an aquifer layer, and the catotelm as an aquitard. The concept definition implies that most runoff will occur within the upper peat layer, close to or at the peat surface as groundwater flow, and that this layer (the acrotelm) has a hydraulic conductivity that is much larger than that of the lower catotelm layer. Reported hydraulic conductivities for the catotelm range from 10^{-4} to 10^2 m d^{-1} (Rycroft et al., 1975; Chason and Siegel, 1986), which sometimes raises the question if the catotelm acts as the aquitard or rather the underlying sediment (Reeve et al., 2000). In the acrotelm hydraulic conductivities are highly variable. Rosa and Larocque (2008) reported hydraulic conductivity variations over a factor of 44 within the upper 40 cm of the acrotelm, and may exceed values of 10^5 m d^{-1} (Holden and Burt, 2003a; van der Schaaf, 2004). Hydraulic conductivities in peat also depend on the formation of methane gas bubbles that may block pores and decrease the hydraulic conductivity (Baird and Gaffney, 1995; Beckwith and Baird, 2001).

Although the acrotelm-catotelm concept has broad utility, it ignores the important

role of macropores and soil pipes in connecting deep and shallow parts of a peat profile (Holden and Burt, 2003b). All ecological, hydrological and biochemical processes and structures have to be explained by a single boundary, rendering the concept inflexible, and incapable of representing a range of ecohydrological phenomena (Morris et al., 2011). These phenomena include heterogeneity in the structure and function of bogs, fast processes occurring near the surface and interactions between peat growth and hydrological processes (Belyea and Baird, 2006). The horizontal spatial heterogeneity found in peat properties is linked to the topographic features found in peatlands (Waddington et al., 2010). This spatial variability impacts flow patterns over the bog (Lapen et al., 2005; Baird et al., 2008; Eppinga et al., 2009). Ronkanen and Kløve (2007) used both oxygen and hydrogen isotopes as well as conventional tracers (KBr, KI) in tracer tests to find water flow paths in a treatment system established on natural peatland in Finland. They found that beside preferential flow paths, water flows mainly in the top of the peat layer. This implies that for the water flow dynamics in peatlands, surface flow processes need to be considered and that an integrated approach of surface and subsurface flow is desired. Considering fast and slow water movement in raised bogs by combining surface runoff and groundwater flow would allow to account for vegetation, related (micro)topography and preferential flowpaths; important three-dimensional components of peatland hydrology (Waddington et al., 2010) that cannot be fitted into the acrotem-catotelm concept. Adding a concept capturing the effect of surface topography on water flow, as a different approach to model peatland hydrology will, even with a simple approach as described in the previous section (Fig. 6.2), increase the understanding of the hydrological functioning of raised bogs.

In ecosystems such as raised bogs and lowland peats, the hydrology and vegetation are adjusted to each other. Besides routing surface runoff, microtopography influences characteristic response times of the groundwater-surface runoff system, the relevance of which we show here by considering the groundwater system as a linear reservoir, drained by a set of parallel streams (Fig. 6.4). In the reservoir, the recession of the groundwater level after cessation of groundwater recharge ($R = 0$) is a function of time (Kraijenhoff van de Leur, 1958):

$$h(t) = h(0)e^{-\frac{t}{j}} \quad (6.1)$$

where $h(t)$ is the groundwater level [L] relative to surface water level at time t [T], $h(0)$ is the initial groundwater level, and j is the reservoir coefficient [T], which is the time in which the groundwater level drops by a factor e^{-1} or by 37 %. For a phreatic aquifer domain in between two parallel streams, schematized in Fig. 6.4, the equation of Kraijenhoff van de Leur (1958) is a good approximation of the reservoir parameter:

$$j = \frac{\mu L^2}{\pi^2 k D} \quad (6.2)$$

where L [L] is the distance between the streams (or ephemeral channels), μ [-] is the phreatic storage coefficient, k [$L T^{-1}$] is the hydraulic conductivity, and D the average thickness of the phreatic aquifer [L]. The reservoir coefficient can be used to simulate the

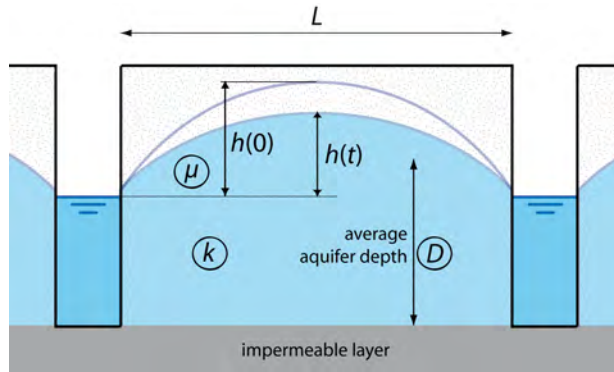


Figure 6.4: Schematization of field between two major streams. L is the distance between the streams, μ the phreatic storage coefficient, k the hydraulic conductivity, D the average thickness of the phreatic aquifer, $h(0)$ is the initial groundwater level between the streams, and $h(t)$ the level at designated time t during the recession period.

dynamics of the groundwater level as a function of groundwater recharge (Kraijenhoff van de Leur, 1958; Bierkens and van den Hurk, 2007). It gives insight in the dynamics of the groundwater level: if j is small, the level reacts quickly to inputs and if j is large it reacts slowly. The j -values range from 1 d for small wet systems to 1000 d for large dry systems. Examples of values of the reservoir parameter and its constituents are given in Table 6.1.

At a smaller scale (j -range less extensive), the reservoir concept is relevant for wetlands too. Small values of j imply that the groundwater level fluctuations are small and the horizontal discharge q , proportional to h , will quickly flatten out the water table. Hence, large systems (large L) that respond slowly lead to a large value of j , while highly conductive materials (coarse sand, gravel) allow groundwater to flow quickly, and lead to a decrease of j . This equation suggests that geometry (L) has a larger effect on groundwater level response than hydraulic properties and neglects slight topographical height variations: the equation mainly emphasizes the importance of the distance between draining streams. Both the loss of storage in time and the resistance to water flow are proportionally related to L , therefore j depends on L^2 . It is interesting, though, that when k and D are large, a large distance L between draining streams will be sufficient to discharge all precipitation in wet periods. Likewise, when water flow in the

Table 6.1: Values for the reservoir parameter and its constituents of two hydrological systems (Werk-groep Herziening Cultuurtechnisch Vademecum, 1988; Hendriks, 2010).

	μ (-)	L (m)	k (m d ⁻¹)	D (m)	j (d)
Managed fen	0.1	10	0.10	4	2.5
Ice pushed ridge	0.3	1000	5	30	203

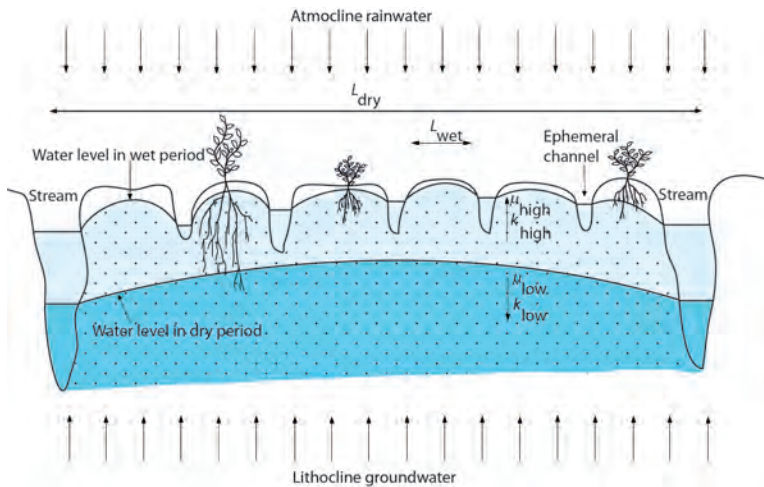


Figure 6.5: Self-organized ecosystem, where feedback processes between hydrology and topography create favorable conditions for various plant species.

soil is slow due to small kD , a fast discharge of precipitation can only be obtained when systems develop a small distance L between draining streams. Such streams develop by soil erosion in wet periods, when saturation excess surface runoff occurs in microchannels. Hence, kD and L are related in (semi-) natural systems.

In wet ecosystems, j varies considerably with the groundwater level. The j -function is an ecosystem feedback function as in wet periods both L and j are small and rainwater is quickly discharged, whereas in dry conditions L and j are large and water is retained. This feedback can be considered an example of hydrologic self-organization.

The surface of natural wetlands is characterized by a complex pattern of ephemeral channels and streams and intermediate higher terrain. A broad variety of patterns has been observed (Larsen and Harvey, 2011), most of which can be conceptualized as a complex of nested systems (Fig. 6.5). In prolonged wet periods, a wetland ecosystem features a small reservoir coefficient because the hydraulic conductivity is large and L_{wet} is small, even though the storage coefficient maybe higher than in dry periods, especially in peat soils. Under prolonged dry conditions (when $L = L_{dry}$ and hydraulic conductivity is small) the reservoir coefficient is large. This corresponds conceptually with the acrotelm-catotelm concept: the fast acrotelm flow is characterized by a small reservoir coefficient and the slow catotelm flow by a large value. The self-organization of the system with regard to the hazards of drought and wetness are in essence captured adequately with the dependence of j on k , L , and μ . The above illustration reveals that horizontal drainage distance is the key determinant of the response time of the system. In essence, the presence of nested systems of streams and channels ensure optimal growth conditions for the wetland vegetation, because these systems enable both the discharge and the storage of water under conditions where either of the two is most needed.

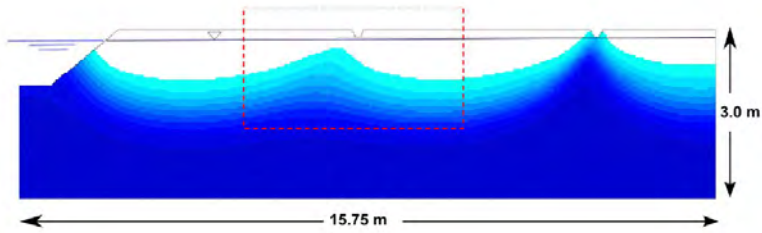


Figure 6.6: Calculated transition zone between young infiltrated precipitation water (white) and older upward seeping groundwater (blue), as affected by small ephemeral channels. Calculations were performed with Hydrus-2D for a loamy sand soil with an upward seepage flux of 0.6 mmd^{-1} . The red dashed box indicates the position of Fig. 6.7.

6.4 Microtopography and spatial distribution of groundwater quality parameters and site factors

As was mentioned in the previous section, it is plausible that complex patterns of ephemeral channels and streams in wetlands affect the hydrological response of the groundwater systems. However, this is not the only impact of draining channels and streams. In areas with upwelling groundwater, infiltrating precipitation water meets groundwater with a different chemical signature and is diverted towards the streams. The volume that is characterized by the atmocline water is lens-shaped and for this reason, such water bodies are called rainwater lenses. The interface between atmocline water and the lithocline deeper groundwater is located deepest at the hydrological divide and monotonously becomes shallower in the direction of streams where exfiltration occurs. This general pattern, depicted by e.g. Schot et al. (2004); Dekker et al. (2005) for fresh water systems and Eeman et al. (2011) for a rainwater lens on saline groundwater, becomes much more complicated when (small) channels convey surface runoff during a limited wet period only. In those periods, part of the infiltrating precipitation does not flow towards the main streams, but towards these more shallow ephemeral channels (Fig. 6.6). Close to these channels, the hydraulic gradient is directed towards the shallow draining channels (Fig. 6.7) and the interface between atmocline and lithocline water becomes situated closer to the soil surface. As Fig. 6.6 shows, the interface cones up at places where channels drain by surface flow, thereby mirroring the topography of the soil surface at these places. The interactions described above will of course depend on the ratio of upward and downward fluxes and the duration of high groundwater levels and consequent activation of ephemeral channels.

Ecologically, the interaction between soil surface and groundwater quality is important. Obviously, the proximity of the phreatic groundwater level is important for the availability of oxygen to plant roots, which directly, via oxygen stress (Bartholomeus et al., 2008) and indirectly, via redox processes (Hinsinger et al., 2009; Koch et al., 1990; van der Welle et al., 2008), and the release of nutrients by mineralization (Koerselman

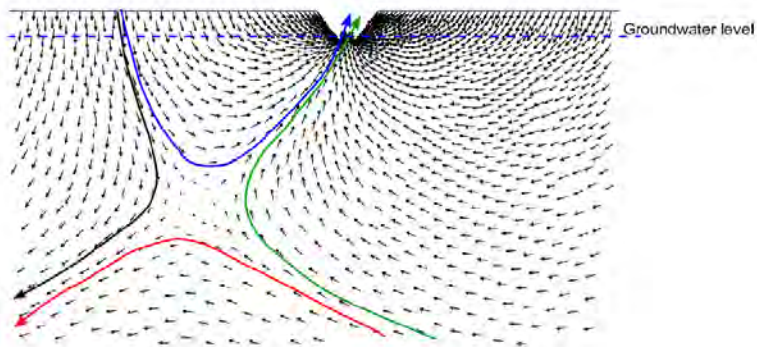


Figure 6.7: Flow pattern as affected by an ephemeral channel during a wet period.

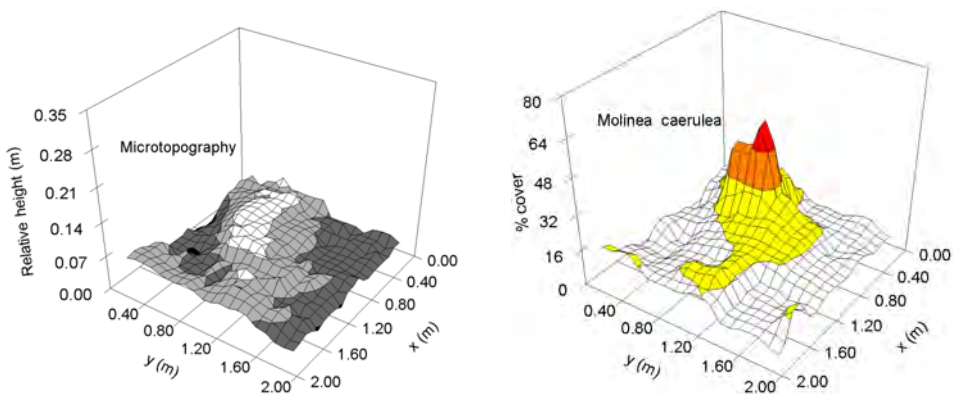


Figure 6.8: Microtopography and relative cover of *Molinia caerulea* in a seepage dependent wetland area. Data from fen meadow reserve “Het Meeuwenkampje” in the Netherlands (Nijp, Nijp). Microtopography was measured with a pinmeter on a 5–10 cm grid. Vegetation was mapped on a 25–25 cm grid.

et al., 1993), affects plant species composition. In view of the different chemical signatures of atmocline and lithocline water, zonation will also occur with regard to acidity, nutrient (NPK) availability, and calcium availability. An illustration of the relation between the occurrence of a plant species (*Molinia caerulea*) and microtopography in a wetland setting is given in Fig. 6.8. *Molinia*, a drought and acid tolerant plant species, is clearly more abundant on the higher and thus dryer and possibly more acid ridges.

As was hypothesized by van Wirdum (1991) and shown by Vivian-Smith (1997) and Peach and Zedler (2006), vegetation can, especially under wet conditions, respond to very subtle topography variations. Although it is clear that microtopography can significantly influence patterns of groundwater flow (Frei et al., 2010), it proves difficult to pinpoint the actual driver for the distribution of plant species over a height gradient.

This is due to the strong correlation between microtopography and important site factors such as soil moisture status, soil aeration and pH. Moreover, the feedback between vegetation and microtopography can be self-enhancing. *Molinea* for instance forms tussocks due to the production of large amounts of litter that is hard to decompose and thus increases local elevation. In a groundwater fed wetland, this increase in elevation will in turn result in more aerated conditions and less influence of groundwater and as a result more acid conditions. This possibly results in competitive advantage for *Molinea* compared to co-occurring species adapted to wet, alkaline conditions.

6.5 Closing remarks

In this paper we have discussed some of the interactions between surface runoff and groundwater flow under the influence of microtopography in flat ecosystems with shallow groundwater levels. Microtopography creates a complex spatiotemporal pattern of ponding and redistribution, which in turn results in variability of infiltration into the soil. Microtopography also influences the exfiltration of groundwater and the residence time of water in the system. The in- and exfiltration fluxes of groundwater directly influence the dynamics of chemical transport in the rainwater lens, deeper groundwater, and in particular the transition zone between the two. Dynamics in fluxes and chemistry impact the occurrence of vegetation, and vegetation enhances the spatial variation of soil saturation and microtopography.

Therefore, aggregating the nested structure of microtopography into a roughness parameter hampers interpretation of the ecohydrology of flat ecosystems with shallow groundwater levels. Despite much ecological research, the impact of flow and (solute) transport processes on vegetation and possible feedbacks have received little attention from the physics point of view, although the impact of e.g. anaerobicity, and acidity on vegetation development have been demonstrated.

To deal with such complexity, both high resolution data and software tools are needed for an improved prediction of surface runoff and soil surface water redistribution. Modelling the interaction between surface runoff and groundwater flow under the influence of surface complexity in a fully physical way remains a computational challenge, permitting the use of simple conceptual alternative modelling strategies. This type of models allows a thorough sensitivity analysis of combining several scales of spatial complexity and examine the effect on spatial variability of hydrological and other site factors in ecosystems with a shallow groundwater level. The increasing availability of detailed topographical data (e.g. LiDAR) of these ecosystems in various regions of the world allows a better investigation of the relation between topography and vegetation patterns. Comparing measured complex topographies with synthetic ones at an increasing level of complexity, will facilitate the understanding of the complex interactions governing the hydrologic responses in these ecosystems.

Acknowledgement

This study was carried out within the framework of the Netherlands Organization for Scientific Research (NWO) CASIMIR programme (018.002.007), the Dutch Water Utility Sector joint research programme (BTO) and the Knowledge for Climate programme.

Parts of this work have been sponsored by the Dutch Ministry of Agriculture OBN-Hoogveen research programme, and Alterra (Wageningen UR), the Netherlands.

Chapter 7

General Discussion

7.1 Summary of results

Surface runoff is the fastest flow route of water through a catchment that transports large amounts of sediment and nutrients. The complexities involved in measuring and modelling surface runoff, especially in flat areas and areas where the climate is such that the process is rare, make that the estimation of surface runoff contribution to the water balance in these areas is not very exact. More specifically, the interactions between surface runoff controls and the role of the soil surface in transporting water to streams has not been given appropriate attention.

The general aim of the research presented in this thesis was *to investigate and quantify the development of surface runoff on relatively flat soils of catchments in temperate climate zones*, based on the questions “What are the main driving mechanisms of surface runoff in these catchments?”, “What rainfall conditions prevail during surface runoff events?”, and “How do flow routes develop during surface runoff events in various types of surface topography?”. The aims and the results of the individual chapters are summarized below.

Aim: to understand how indicators of hydrological connectivity respond to spatial heterogeneity in terms of microtopography and infiltration parameters.

For synthetic surfaces with identical statistics, but varying spatial positioning of microtopography, normalized surface runoff curves can be used as an indicator for hydrologic connectivity, both on impermeable and infiltrating surfaces. The microtopography smoothens away spatial variability of infiltration characteristics as long as the typical length scales of these characteristics do not exceed that of the microtopography.

Aim: use various monitoring and auxiliary information to give an integrated narrative of surface runoff for two field sites in flat, lowland catchments in the sandy part of The Netherlands.

Under the rare conditions required to generate a surface runoff flux to the open water system, up to 10 % of the event precipitation can leave the field as surface runoff, both for loamy and sandy soils and easily overcoming storage thresholds from mesotopography features on the soil surface. Large contributing areas were observed during the surface runoff events, with multiple spillpoints towards streams and ditches. Snowmelt surface runoff events were of smaller size and impact than saturation excess surface runoff events. In this type of catchments, the formation of surface runoff is a two-stage process with thresholds from storage capacity of the unsaturated zone and the surface topography.

Aim: to quantitatively understand how surface runoff development is affected by the presence of a shallow groundwater table, and how micro- and mesotopography affect surface runoff development under saturation excess conditions.

The feedbacks included in the FAST-Runoff model (Chapter 4) provided dynamic sorptivity and specific yield. The specific yield feedback was clearly visible in the increased non-linearity of the groundwater table increase and decrease. Under saturation excess conditions, the amplitude of the microtopography is more important for the surface runoff behaviour than its spatial structure. Mesotopography affects surface runoff development under saturation excess conditions by actually rerouting ponding water over longer distances. The infiltration of water in mesotopographic depressions decreased the gradient of the groundwater table over a large part of each field, thereby decreasing groundwater flow.

Aim: to explain differences in measured surface runoff volumes and nutrient concentrations of surface runoff between fields by characteristics of their meso- and microtopography and to investigate whether the performed plot scale measurements were representative for the surface runoff behaviour of the whole field.

The effect that microrelief has on flow route shapes in flat fields can be quantified with metrics from simple surface runoff curves. The groundwater dynamics and the depth of the unsaturated zone were found to account for a spatially variable initiation of ponding and surface runoff. However, this spatial variability could not be linked to the full meso- and microtopographies of the fields. The FAST-Runoff model (Chapter 4) could not be operated on the desired scale and discretization. Even though the model complexity was reduced, the non-linearities introduced by the dynamic specific yield, could only be treated at very small timesteps resulting in very long computation times.

Aim: to discuss the influence of microtopography on mass transfer processes just above and under the surface from an ecohydrological perspective in flat ecosystems.

Aggregating the nested structure of microtopography into a roughness parameter hampers interpretation of the ecohydrology of flat ecosystems with shallow groundwater levels. The increasing availability of detailed topographical data and development of conceptual alternative modelling strategies, such as proposed in Chapter 6 for raised bogs, allow a better investigation of the relation between topography and vegetation patterns by means of thorough sensitivity analyses combining several scales of spatial complexity.

Though process oriented studies on surface runoff in flat, agricultural areas as described here, have been performed before, there has been little systematic investigation into controls on and relations between driving mechanisms of surface runoff in these areas. The results presented in this thesis provide new insights into the complexity of processes and feedbacks involved in surface runoff generation on flat surfaces under conditions of infiltration and saturation excess. The results can be used to parameterize larger scale distributed models and suggest the steps that are needed to improve larger scale estimations of surface runoff risk and impact.

7.2 Synthesis

As the measurement campaigns presented in this thesis show once more, surface runoff events are rare in flat, well-drained, agricultural catchments in temperate climate zones. Events occurred in winter and early spring and were driven by saturation excess. Though the time period over which the measurements presented in Chapter 3 were performed, was shorter than that of the measurements presented in Chapter 5, the events of winter 2010 occurred during the same days at the two locations (they are approximately 100 km apart). This suggests that larger scale rainfall characteristics are the dominant factor in creating the right initial conditions for surface runoff to occur somewhere during a short time period. The total volumes of surface runoff measured at the field sites was fairly small as were the nutrient loads involved, even though some of the numbers presented in Chapter 5 underestimated the total volumes and loads, because one of the major surface runoff events was not measured. The variation in the number of events per season that was found in Chapter 5, was also reflected in the mesotopography simulations of Chapter 4, where stochastically generated rainfall timeseries resulted in differences of cumulative surface runoff volumes of up to one order of magnitude. Whereas surface runoff events were mainly measured from January to April, the simulations featured the largest events in October and November. This might be due to some artefacts of the rainfall timeseries (parameters for the rainfall simulation model were derived from 10 year rainfall data, a timespan that may have been too short) or to the use of constant boundary conditions in the simulations, whereas ditch levels rise during the winter season.

Given the dominance of saturation excess over infiltration excess as a driving mechanism, the formation of surface runoff flow paths towards streams and ditches is a two-stage process. The storage capacity of the unsaturated zone and surface topography are both thresholds that need to be exceeded to form a continuous flow path over the soil surface. The filling of the surface topography (i.e. overcoming the second threshold) starts when the rainfall rate exceeds the groundwater flux, which determines the infiltration rate under saturated conditions. This type of surface runoff initiation could also be characterized as the “Dunton” hybrid mechanism that contains both aspects from saturation and infiltration excess runoff (Loague et al., 2010).

The importance of initial wetness of the soil on surface runoff was also emphasized in the numerical experiments of Chapter 4. The smaller the average soil water storage capacity is, the earlier surface runoff will spill from field to ditch: the first threshold is relatively small. However, the spatial distribution of soil water storage capacity also plays a role. For a specified average storage capacity, in a field with a larger spatial variability there are locations that are closer to saturation than in a field with a smaller variability. These close-to-saturation patches will spill excess water to adjacent locations and contribute to a faster growth of saturated areas throughout the field.

The spatial structure of microtopography, i.e. random, rivers, or craters in the microscale, determined the development of hydrological connectivity in otherwise statistically identical surface topographies under infiltration excess conditions (Chapter

2). The average elevation of spillpoints of the depressions differed in these spatial structures and resulted in different ratios between contributing area and ponding area of these topographies. Spatially varying infiltration characteristics delayed the filling of the depressions and the formation of flow routes. However, the mutual activation of these routes was not so much affected, because the filling of the depressions in the microtopographies provided an averaging mechanism. The patterns of development of hydrological connectivity of the different spatial structures remain distinctively different from each other and similar to their no-infiltration characteristic, as long as the correlation scales of infiltration characteristics have the same size as those of the microtopography.

Under saturation excess conditions the correlation scale of the infiltration characteristics (in this case not determined by hydraulic conductivity, but by soil water storage capacity) are larger than the correlation scale of the microtopography, so one would expect flow routes to change a lot. They do in such a way that the spatial structure of the topographies is not distinguishable anymore (Chapter 4). Since ponding now starts in the middle of the field, there is no gradual growing inward from flow routes originating at the field boundaries. Instead, there are only breakthroughs of large, saturated and completely filled depressions, merged into a single flow route. The structures of the microtopographies are too small to have an effect on the hydrological connectivity development. Only their function of surface storage, i.e. the second threshold of the surface runoff process (Chapter 3), remains.

In the schematized fields with mesotopography presented in Chapter 4, excess water was rerouted to a location in the field that was not necessarily as close to saturation as the location where it originated from. The infiltration of water in mesotopographic depressions decreased the gradient of the groundwater table over a large part of each field, thereby decreasing groundwater flow. This effect increased when the mesotopographic depressions were located closer to the ditches, because the area over which the groundwater table was levelled increased. The combined effect of reinfiltration and groundwater flow, increased the variability of surface runoff discharge into the ditches under statistically similar precipitation events.

In the real agricultural fields of Chapter 5, mesotopography was not schematized and microtopography was not exclusively Gaussian. Where distinctive mesotopographic lows were present, initiation of ponding shifted from right between the ditches towards these lows. The simulation of ploughing rills on the mesotopographies actually affected surface runoff patterns in the context of a changing hydrological connectivity, because they transported water over large distances. In these fields, the interactions between mesotopography, microtopography, and groundwater recharge and drainage were more complex, resulting in large spatial differences of ponding development. Unfortunately, applying the FAST-Runoff model to these fields to investigate this rerouting proved to be infeasible. The timestep criterion based on the size of the specific yield (Chapter 4), resulted in very small timesteps when part of the field was close to saturation. The

relatively small grid cell size chosen in the fields to characterize the microtopography resulted in an excessive computation time. An improvement of the FAST-Runoff model should therefore consist of a reduction of the number of calculations to be performed. Such a reduction can be achieved by assuming that soil columns have a larger area than the soil surface grid cells. Conceptually, such an assumption would be reasonable, because it is very unlikely that the groundwater table shows the same amount of roughness as the soil surface: instead it is much smoother and may be more closely related to a coarse DEM than a fine DEM (Sørensen and Seibert, 2007).

Considering these limitations of the FAST-Runoff model that I developed in the framework of this thesis, one might wonder, why not use HydroGeoSphere (Therrien et al., 2008) after all? A full sensitivity analysis would not have been possible, but at least one full simulation might have succeeded. To my opinion this would not have created much extra insight into the interactions between the various surface runoff controls. The relationships between these controls, i.e. the microtopography, the groundwater levels, infiltration characteristics, are in itself so complex and partly erratic that it would be very complicated to really figure out what the model was trying to communicate (Tipper, 2008).

The focus areas of this PhD project were flat agricultural areas such as those found in The Netherlands. However, the concepts and modelling as developed in this research can be applied to other flat shallow groundwater ecosystems where flow patterns and runoff generation are a result of filling and spilling of depressions. This may provide options to improve the characterization of site factors in wet ecosystems, such as in the raised bogs presented in Chapter 6.

7.3 Perspectives for process oriented research

Follow up opportunities with respect to modelling and measuring small scale surface runoff generation are:

- In addition to the measuring of discharge at spillpoints around a field, the monitoring of ponding location and extent throughout a field and the monitoring of groundwater levels in a dense grid in such a field would yield more process insight in the activation of flow routes and the effects of reinfiltration on groundwater patterns.
- The increased availability of high resolution elevation data of mesotopography provides an excellent opportunity to further investigate generic properties of the mesotopography, similar to the statistical characterization that was provided in this thesis for microtopography. It would also be interesting to combine these elevation data with remotely sensed data of surface wetness, to analyze ponding and surface runoff patterns.
- If computation times of surface runoff models can be reduced, relevant feedbacks on dynamics of the system itself under surface runoff generation (i.e. erosion and

sedimentation and the associated decrease of saturated hydraulic conductivity) can be included in the process modelling.

7.4 Perspectives for impact oriented research

To arrive at an improved estimation of surface runoff risk and impact on regional or catchment scale, the following steps could be taken:

- It is not feasible to measure surface runoff in every field of a catchment. However, the acquisition of soft data in the form of a Post Event Field Survey, as performed in Brauer et al. (2011), during a very wet winterweek to map ponding extent and spillpoint locations would presumably give more insight in the spatial variability of surface runoff events and ponding conditions.
- The combination of spatial databases on elevation, soil types, groundwater classes, and land use can be combined to derive sets of dynamic storage and surface runoff relationships for fields in a catchment. Similar to the use of the curves in Chapter 2, these relationships could be used as indicators of hydrological connectivity throughout a catchment.

7.5 Final conclusions

In order to come to a good quantification of surface runoff in flat, well-drained agricultural catchments in temperate climate zones, the controls on the generating mechanisms and the feedbacks between those need to be understood. When the generating mechanisms in a field are properly quantified, the activation of flow routes through micro- and mesotopography can be determined. This thesis has shown the dominance of saturation excess as a generating mechanism for surface runoff events in The Netherlands. The formation of surface runoff flow paths towards streams and ditches is therefore a double-threshold process, during which both the storage capacity of the unsaturated zone and that of the surface topography need to be exceeded. The activation of the flow paths in the micro- and mesotopography of a field depends on the generating mechanism. Spatial structures of microtopography are relevant in flow pattern delineation under infiltration excess surface runoff, and were statistically quantified in this thesis. Under saturation excess conditions, Gaussian patterns of microtopography only provide surface depression storage, whereas mesotopography position within a field affects the flow path behaviour, because excess water is routed over longer distances and the groundwater gradient is influenced by reinfiltration of water in the depressions. Although interfacing data with simplified models remains difficult, these results contribute to an increased understanding of the variables to monitor when a catchment is analyzed for surface runoff risk.

Appendix A

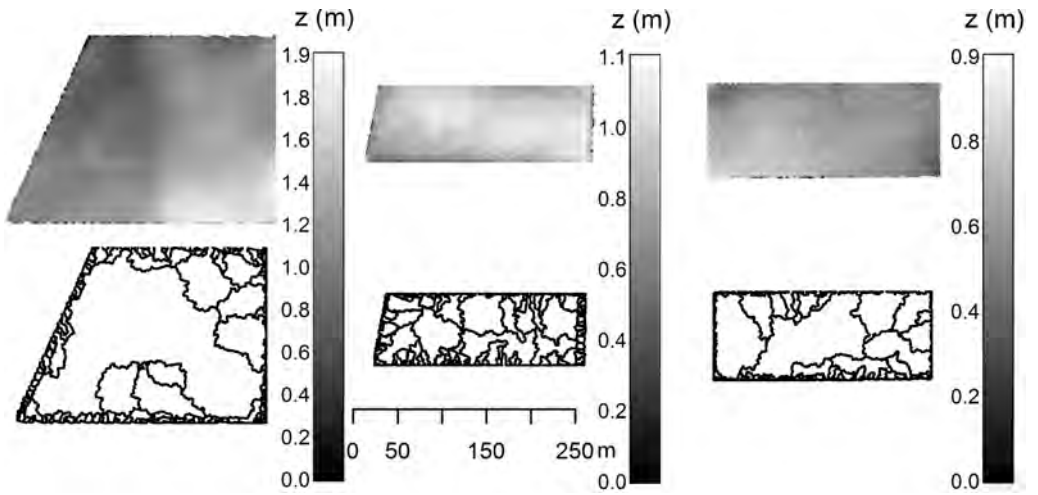


Figure A.1: DEMs of the fields with microtopography realization RA, grid cell size 0.1 m. In the second row, the flow route maps of the fields, obtained from the analysis with the FAST-Runoff model. From left to right field A, G, and H.

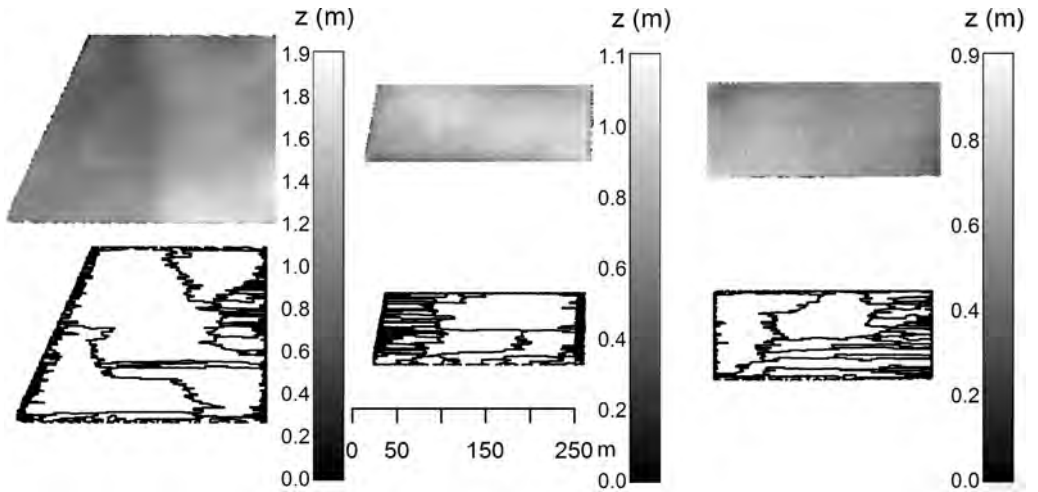


Figure A.2: DEMs of the fields with microtopography realization LH, grid cell size 0.1 m. In the second row, the flow route maps of the fields, obtained from the analysis with the FAST-Runoff model. From left to right field A, G, and H.

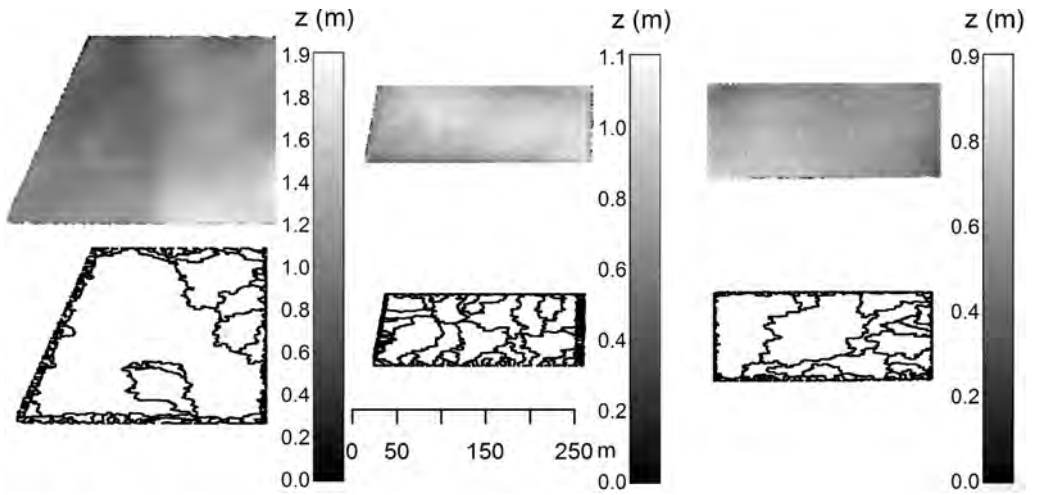


Figure A.3: DEMs of the fields with microtopography realization SH, grid cell size 0.1 m. In the second row, the flow route maps of the fields, obtained from the analysis with the FAST-Runoff model. From left to right field A, G, and H.

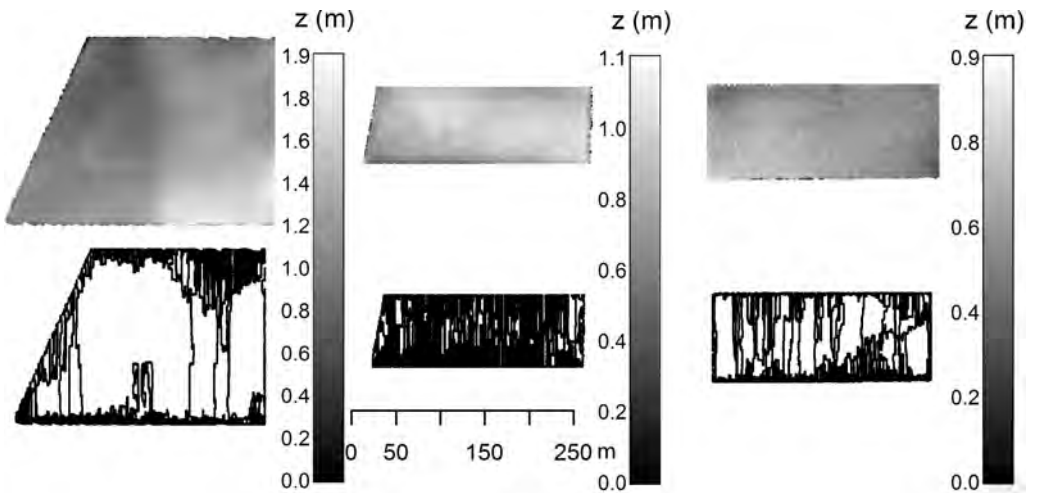


Figure A.4: DEMs of the fields with microtopography realization LV, grid cell size 0.1 m. In the second row, the flow route maps of the fields, obtained from the analysis with the FAST-Runoff model. From left to right field A, G, and H.

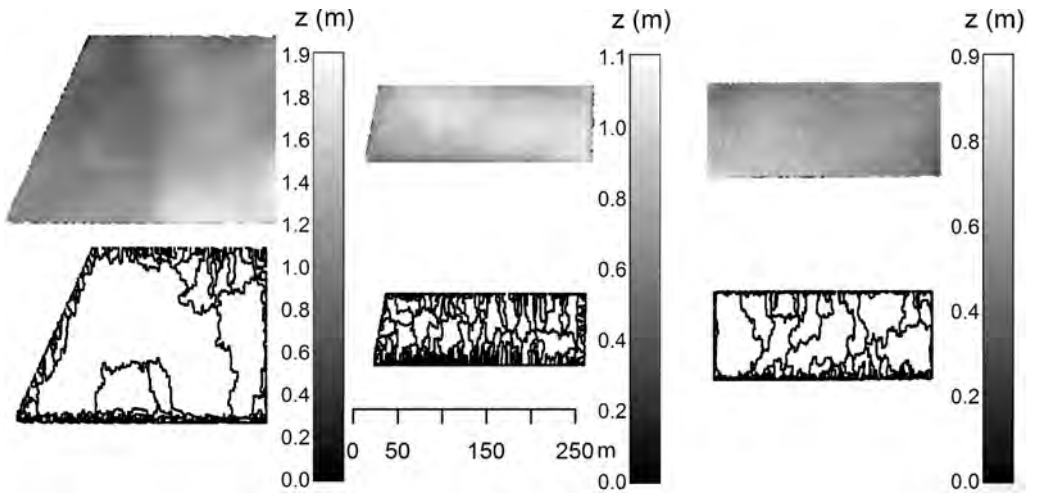


Figure A.5: DEMs of the fields with microtopography realization SV, grid cell size 0.1 m. In the second row, the flow route maps of the fields, obtained from the analysis with the FAST-Runoff model. From left to right field A, G, and H.

Summary / Samenvatting

English summary

Surface runoff is an important process that affects the local water balance and causes soil erosion and rapid solute transport towards ditches, streams, and rivers. Surface runoff is relatively rare in flat, agricultural areas in temperate climate zones and measuring and modelling the process is quite complicated. For this reason, there has been little systematic investigation into the controls on and the relations between driving mechanisms of surface runoff in The Netherlands, though surface runoff budget studies have been performed before. More specifically, the interactions between surface runoff controls and the role of the soil surface in transporting water to streams has not been given appropriate attention. The general aim of this thesis is to investigate and quantify the development of surface runoff on relatively flat soils of catchments in temperate climate zones.

In Chapter 2, a ponding and redistribution model is presented that simulates the flow of water over a surface with a heterogeneous microtopography with or without infiltration of water into the soil. With this model, the functional hydrological connectivity of synthetical elevation fields with varying statistical properties was investigated. The connectivity behaviour was determined by the presence of depressions with a large area compared to the field area and by the spatial organization of the microtopography in rills or channels. The presence of microdepressions suppressed the effect of the spatial variation of infiltration properties. In Chapter 3, surface runoff measurements from two agricultural fields in the sandy part of The Netherlands are presented. These data were combined with auxiliary information to give an integrated narrative of surface runoff in flat, lowland catchments. During the seven events that occurred during the measurement period, up to 10 % of the event precipitation left the field as surface runoff. When the events resulted from a combination of rainfall and melting snow, the area contributing to surface runoff was small and located close to the field boundaries. When the events were driven by saturation excess, the area contributing to surface runoff was larger and flow paths were relatively long, because the wettest locations within the fields were found at a large distance from the ditches. In the days preceding the events, ponding of water occurred in micro- and mesotopography at these wet locations. In this type of catchment, the formation of surface runoff was a two-stage process with thresholds from storage capacity of the unsaturated zone and the surface topography. The ponding and redistribution model was extended with a 2D groundwater model to further examine surface runoff generation in fields with micro- or mesotopography under saturation excess conditions (Chapter 4). When the groundwater table is shallow, a small addition of water to the groundwater reservoir can lead to a large rise of the water table. These dynamics were included in the model. Under saturation excess conditions, the amplitude of the microtopography was more important for the surface runoff behaviour than its spatial structure. Mesotopography affected surface runoff development under saturation excess conditions by actually rerouting ponding water over longer distances. The infiltration of water in mesotopographic depressions

decreased the gradient of the groundwater table over a large part of each field, thereby decreasing groundwater flow. The presence of mesodepressions effectively resulted in a nested hydrological system where smaller water bodies were activated when the amount of water stored in the system was large. Because of the nested activation, the effect of the specific structure of rainfall series was large and led to differences in total volume of surface runoff generated per season of one order of magnitude for statistically identical rainfall timeseries. The model developed in Chapter 4 was applied to real fields with varying micro- and mesotopography in Chapter 5 with the goal of explaining differences in measured surface runoff volumes and nutrient loads of surface runoff between those fields. The groundwater dynamics and the depth of the unsaturated zone were found to account for a spatially variable initiation of ponding and surface runoff. However, this spatial variability could not be linked to the full meso- and microtopographies of the fields. Even though the model complexity was reduced, the non-linearities introduced by the dynamic specific yield, could only be treated at very small timesteps resulting in too long computation times. In Chapter 6, the intricate relationships between microtopography, surface runoff, and ecohydrology in ecosystems with shallow groundwater tables are reviewed. The use of microtopography in modeling approaches was illustrated with two examples that feature a typical ecosystem with shallow groundwater under influence of microtopography. Microtopography could add flexibility to the acrotelm-catotelm concept in raised bog hydrology, by accounting for fill and spill processes along the sides of the bogs. Also, the effects of microtopography and surface runoff on the mixing of water with different chemical signatures and the subsequent results in variations of the occurrence of plant species were demonstrated.

In order to come to a good quantification of surface runoff in flat, well-drained agricultural catchments in temperate climate zones, the controls on its generating mechanisms and the feedbacks between those need to be understood. When the generating mechanisms in a field are properly quantified, the activation of flow routes through micro- and mesotopography can be determined. The results presented in this thesis provide new insights into the complexity of processes and feedbacks involved in surface runoff generation on flat surfaces under conditions of infiltration and saturation excess. The results can be used to parameterize larger scale distributed models and suggest the steps that are needed to improve larger scale estimations of surface runoff risk and impact.

Nederlandse samenvatting

Oppervlakkige afvoer is een belangrijk proces dat de lokale waterbalans beïnvloedt en de oorzaak is van bodemerosie en snel transport van opgeloste stoffen naar sloten, beken en rivieren. Oppervlakkige afvoer is tamelijk zeldzaam in vlakke landbouwgebieden in gematigde klimaatzones en het meten en modelleren ervan is complex. Alhoewel er verschillende meetstudies zijn uitgevoerd in Nederland, is er weinig systematisch onderzoek gedaan naar de mechanismes die het ontstaan van oppervlakkige afvoer sturen en de relaties tussen deze mechanismes. Preciezer geformuleerd, er is nog te weinig aandacht besteed aan de relaties tussen de sturende processen van oppervlakkige afvoer en de rol van het maaiveld in de afvoer van water naar het oppervlaktewater. Het doel van dit proefschrift is het onderzoeken en kwantificeren van de ontwikkeling van oppervlakkige afvoer op vlakke bodems van stroomgebieden in gematigde klimaatzones.

In hoofdstuk 2 wordt een model gepresenteerd dat de stroming van water simuleert over een oppervlak met een ruwe microtopografie met of zonder infiltratie van water in de bodem. Met dit model werd de functionele hydrologische connectiviteit onderzocht van synthetische topografieën met verschillende statistische eigenschappen. De ontwikkeling van connectiviteit werd bepaald door de aanwezigheid van depressies met een groot oppervlak ten opzichte van het totale oppervlak van het veld en door het ruimtelijke patroon van de microtopografie, variërend van ruggen tot kanaaltjes. De aanwezigheid van microdepressies onderdrukte het effect van ruimtelijke variatie van infiltratie-eigenschappen. In hoofdstuk 3 worden metingen van oppervlakkige afvoer van twee landbouwpercelen op zandgrond in Nederland gepresenteerd. De eigen meetgegevens werden gecombineerd met extra informatie om een kwalitatieve reconstructie te maken van oppervlakkige afvoer in platte, laaglandstroomgebieden. Tijdens de zeven afvoermomenten in de meetperiode werd maximaal 10 % van de neerslag afgevoerd als oppervlakkige afvoer. Sommige incidenten ontstonden uit de combinatie van regen en smeltende sneeuw. In deze gevallen werd oppervlakkige afvoer vlakbij de sloten gegenereerd en was het oppervlak dat bijdroeg aan afvoer klein. In de gevallen dat een volledig verzadigde bodem de oorzaak was van oppervlakkige afvoer was het oppervlak dat bijdroeg aan afvoer groter en de stroompaden relatief lang, omdat de natste plekken van de percelen op grotere afstand van de sloten ontstonden. Plassen ontstonden op deze natte plekken in micro- en mesotopografie in de dagen voorafgaand aan de incidenten. Het ontstaan van oppervlakkige afvoer was op deze velden een proces met twee fases die gescheiden werden door drempels van bergingscapaciteit: een van berging in de onverzadigde zone en een van berging in de topografie van het bodemoppervlak. Het model voor waterstroming over een ruw oppervlak werd uitgebreid met een tweedimensionaal grondwatermodel om het ontstaan van oppervlakkige afvoer onder verzadigde omstandigheden verder te analyseren (hoofdstuk 4). Als de grondwaterspiegel ondiep is, kan een kleine toevoeging van water aan de verzadigde zone leiden tot een grote stijging van de grondwaterspiegel. Het model simuleert deze dynamiek. Onder verzadigde omstandigheden is de afmeting van de microtopografie

belangrijker dan de ruimtelijke structuur voor de ontwikkeling van oppervlakkige afvoer. De infiltratie van water in grotere plassen verkleinde de gradiënt van de grondwaterspiegel in een groot deel van de percelen en verlaagde daarmee de horizontale grondwaterstroming. De aanwezigheid van mesotopografie resulteerde daarmee in een genest hydrologisch systeem waarin kleinere waterlopen geactiveerd werden wanneer er meer water in het systeem geborgen werd. Door de geneste activering, was het effect van de specifieke volgorde van regenbuien groot en leidde dat tot verschillen in totale oppervlakkige afvoer per seizoen van één orde grootte voor statistisch identieke neerslagseries. Het complete model werd toegepast op drie percelen in Noord-Limburg met als doel het verklaren van gemeten verschillen in volumes van oppervlakkige afvoer en de nutriëntvrachten in die afvoer op de percelen (hoofdstuk 5). Grondwaterdynamiek en de diepte van de onverzadigde zone waren de belangrijkste factoren in het ruimtelijk variërende patroon van begin van plasmvorming en oppervlakkige afvoer. Helaas kon deze ruimtelijke variatie niet worden verbonden aan de complete meso- en microtopografie van de percelen. Zelfs met het versimpelde model konden de niet-lineaire vergelijkingen alleen maar opgelost worden met hele kleine tijdstappen, waardoor de rekentijd te lang werd. In hoofdstuk 6 worden de intrinsieke relaties tussen microtopografie, oppervlakkige afvoer en ecohydrologie in ecosystemen met ondiepe grondwaterspiegels bekeken. Het gebruik van microtopografie in modelaanpakken werd geïllustreerd aan de hand van twee voorbeelden van typische ecosystemen met een ondiepe grondwaterspiegel en invloed van microtopografie. In vergelijking met het acrotelm-catotelm concept, kan microtopografie meer flexibiliteit bieden in het modelleren van de hydrologie van hoogvenen, door het vullen en overstromen van plassen op de flanken van het hoogveen te simuleren. Daarnaast werden de effecten van microtopografie en oppervlakkige afvoer op het mixen van water met verschillend chemische afdranken en de resulterende variaties van standplaatsfactoren (vegetatiepatronen) aangetoond.

Om te komen tot een goede kwantificering van oppervlakkige afvoer in platte, goed-gedraineerde, agrarische stroomgebieden in gematigde klimaatzones, moeten de mechanismes die het ontstaan van oppervlakkige afvoer sturen en de terugkoppelingen tussen deze sturende mechanismes worden begrepen. Wanneer de processen die afvoer genereren gekwantificeerd zijn, kan de activering van stroompaden door micro- en mesotopografie bepaald worden. De resultaten die in dit proefschrift worden gepresenteerd geven nieuwe inzichten in de complexiteit van de processen en terugkoppelingen die leiden tot oppervlakkige afvoer in vlakke velden wanneer de neerslagintensiteit groter is dan de infiltratiecapaciteit of wanneer het waterbergend vermogen van de bodem is overschreden. De resultaten kunnen worden gebruikt om hydrologische modellen die op een grotere ruimtelijke schaal worden toegepast te parameteriseren en geven een indicatie van de stappen die genomen moeten worden om te komen tot een schatting van risico en impact van oppervlakkige afvoer op grotere ruimtelijke schalen.

Bibliography

- Abbott, M. B., J. C. Bathurst, J. A. Cunge, P. E. O'Connell, and J. Rasmussen (1986). An introduction to the European Hydrological System — Système Hydrologique Européen, "SHE": Structure of a physically-based, distributed modelling system. *Journal of Hydrology* 87, 61–77.
- Abrahams, A. D., A. J. Parsons, and J. Wainwright (1994). Resistance to overland flow on semiarid grassland and shrubland hillslopes, Walnut Gulch, southern Arizona. *Journal of Hydrology* 156(1-4), 431–446.
- Abrahams, A. D., A. J. Parsons, and J. Wainwright (2003). Disposition of rainwater under creosotebush. *Hydrological Processes* 17(13), 2555–2566.
- Ajayi, A. E., N. van de Giesen, and P. Vlek (2008). A numerical model for simulating Hortonian overland flow on tropical hillslopes with vegetation elements. *Hydrological Processes* 22(8), 1107–1118.
- Alvarez-Mozos, J., M. Angel Campo, R. Gimenez, J. Casali, and U. Leibar (2011). Implications of scale, slope, tillage operation and direction in the estimation of surface depression storage. *Soil & Tillage Research* 111(2), 142–153.
- Antoine, M., M. Javaux, and C. Bielders (2009). What indicators can capture runoff-relevant connectivity properties of the micro-topography at the plot scale? *Advances in Water Resources* 32(8), 1297–1310.
- Appels, W. M., P. W. Bogaart, and S. E. A. T. M. van der Zee (2011). Influence of spatial variations of microtopography and infiltration on surface runoff and field scale hydrological connectivity. *Advances in Water Resources* 34(2), 303–313.
- Augeard, B., C. Kao, C. Chaumont, and M. Vauclin (2005). Mechanisms of surface runoff genesis on a subsurface drained soil affected by surface crusting: A field investigation. *Physics and Chemistry of the Earth, Parts A/B/C* 30(8-10), 598–610.
- Baird, A. J., P. A. Eades, and B. W. J. Surridge (2008). The hydraulic structure of a raised bog and its implications for ecohydrological modelling of bog development. *Ecohydrology* 1(4), 289–298.
- Baird, A. J. and S. W. Gaffney (1995). A partial explanation of the dependency of hydraulic conductivity on positive pore water pressure in peat soils. *Earth Surface Processes and Landforms* 20(6), 561–566.
- Bartholomeus, R. P., J.-P. M. Witte, P. M. van Bodegom, J. C. van Dam, and R. Aerts (2008). Critical soil conditions for oxygen stress to plant roots: Substituting the Feddes-function by a process-based model. *Journal of Hydrology* 360(1-4), 147–165.

- Bates, P. D., M. G. Anderson, L. Baird, D. E. Walling, and D. Simm (1992). Modeling floodplain flows using a 2-dimensional finite-element model. *Earth Surface Processes and Landforms* 17(6), 575–588.
- Bates, P. D., M. S. Horritt, C. N. Smith, and D. Mason (1997). Integrating remote sensing observations of flood hydrology and hydraulic modelling. *Hydrological Processes* 11(14), 1777–1795.
- Beckwith, C. W. and A. J. Baird (2001). Effect of biogenic gas bubbles on water flow through poorly decomposed blanket peat. *Water Resources Research* 37(3), 551–558.
- Belyea, L. R. (2007). Climatic and topographic limits to the abundance of bog pools. *Hydrological Processes* 21(5), 675–687.
- Belyea, L. R. and A. J. Baird (2006). Beyond "the limits to peat bog growth": cross-scale feedback in peatland development. *Ecological Monographs* 76(3), 299–322.
- Belyea, L. R. and R. S. Clymo (2001). Feedback control of the rate of peat formation. *Proceedings of the Royal Society of London Series B-Biological Sciences* 268(1473), 1315–1321.
- Bergkamp, G. (1998). A hierarchical view of the interactions of runoff and infiltration with vegetation and microtopography in semiarid shrublands. *Catena* 33(3-4), 201–220.
- Beven, K. J. (2002). *Rainfall-runoff modelling, the Primer*. Chichester, England: John Wiley and Sons.
- Beven, K. J. (2004). Robert E. Horton's perceptual model of infiltration processes. *Hydrological Processes* 18(17), 3447–3460.
- Beven, K. J., R. Lamb, P. Quinn, R. Romanowicz, and J. Freer (1995). Topmodel. In V. P. Singh (Ed.), *Computer Models of Watershed Hydrology*, pp. 627–668. Water Resources Publications.
- Bierkens, M. F. P. and B. J. J. M. van den Hurk (2007). Groundwater convergence as a possible mechanism for multi-year persistence in rainfall. *Geophysical Research Letters* 34(2).
- Blanchoud, H., E. Moreau-Guigon, F. Farrugia, M. Chevreuil, and J. M. Mouchel (2007). Contribution by urban and agricultural pesticide uses to water contamination at the scale of the Marne watershed. *Science of the Total Environment* 375(1-3), 168–179.
- Bolinder, M. A., R. R. Simard, S. Beauchemin, and K. B. MacDonald (2000). Indicator of risk of water contamination by P for Soil Landscape of Canada polygons. *Canadian Journal of Soil Science* 80(1), 153–163.

- Bracken, L. J. and J. Croke (2007). The concept of hydrological connectivity and its contribution to understanding runoff-dominated geomorphic systems. *Hydrological Processes* 21(13), 1749–1763.
- Brauer, C. C., A. J. Teuling, A. Overeem, Y. van der Velde, P. Hazenberg, P. M. M. Warmerdam, and R. Uijlenhoet (2011). Anatomy of extraordinary rainfall and flash flood in a Dutch lowland catchment. *Hydrology and Earth System Sciences* 15(6), 1991–2005.
- Bronstert, A. and A. Bárdossy (2003). Uncertainty of runoff modelling at the hillslope scale due to temporal variations of rainfall intensity. *Physics and Chemistry of the Earth, Parts A/B/C* 28(6-7), 283–288.
- Brutsaert, W. (2005). *Hydrology An Introduction*. New York: Cambridge University Press.
- Burton, A., C. G. Kilsby, H. J. Fowler, P. S. P. Cowpertwait, and P. E. O’Connell (2008). RainSim: a spatial-temporal stochastic rainfall modelling system. *Environmental Modelling & Software* 23(12), 1356–1369.
- Campbell, G. S. (1974). Simple method for determining unsaturated conductivity from moisture retention data. *Soil Science* 117(6), 311–314.
- Camporese, M., C. Paniconi, M. Putti, and S. Orlandini (2010). Surface-subsurface flow modeling with path-based runoff routing, boundary condition-based coupling, and assimilation of multisource observation data. *Water Resources Research* 46, W02512.
- Chason, D. B. and D. I. Siegel (1986). Hydraulic conductivity and related physical-properties of peat, lost river peatland, northern Minnesota. *Soil Science* 142(2), 91–99.
- Church, M. and M.-K. Woo (1999). Geography of surface runoff: some lessons for research. In M. G. Anderson and T. P. Burt (Eds.), *Process Studies in Hillslope Hydrology*. Chichester, England: John Wiley and Sons.
- Cirkel, D. G., J. P. M. Witte, P. M. van Bodegom, J. J. Nijp, and S. E. A. T. M. van der Zee (2012). The influence of spatiotemporal variability and adaptations to hypoxia on empirical relationships between soil acidity and vegetation. *Ecohydrology*.
- Cirkel, D. G., J.-P. M. Witte, and S. E. A. T. M. van der Zee (2010). Estimating seepage intensities from groundwater level time series by inverse modelling: A sensitivity analysis on wet meadow scenarios. *Journal of Hydrology* 385(1-4), 132–142.
- Clapp, R. B. and G. M. Hornberger (1978). Empirical equations for some soil hydraulic-properties. *Water Resources Research* 14(4), 601–604.
- Clymo, R. S. (1984). The limits to peat bog growth. *Philosophical Transactions of the Royal Society B: Biological Sciences* 303(1117), 605–654.

- Clymo, R. S. (1992). Models of peat growth. *Suo (Helsinki)* 43(4-5), 127–136.
- Cremers, N. H. D. T., P. M. van Dijk, A. P. J. DeRoo, and M. A. Verzandvoort (1996). Spatial and temporal variability of soil surface roughness and the application in hydrological and soil erosion modelling. *Hydrological Processes* 10(8), 1035–1047.
- Darboux, F., P. Davy, and C. Gascuel-Oudou (2002a). Effect of depression storage capacity on overland-flow generation for rough horizontal surfaces: Water transfer distance and scaling. *Earth Surface Processes and Landforms* 27(2), 177–191.
- Darboux, F., P. Davy, C. Gascuel-Oudou, and C. Huang (2001). Evolution of soil surface roughness and flowpath connectivity in overland flow experiments. *Catena* 46(2-3), 125–139.
- Darboux, F., C. Gascuel-Oudou, and P. Davy (2002b). Effects of surface water storage by soil roughness on overland-flow generation. *Earth Surface Processes and Landforms* 27(3), 223–233.
- De Baets, S., J. Poesen, G. Gyssels, and A. Knapen (2006). Effects of grass roots on the erodibility of topsoils during concentrated flow. *Geomorphology* 76(1-2), 54–67.
- de Vries, J. (1994). Dynamics of the interface between streams and groundwater systems in lowland areas, with reference to stream net evolution. *Journal of Hydrology* 155(1-2), 39–56.
- de Vries, J. (1995). Seasonal expansion and contraction of stream networks in shallow groundwater systems. *Journal of Hydrology* 170(1-4), 15–26.
- de Zeeuw, J. and F. Hellinga (1958). Neerslag en afvoer. *Landbouwkundig Tijdschrift* 70, 405–422.
- Deasy, C., R. E. Brazier, A. L. Heathwaite, and R. Hodgkinson (2009). Pathways of runoff and sediment transfer in small agricultural catchments. *Hydrological Processes* 23(9), 1349–1358.
- Deasy, C., A. L. Heathwaite, and R. E. Brazier (2008). A field methodology for quantifying phosphorus transfer and delivery to streams in first order agricultural catchments. *Journal of Hydrology* 350(3-4), 329–338.
- Dekker, S. C., A. Barendregt, M. C. Bootsma, and P. P. Schot (2005). Modelling hydrological management for the restoration of acidified floating fens. *Hydrological Processes* 19(20), 3973–3984.
- Delestre, O., S. Cordier, F. Darboux, M. Du, F. James, C. Laguerre, C. Lucas, and O. Planchon (2012). FullSWOF: a software for overland flow simulation / FullSWOF: un logiciel pour la simulation du ruissellement. *arXiv*, arXiv:1204.3210.

- Dooge, J. C. I. (1957). The rational method for estimating flood peaks. *Engineering* 184, 311–313,374–377.
- Dunne, T. and R. D. Black (1970). An experimental investigation of runoff production in permeable soils. *Water Resources Research* 6(2), 478–490.
- Dunne, T., W. H. Zhang, and B. F. Aubry (1991). Effects of rainfall, vegetation, and microtopography on infiltration and runoff. *Water Resources Research* 27(9), 2271–2285.
- Eeman, S., A. Leijnse, P. A. C. Raats, and S. E. A. T. M. van der Zee (2011). Analysis of the thickness of a fresh water lens and of the transition zone between this lens and upwelling saline water. *Advances in Water Resources* 34(2), 291–302.
- Eggelsmann, R. (1967). Oberflächengefälle und Abflussregime der Hochmoore. *Wasser Boden* 19, 247–252.
- Egner, H., H. Riehm, and W. R. Domingo (1960). Investigations on chemical soil analysis as the basis for estimating soil fertility. II. Chemical extraction methods for phosphorus and potassium determination. *Kungliga Lantbrukshogskolans Annaler* 26, 199–215.
- Eppinga, M. B., P. C. de Ruiter, M. J. Wassen, and M. Rietkerk (2009). Nutrients and hydrology indicate the driving mechanisms of peatland surface patterning. *The American Naturalist* 173(6), 803–818.
- Ernst, L. F. (1956). Calculation of the steady flow of groundwater in vertical cross-sections. *Netherlands Journal of Agricultural Science* 4, 126–131.
- FAO (2008). FAO-UNESCO Soil map of the world. Revised legend. World Soil Resources Report 60, FAO, Rome, Italy.
- Fiedler, F. R., G. W. Frasier, J. A. Ramirez, and L. R. Ahuja (2002). Hydrologic response of grasslands: Effects of grazing, interactive infiltration, and scale. *Journal of Hydrologic Engineering* 7(4), 293–301.
- Fiedler, F. R. and J. A. Ramirez (2000). A numerical method for simulating discontinuous shallow flow over an infiltrating surface. *International Journal for Numerical Methods in Fluids* 32(2), 219–240.
- Freeze, R. and R. Harlan (1969). Blueprint for a physically-based, digitally-simulated hydrologic response model. *Journal of Hydrology* 9(3), 237–258.
- Frei, S., G. Lischeid, and J. H. Fleckenstein (2010). Effects of micro-topography on surface-subsurface exchange and runoff generation in a virtual riparian wetland - A modeling study. *Advances in Water Resources* 33(11), 1388–1401.

- Frolking, S., N. T. Roulet, T. R. Moore, P. J. H. Richard, M. Lavoie, and S. D. Muller (2001). Modeling northern peatland decomposition and peat accumulation. *Ecosystems* 4(5), 479–498.
- Glover, F. and L. Dumm (1960). Validity and use of the transient flow concept in subsurface drainage. *Proceedings of the American Society of Agricultural Engineers Meeting*, 4–7.
- Green, J. C. (2005). Modelling flow resistance in vegetated streams: review and development of new theory. *Hydrological Processes* 19(6), 1245–1259.
- Hairsine, P. B. and C. W. Rose (1992). Modeling Water Erosion Due to Overland-Flow Using Physical Principles .1. Sheet Flow. *Water Resources Research* 28(1), 237–243.
- Hansen, B., P. Schjonning, and E. Sibbesen (1999). Roughness indices for estimation of depression storage capacity of tilled soil surfaces. *Soil and Tillage Research* 52(1-2), 103–111.
- Hart, M. R. and P. S. Cornish (2012). Available soil phosphorus, phosphorus buffering and soil cover determine most variation in phosphorus concentration in runoff from pastoral sites. *Nutrient Cycling in Agroecosystems* 93(2), 227–244.
- Haygarth, P. M., A. L. Heathwaite, S. C. Jarvis, and T. R. Harrod (2000). Hydrological factors for phosphorus transfer from agricultural soils. *Advances in Agronomy* 69, 153–178.
- He, G., V. Engel, L. Leonard, A. Croft, D. Childers, M. Laas, Y. Deng, and H. M. Solo-Gabriele (2010). Factors controlling surface water flow in a low-gradient subtropical wetland. *Wetlands* 30(2), 275–286.
- Heathwaite, A. L., P. F. Quinn, and C. J. M. Hewett (2005). Modelling and managing critical source areas of diffuse pollution from agricultural land using flow connectivity simulation. *Journal of Hydrology* 304(1-4), 446–461.
- Helming, K., M. J. M. Romkens, and S. N. Prasad (1998). Surface roughness related processes of runoff and soil loss: A flume study. *Soil Science Society of America Journal* 62(1), 243–250.
- Hendriks, M. R. (2010). *Introduction to Physical Hydrology*. Oxford, England: Oxford University Press.
- Herron, N. F. and P. B. Hairsine (1998). A scheme for evaluating the effectiveness of riparian zones in reducing overland flow to streams. *Australian Journal of Soil Research* 36(4), 683–698.
- Hillel, D. (1980). *Applications of Soil Physics*. New York: Academic Press, INC.

- HilleRisLambers, R., M. Rietkerk, F. van den Bosch, H. H. T. Prins, and H. de Kroon (2001). Vegetation pattern formation in semi-arid grazing systems. *Ecology* 82(1), 50–61.
- Hinsinger, P., A. G. Bengough, D. Vetterlein, and I. M. Young (2009). Rhizosphere: biophysics, biogeochemistry and ecological relevance. *Plant and Soil* 321(1-2), 117–152.
- Holden, J. and T. P. Burt (2003a). Hydraulic conductivity in upland blanket peat: measurement and variability. *Hydrological Processes* 17(6), 1227–1237.
- Holden, J. and T. P. Burt (2003b). Hydrological studies on blanket peat: the significance of the acrotelm-catotelm model. *Journal of Ecology* 91(1), 86–102.
- Holden, J., M. J. Kirkby, S. N. Lane, D. G. Milledge, C. J. Brookes, V. Holden, and A. T. McDonald (2008). Overland flow velocity and roughness properties in peatlands. *Water Resources Research* 44(6), 1–11.
- Hooghoudt, S. B. (1940). Algemene beschouwing van het probleem van detailontwatering en de infiltratie door middel van parallel lopende drains, greppels, sloten en kanalen. Verslag Landbouwkundig Onderzoek 46(14).
- Horton, R. E. (1933). The role of infiltration in the hydrologic cycle. *Transactions of the American Geophysical Union* 14, 446–460.
- Ingram, H. A. P. (1978). Soil layers in mires: function and terminology. *Journal of Soil Science* 29(2), 224–227.
- Ivanov, K. E. (1981). *Water movement in mirelands*. London: Academic Press Inc.
- Ivanov, V. Y., E. R. Vivoni, R. L. Bras, and D. Entekhabi (2004). Catchment hydrologic response with a fully distributed triangulated irregular network model. *Water Resources Research* 40(11).
- Kamphorst, E. C., V. Jetten, J. Guerif, J. Pitkanen, B. V. Iversen, J. T. Douglas, and A. Paz (2000). Predicting depressional storage from soil surface roughness. *Soil Science Society of America Journal* 64(5), 1749–1758.
- Kirchner, J. W. (2006). Getting the right answers for the right reasons: Linking measurements, analyses, and models to advance the science of hydrology. *Water Resources Research* 42(3), doi:10.1029/2005WR004362.
- Kirkby, M. J. (1975). Hydrograph modelling strategies. In R. Peel, M. Chisholm, and P. Haggett (Eds.), *Processes in Human and Physical Geography*, pp. 69–90. London: Heinemann.
- Kleinhans, M. G., C. J. J. Buskes, and H. W. de Regt (2005). Terra Incognita: Explanation and Reduction in Earth Science. *International Studies in the Philosophy of Science* 19(3), 289–317.

- Klijn, F. and J. P. M. Witte (1999). Eco-hydrology: Groundwater flow and site factors in plant ecology. *Hydrogeology Journal* 7(1), 65–77.
- Koch, M. S., I. A. Mendelssohn, and K. L. Mckee (1990). Mechanism for the hydrogen sulfide-induced growth limitation in wetland macrophytes. *Limnology and Oceanography* 35(2), 399–408.
- Koerselman, W., M. B. Vankerkhoven, and J. T. A. Verhoeven (1993). Release of inorganic N, P and K in peat soils - effect of temperature, water chemistry and water-level. *Biogeochemistry* 20(2), 63–81.
- Kollet, S. J. and R. M. Maxwell (2006). Integrated surface-groundwater flow modeling: A free-surface overland flow boundary condition in a parallel groundwater flow model. *Advances in Water Resources* 29(7), 945–958.
- Kraijenhoff van de Leur, D. A. (1958). A study of non-steady groundwater flow with special reference to a reservoir coefficient. *De Ingenieur* 70, 87–94.
- Kronvang, B., A. Laubel, and R. Grant (1997). Suspended sediment and particulate phosphorus transport and delivery pathways in an arable catchment, Gelbaek Stream, Denmark. *Hydrological Processes* 11(6), 627–642.
- Kvarner, J. and B. Klove (2006). Tracing sources of summer streamflow in boreal headwaters using isotopic signatures and water geochemical components. *Journal of Hydrology* 331(1–2), 186–204.
- Lane, S. N. (1998). Hydraulic modelling in hydrology and geomorphology: A review of high resolution approaches. *Hydrological Processes* 12(8), 1131–1150.
- Lane, S. N. and R. J. Hardy (2002). Porous rivers: a new way of conceptualising river and floodplain flows? In D. B. Ingham and I. Pop (Eds.), *Transport Phenomena in Porous Media*. Pergamon.
- Lane, S. N., S. M. Reaney, and A. L. Heathwaite (2009). Representation of landscape hydrological connectivity using a topographically driven surface flow index. *Water Resources Research* 45, doi:10.1029/2008WR007336.
- Langlois, J. L. and G. R. Mehuys (2003). Intra-storm study of solute chemical composition of overland flow water in two agricultural fields. *Journal of Environmental Quality* 32(6), 2301–2310.
- Lapen, D. R., J. S. Price, and R. Gilbert (2005). Modelling two-dimensional steady-state groundwater flow and flow sensitivity to boundary conditions in blanket peat complexes. *Hydrological Processes* 19(2), 371–386.
- Larsen, L. G. and J. W. Harvey (2011). Modeling of hydroecological feedbacks predicts distinct classes of landscape pattern, process, and restoration potential in shallow aquatic ecosystems. *Geomorphology* 126(3-4), 279–296.

- Lexartza-Artza, I. and J. Wainwright (2009). Hydrological connectivity: Linking concepts with practical implications. *Catena* 79(2), 146–152.
- Loague, K., C. S. Heppner, B. A. Ebel, and J. E. VanderKwaak (2010). The quixotic search for a comprehensive understanding of hydrologic response at the surface: Horton, Dunne, Dunton, and the role of concept-development simulation. *Hydrological Processes* 24(17), 2499–2505.
- Louchart, X., M. Voltz, P. Andrieux, and R. Moussa (2001). Herbicide transport to surface waters at field and watershed scales in a Mediterranean vineyard area. *Journal of Environmental Quality* 30(3), 982–991.
- Ludwig, J. A., B. P. Wilcox, D. D. Breshears, D. J. Tongway, and A. C. Imeson (2005). Vegetation patches and runoff-erosion as interacting ecohydrological processes in semiarid landscapes. *Ecology* 86(2), 288–297.
- Luhar, M., J. Rominger, and H. Nepf (2008). Interaction between flow, transport and vegetation spatial structure. *Environmental Fluid Mechanics* 8(5-6), 423–439.
- Martinec, J. and A. Rango (1986). Parameter values for snowmelt runoff modelling. *Journal of Hydrology* 84, 197–219.
- Massop, H. T. L., I. G. A. M. Noij, W. M. Appels, and A. van den Toorn (2012). Oppervlakkige afspoeling op landbouwgronden. Metingen op zandgrond in Limburg. Scientific report 2270, Alterra, Research Institute for the Green World, Wageningen.
- Mayor, A. G., S. Bautista, E. E. Small, M. Dixon, and J. Bellot (2008). Measurement of the connectivity of runoff source areas as determined by vegetation pattern and topography: A tool for assessing potential water and soil losses in drylands. *Water Resources Research* 44(10).
- McDonnell, J. J., M. Sivapalan, K. Vache, S. Dunn, G. Grant, R. Haggerty, C. Hinz, R. Hooper, J. W. Kirchner, M. L. Roderick, J. Selker, and M. Weiler (2007). Moving beyond heterogeneity and process complexity: A new vision for watershed hydrology. *Water Resources Research* 43(7), doi:10.1029/2006WR005467.
- Meng, H., T. R. Green, J. D. Saias, and L. R. Ahuja (2008). Development and testing of a terrain-based hydrologic model for spatial Hortonian infiltration and Runoff/On. *Environmental Modelling & Software* 23(6), 794–812.
- Moore, I. D. and C. L. Larson (1979). Estimating Micro-Relief surface storage from point data. *Transactions of the ASAE* 22(5), 1073–1077.
- Morbidelli, R., C. Corradini, and R. S. Govindaraju (2006). A field-scale infiltration model accounting for spatial heterogeneity of rainfall and soil saturated hydraulic conductivity. *Hydrological Processes* 20(7), 1465–1481.

- Morris, P. J., J. M. Waddington, B. W. Benscoter, and M. R. Turetsky (2011). Conceptual frameworks in peatland ecohydrology: looking beyond the two-layered (acrotelm-catotelm) model. *Ecohydrology* 4(1), 1–11.
- Moser, K., C. Ahn, and G. Noe (2007). Characterization of microtopography and its influence on vegetation patterns in created wetlands. *Wetlands* 27(4), 1081–1097.
- Mueller, E. N., J. Wainwright, and A. J. Parsons (2007). Impact of connectivity on the modeling of overland flow within semiarid shrubland environments. *Water Resources Research* 43(9), doi:10.1029/2006WR005006.
- Mulder, J., N. Christophersen, K. Kopperud, and P. H. Fjeldal (1995). Water flow paths and the spatial distribution of soils as a key to understanding differences in streamwater chemistry between three catchments (Norway). *Water, Air, & Soil Pollution* 81(1–2), 67–91.
- Nachabe, M. H. (2002). Analytical expressions for transient specific yield and shallow water table drainage. *Water Resources Research* 38(10), doi:10.1029/2001WR001071.
- Nepf, H. M. (1999). Drag, turbulence, and diffusion in flow through emergent vegetation. *Water Resources Research* 35(2), 479–489.
- Nijp, J. J. Spatial heterogeneity of microtopography, soil water acidity, and vegetation composition in a *Cirsio-Molinietum-Caricetum elatae* gradient. MSc thesis, Wageningen University, Wageningen, The Netherlands.
- NIST (2010). *NIST Handbook of Mathematical Functions*. Cambridge, England: Cambridge University Press.
- Noij, I. G. A. M., P. J. T. van Bakel, R. A. Smidt, H. T. L. Massop, and W. J. Chardon (2007). Fosfaatpilot Noord- en Midden-Limburg. plan van aanpak en monitoring. Scientific report 1255, Alterra, Research Institute for the Green World, Wageningen.
- Noij, I. G. A. M., C. van der Salm, H. T. L. Massop, E. M. P. M. van Boekel, C. Schuiling, M. Pleijter, O. Clevering, P. J. T. van Bakel, W. J. Chardon, and D. J. J. Walvoort (2009). Beleidskader fosfaat voor Noord- en Midden-Limburg. wetenschappelijke onderbouwing. Scientific report 1894, Alterra, Research Institute for the Green World, Wageningen.
- Novozamsky, I., R. Vaneck, V. J. G. Houba, and J. J. Vanderlee (1986). Use of Inductively Coupled Plasma Atomic Emission-Spectrometry for Determination of Iron, Aluminum and Phosphorus in Tamm Soil Extracts. *Netherlands Journal of Agricultural Science* 34(2), 185–191.
- Oenema, O., L. van Liere, and O. Schoumans (2005). Effects of lowering nitrogen and phosphorus surpluses in agriculture on the quality of groundwater and surface water in The Netherlands. *Journal of Hydrology* 304(1-4), 289–301.

- Onstad, C. A. (1984). Depressional storage on tilled soil surfaces. *Transactions of the ASAE* 27(3), 729–732.
- Orlandini, S., M. Mancini, C. Paniconi, and R. Rosso (1996, July). Local contributions to infiltration excess runoff for a conceptual catchment scale model. *Water Resources Research* 32(7), 2003–2012.
- Ouyang, W., H. Huang, F. Hao, Y. Shan, and B. Guo (2012). Evaluating spatial interaction of soil property with non-point source pollution at watershed scale: The phosphorus indicator in Northeast China. *Science of the Total Environment* 432, 412–421.
- Overeem, A., T. A. Buishand, and I. Holleman (2009a). Extreme rainfall analysis and estimation of depth-duration-frequency curves using weather radar. *Water Resources Research* 45, doi:10.1029/2009WR007869.
- Overeem, A., I. Holleman, and T. A. Buishand (2009b). Derivation of a 10-year radar-based climatology of rainfall. *Journal of Applied Meteorology and Climatology* 48, 1448–1463.
- Paniconi, C. and E. F. Wood (1993, June). A detailed model for simulation of catchment scale subsurface hydrologic processes. *Water Resources Research* 29(6), 1601–1620.
- Pärn, J., G. Pinay, and U. Mander (2012). Indicators of nutrients transport from agricultural catchments under temperate climate: A review. *Ecological Indicators* 22, 4–15.
- Peñuela, A., M. Javaux, and C. L. Bièlders (2013). Scale effect on overland flow connectivity at the plot scale. *Hydrology and Earth System Sciences* 17(1), 87–101.
- Peach, M. and J. B. Zedler (2006). How tussocks structure sedge meadow vegetation. *Wetlands* 26(2), 322–335.
- Philip, J. R. (1957a). The Theory of Infiltration: 1. The Infiltration Equation and Its Solution. *Soil Science* 83(5), 345–358.
- Philip, J. R. (1957b). The Theory of Infiltration: 4. Sorptivity and Algebraic Infiltration Equations. *Soil Science* 84(3), 257–264.
- Piper, A. M. (1953). A graphic procedure for the geo-chemical interpretation of water analysis. USGS Groundwater Note 12, USGS.
- Poethig, R., H. Behrendt, D. Opitz, and G. Furrer (2010). A universal method to assess the potential of phosphorus loss from soil to aquatic ecosystems. *Environmental Science and Pollution Research* 17(2), 497–504.
- Pouliot, R., L. Rochefort, and E. Karofeld (2011). Initiation of microtopography in revegetated cutover peatlands. *Applied Vegetation Science* 14(2), 158–171.

- Probst, J. L. (1985). Nitrogen and phosphorus exportation in the Garonne Basin (France). *Journal of Hydrology* 76(3-4), 281–305.
- Puustinen, M., E. Turtola, M. Kukkonen, J. Koskiaho, J. Linjama, R. Niinioja, and S. Tattari (2010). VIHMA-A tool for allocation of measures to control erosion and nutrient loading from Finnish agricultural catchments. *Agriculture, Ecosystems & Environment* 138(3-4), 306–317.
- Quinton, W. L. and N. T. Roulet (1998). Spring and summer runoff hydrology of a subarctic patterned wetland. *Arctic and Alpine Research* 30(3), 285–294.
- R Development Core Team (2010). R: A language and environment for statistical computing.
- Rango, A. and J. Martinec (1995). Revisiting the degree-day method for snowmelt computations. *Water Resources Bulletin* 31(4), 657–669.
- Rawls, W. J. (1992). Infiltration and soil water movement. In *Handbook of Hydrology*. McGraw-Hill. Inc, USA.
- Reaney, S. M., L. J. Bracken, and M. J. Kirkby (2007). Use of the connectivity of runoff model (CRUM) to investigate the influence of storm characteristics on runoff generation and connectivity in semi-arid areas. *Hydrological Processes* 21(7), 894–906.
- Reeve, A., D. Siegel, and P. Glaser (2000). Simulating vertical flow in large peatlands. *Journal of Hydrology* 227(1–4), 207–217.
- Rezanezhad, F., W. L. Quinton, J. S. Price, T. R. Elliot, D. Elrick, and K. R. Shook (2010). Influence of pore size and geometry on peat unsaturated hydraulic conductivity computed from 3D computed tomography image analysis. *Hydrological Processes* 24(21), 2983–2994.
- Rietkerk, M., M. C. Boerlijst, F. van Langevelde, R. HilleRisLambers, J. van de Koppel, L. Kumar, H. H. T. Prins, and A. M. de Roos (2002). Self-organization of vegetation in arid ecosystems. *American Naturalist* 160(4), 524–530.
- Romanov, V. V. (1968). *Hydrophysics of bogs (translated)*. Jerusalem, Israel: Israel program of scientific translations.
- Romkens, M. J. M., K. Helming, and S. N. Prasad (2002). Soil erosion under different rainfall intensities, surface roughness, and soil water regimes. *Catena* 46(2-3), 103–123.
- Ronkanen, A.-K. and B. Kløve (2007). Use of stable isotopes and tracers to detect preferential flow patterns in a peatland treating municipal wastewater. *Journal of Hydrology* 347(3–4), 418–429.

- Rosa, E. and M. Larocque (2008). Investigating peat hydrological properties using field and laboratory methods: application to the Lanoraie peatland complex (southern Quebec, Canada). *Hydrological Processes* 22(12), 1866–1875.
- Rozemeijer, J. C. (2010). *Dynamics in groundwater and surface water quality: From field-scale processes to catchment-scale monitoring*. PhD thesis, Utrecht University, Utrecht, The Netherlands.
- Rycroft, D. W., D. J. A. Williams, and H. A. P. Ingram (1975). The transmission of water through peat: II. Field experiments. *Journal of Ecology* 63(2), 557–568.
- Salvucci, G. D. and D. Entekhabi (1994). Equivalent steady soil-moisture profile and the time compression approximation in water-balance modeling. *Water Resources Research* 30(10), 2737–2749.
- Schot, P. P., S. C. Dekker, and A. Poot (2004). The dynamic form of rainwater lenses in drained fens. *Journal of Hydrology* 293(1-4), 74–84.
- Sharma, M. L., G. A. Gander, and C. G. Hunt (1980). Spatial variability of infiltration in a watershed. *Journal of Hydrology* 45(1-2), 101–122.
- Sharpley, A. N., J. L. Weld, D. B. Beegle, P. J. A. Kleinman, W. J. Gburek, P. A. Moore, and G. Mullins (2003). Development of phosphorus indices for nutrient management planning strategies in the United States. *Journal of Soil and Water Conservation* 58(3), 137–152.
- Simard, R. R., S. Beauchemin, and P. M. Haygarth (2000). Potential for preferential pathways of phosphorus transport. *Journal of Environmental Quality* 29(1), 97–105.
- Sissingh, H. A. (1971). Analytical technique of Pw method, used for assessment of phosphate status of arable soils in The Netherlands. *Plant and Soil* 34(2), 483–486.
- Sivapalan, M. and P. C. D. Milly (1989). On the relationship between the time condensation approximation and the flux concentration relation. *Journal of Hydrology* 105(3-4), 357–367.
- Sjors, H. (1990). Divergent successions in mires a comparative study. *Aquilo Ser Botanica* 28, 67–78.
- Smith, M. W., N. J. Cox, and L. J. Bracken (2010). Terrestrial laser scanning soil surfaces: a field methodology to examine soil surface roughness and overland flow hydraulics. *Hydrological Processes* 25.
- Smith, R. E. and R. H. B. Hebbert (1983). Mathematical simulation of interdependent surface and subsurface hydrologic processes. *Water Resources Research* 19(4), 987–1001.

- Sophocleous, M. (2002). Interactions between groundwater and surface water: The state of the science. *Hydrogeology Journal* 10(1), 52–67.
- Sørensen, R. and J. Seibert (2007). Effects of DEM resolution on the calculation of topographical indices: TWI and its components. *Journal of Hydrology* 347(1-2), 79–89.
- Sterling, A., B. Peco, M. A. Casado, E. F. Galiano, and F. D. Pineda (1984). Influence of microtopography on floristic variation in the ecological succession in grassland. *Oikos* 42(3), 334–342.
- Stiff, H. (1951). The interpretation of chemical water analysis by means of patterns. *Transactions of the American Institute of Mining and Metallurgical Engineers* 192, 376–378.
- Stolte, J., C. J. Ritsema, and H. Wösten (2000). Oppervlakte-afvoer: een combinatie van helling, bodem, gewas en regen. *Stromingen* 6(4), 27–36.
- Stuyfzand, P. J. (1986). Een nieuwe hydrochemische classificatie van watertypen, met Nederlandse voorbeelden van toepassing. *H₂O* 19, 562–568.
- Sumner, D. M. (2007). Effects of capillarity and microtopography on wetland specific yield. *Wetlands* 27(3), 693–701.
- Taskinen, A., H. Sirviö, and M. Bruen (2008). Generation of two-dimensionally variable saturated hydraulic conductivity fields: Model theory, verification and computer program. *Computers & Geosciences* 34(8), 876–890.
- Tayfur, G. and M. L. Kavvas (1998). Areally-averaged overland flow equations at hillslope scale. *Hydrological Sciences Journal — Journal Des Sciences Hydrologiques* 43(3), 361–378.
- Therrien, R., R. G. McLaren, E. A. Sudicky, and S. M. Panday (2008). HydroGeoSphere a threedimensional numerical model describing fully-integrated subsurface and surface flow and solute transport. Manual, University of Waterloo, Groundwater Simulations Group, Waterloo.
- Thompson, S. E., G. G. Katul, and A. Porporato (2010). Role of microtopography in rainfall-runoff partitioning: An analysis using idealized geometry. *Water Resources Research* 46, 11 PP.
- Tipper, J. C. (2008). Models that talk back. In P. de Boer, G. Postma, K. van der Zwan, P. Burgess, and P. Kukla (Eds.), *Analogue and Numerical Modelling of Sedimentary Systems: from Understanding to Prediction*, pp. 287–306. Chicester, England: John Wiley and Sons.
- TNO-NITG (2012, nov). Dinoloket. <http://www.dinoloket.nl>.

- Tsuboya, T., K. Takagi, H. Takahashi, Y. Kurashige, and N. Tase (2001). Effect of pore structure on redistribution of subsurface water in Sarobetsu Mire, northern Japan. *Journal of Hydrology* 252(1–4), 100–115.
- Turtola, E. and A. Jaakkola (1995). Loss of phosphorus by surface runoff and leaching from a heavy clay soil under barley and grass ley in Finland. *Acta Agriculturae Scandinavica Section B-Soil and Plant Science* 45(3), 159–165.
- van Beek, C. L., C. van der Salm, A. C. C. Plette, and H. v. d. Weerd (2009). Nutrient loss pathways from grazed grasslands and the effects of decreasing inputs: experimental results for three soil types. *Nutrient Cycling in Agroecosystems* 83(2).
- van Breemen, N. (1995). How sphagnum bogs down other plants. *Trends in ecology & evolution* 10(7), 270–275.
- van den Akker, J. J. H. (2004). SOCOMO: a soil compaction model to calculate soil stresses and the subsoil carrying capacity. *Soil & Tillage Research* 79(1), 113–127.
- van der Ploeg, M. J., W. M. Appels, D. G. Cirkel, M. R. Oosterwoud, J.-P. M. Witte, and S. E. A. T. M. van der Zee (2012). Microtopography as a driving mechanism for ecohydrological processes in shallow groundwater systems. *Vadose Zone Journal* 11(3), vzj2011.0098.
- van der Salm, C., A. van den Toorn, W. J. Chardon, and G. F. Koopmans (2012). Water and nutrient transport on a heavy clay soil in a fluvial plain in the Netherlands. *Journal of Environmental Quality* 41(1).
- van der Schaaf, S. (2004). A single well pumping and recovery test to measure in situ acrotelm transmissivity in raised bogs. *Journal of Hydrology* 290(1–2).
- van der Velde, Y., G. H. de Rooij, and P. J. J. F. Torfs (2009). Catchment-scale non-linear groundwater-surface water interactions in densely drained lowland catchments. *Hydrology and Earth System Sciences* 13(10), 1867–1885.
- van der Velde, Y., J. C. Rozemeijer, G. H. de Rooij, F. C. van Geer, and H. P. Broers (2010). Field-Scale measurements for separation of catchment discharge into flow route contributions. *Vadose Zone Journal* 9(1), 25–35.
- van der Velde, Y., P. J. J. F. Torfs, S. E. A. T. M. van der Zee, and R. Uijlenhoet (2012). Quantifying catchment-scale mixing and its effect on time-varying travel time distributions. *Water Resources Research* 48(6).
- van der Welle, M. E. W., J. G. M. Roelofs, and L. P. M. Lamers (2008). Multi-level effects of sulphur-iron interactions in freshwater wetlands in The Netherlands. *Science of the Total Environment* 406(3), doi:10.1016/j.scitotenv.2008.05.056.

- van der Zee, S. E. A. T. M., W. H. van Riemsdijk, and F. A. M. de Haan (1990). The protocol of phosphate saturated soils. Part I: Explanation. Scientific report, Department of soil science and plant nutrition, Wageningen University, Wageningen, The Netherlands.
- van Genuchten, M. T. (1980). A closed-form equation for predicting the hydraulic conductivity of unsaturated soils. *Soil Science Society of America Journal* 44(5), 892–898.
- van Wirdum, G. (1991). *Vegetation and hydrology of floating rich-fens*. PhD thesis, University of Amsterdam, Amsterdam, The Netherlands.
- Vellidis, G., R. Lowrance, P. Gay, and R. K. Hubbard (2003). Nutrient transport in a restored riparian wetland. *Journal of Environmental Quality* 32(2), 711–726.
- Vivian-Smith, G. (1997). Microtopographic heterogeneity and floristic diversity in experimental wetland communities. *Journal of Ecology* 85(1), 71–82.
- Waddington, J. M., E. Kellner, M. Strack, and J. S. Price (2010). Differential peat deformation, compressibility, and water storage between peatland microforms: Implications for ecosystem function and development. *Water Resources Research* 46(7), 1–12.
- Wallen, B., U. Falkengrengrerup, and N. Malmer (1988). Biomass, Productivity and Relative Rate of Photosynthesis of Sphagnum at Different Water Levels on a South Swedish Peat Bog. *Holarctic Ecology* 11(1), 70–76.
- Weiler, M. and F. Naef (2003). An experimental tracer study of the role of macropores in infiltration in grassland soils. *Hydrological Processes* 17(2), 477–493.
- Werkgroep Herziening Cultuurtechnisch Vademecum (1988). Cultuurtechnisch Vademecum.
- Western, A. W., G. Blöschl, and R. B. Grayson (2001). Toward capturing hydrologically significant connectivity in spatial patterns. *Water Resources Research* 37(1), 83–97.
- Withers, P. J. A., R. H. Hodgkinson, H. Adamson, and G. Green (2007). The impact of pasture improvement on phosphorus concentrations in soils and streams in an upland catchment in Northern England. *Agriculture Ecosystems & Environment* 122(2), 220–232.
- Withers, P. J. A., B. Ulén, C. Stamm, and M. Bechmann (2003). Incidental phosphorus losses — are they significant and can they be predicted? *Journal of Plant Nutrition and Soil Science* 166(4), 459–468.
- Wolf, J., A. H. W. Beusen, P. Groenendijk, T. Kroon, R. Rotter, and H. van Zeijts (2003). The integrated modeling system STONE for calculating nutrient emissions from agriculture in The Netherlands. *Environmental Modelling & Software* 18(7), 597–617.

Wösten, J. H. M., G. J. Veerman, W. J. M. de Groot, and J. Stolte (2001).

Doorlatendheidskarakteristieken van boven- en ondergronden in Nederland: de Staringreeks. Alterra-rapport 153, Alterra, Research Instituut voor de Groene Ruimte, Wageningen.

Zimmerman, R. W. and G. S. Bodvarsson (1995). Estimation of hydraulic conductivities of Yucca Mountain tuffs from sorptivity and water retention measurements. Scientific report, Lawrence Berkeley Laboratory, University of California, Berkeley.

Zinn, B. and C. F. Harvey (2003). When good statistical models of aquifer heterogeneity go bad: A comparison of flow, dispersion, and mass transfer in connected and multivariate gaussian hydraulic conductivity fields. *Water Resources Research* 39(3), doi:10.1029/2001WR001146.

Dankwoord

Het is eindelijk af! En hoewel dit boekje het harde bewijs is van mijn persoonlijke leercurve de afgelopen jaren, had ik het natuurlijk nooit alleen kunnen doen.

Zoals met zoveel dingen, rolde ik via-via dit onderzoek in. Een gesprek tussen Henny van Werven en Sjoerd van der Zee (H: “Sjoerd, dit was een student van ons, heb je niet een baan voor haar?” S: “Ja, maar het is wel een promotietraject, vind je dat erg?” W: “Nee, dat is prima.”) resulteerde in een gesprek met alle projectpartners en een maand later in de transformatie van secretaresse bij Alterra naar AiO bij de leerstoelgroep SEG. Sjoerd, bedankt voor je immense hoeveelheid proefballonnen, je verzekering dat de resultaten wel degelijk interessant waren, je kritische blik op vrijwel alles en de ruimte die je gaf om zelf uit te vinden wat relevant en nieuw was. Patrick, je raakte gaandeweg meer bij mijn onderzoek betrokken en werd uiteindelijk officieel co-promotor. Zonder jouw ideeën en fenomenale kennis van wat er allemaal gedaan is en waar aanknopingspunten liggen was ik niet zover gekomen. De discussies met zijn drie-en waren af en toe behoorlijk fel, maar volgens mij waren we aan elkaar gewaagd en ik ben dan ook heel tevreden met jullie als begeleidingsteam! Het was fantastisch dat jullie op het eind zoveel tijd hebben vrijgemaakt om alle stukken op tijd af te maken. Naast de dagelijkse begeleiding heb ik veel gebruik gemaakt van de theoretische en technische ondersteuning van Toon Leijnse en Pieter Hazenberg.

De aanzet voor en de financiering van dit onderzoek was afkomstig van Alterra en mijn dank gaat uit naar iedereen die in eerdere of latere instantie betrokken was bij het uitzetten van de richting van het onderzoek, het opzetten van de veldproeven en het uitvoeren ervan (Frank, Ab, Piet, Rob, Han, Antonie, Jan). Een tweede samenwerking met Alterra kwam tot stand via het oppervlakkige afvoerproject van Gert-Jan Noij en Harry Massop en resulteerde in hoofdstuk vijf.

Collega's van SEG, het waren vijf fantastische jaren en ik ben blij dat ik met jullie heb kunnen samenwerken. Discussies over hoe het allemaal anders en beter kan, het vieren van piekmomenten en het ventileren van frustraties: het SEG-HWM koffiehalfuurtje, de lunch en de vrijdagmiddagborrels met of zonder afzakkertje met de usual suspects zal ik niet snel vergeten.

Sommige collega's hebben mijn promotietraject van dichterbij meegemaakt dan anderen: de eerste anderhalf jaar deelden Marieke en ik een luxueuze hoekkamer in Atlas met Peter, Ria en Han, later verkasten we naar een kamer op de SEG-gang waar Gijsbert onze vaste donderdaggast was. Met zijn drieën zaten we redelijk op hetzelfde tijdsschema, maar onze pieken en dalen kwamen gelukkig steeds op verschillende momenten, zodat er altijd wel iemand was om je ergens doorheen te praten. Ik ben dan

ook erg blij dat jullie naast mij op het podium staan. Marieke, ik kon me geen beter spiegelbeeld wensen; het blijft teleurstellend om nu langs mijn beeldscherm heen te kijken en alleen een cubicle-wand te zien.

Ik heb niet vijf jaar lang alleen maar gewerkt en mijn sociale kring bestaat uit meer dan collega's. Dat ging ik deste meer waarderen toen mijn contract was afgelopen, er nog een berg werk achterbleef en de stress exponentieel toenam. In willekeurige volgorde dank aan: de dames voor de bulk-emails, fietsvakanties, en feestjes ter ere van dertig worden; G7 flatmates for lovely dinners, lively discussions, parties, and the trips abroad; UMAten, Caprice en Daniëlle voor de enige echte manier van afleiding: hobo spelen; alle vrienden en collega's die me de laatste maanden op regelmatige basis van eten en drinken voorzagen; en mamma, pappa en Mark voor alle bevestiging en bemoediging en een plek om naar toe te rennen als het werk me boven het hoofd groeide.

Een PhD doen is echt fantastisch, maar het zou bloedsaai zijn in je eentje, dus uit de grond van mijn hart: **BEDANKT!**

Curriculum Vitae

Willemijn Maria Appels — 28 September 1981 — Helmond

1993–1999	Pre-university education Carolus Borromeus College & Stedelijk Gymnasium Arnhem	Helmond & Arnhem
2000–2004	BSc. Soil, Water, and Atmosphere Wageningen University	Wageningen
2004–2006	MSc. Hydrology and Water Quality Wageningen University	Wageningen
2006	Traineeship Hydrology Xi'an University of Architecture and Technology	Xi'an (China)
2007–2012	PhD Candidate Soil Physics, Ecohydrology and Groundwater Management Group Wageningen University	Wageningen
2012–present	Postdoctoral Fellow Global Institute for Water Security University of Saskatchewan	Saskatoon (Canada)

Publications related to this thesis:

- Appels, W.M., P.W. Bogaart, and S.E.A.T.M. van der Zee. 2011. Influence of spatial variations of microtopography and infiltration on surface runoff and field scale hydrological connectivity. *Advances in Water Resources* 34(2). 303–313.
- Van der Ploeg, M.J., W.M. Appels, D.G. Cirkel, M.R. Oosterwoud, J.-P.M. Witte, and S.E.A.T.M. van der Zee. 2012. Microtopography as a driving mechanism for ecohydrological processes in shallow groundwater systems. *Vadose Zone Journal* 11(3). vzt2011.0098.



Netherlands Research School for the
Socio-Economic and Natural Sciences of the Environment

C E R T I F I C A T E

The Netherlands Research School for the
Socio-Economic and Natural Sciences of the Environment
(SENSE), declares that

Willemijn Maria Appels

born on 28 September 1981 in Helmond, the Netherlands

has successfully fulfilled all requirements of the
Educational Programme of SENSE.

Wageningen, 19 March 2013

the Chairman of the SENSE board

Prof. dr. Rik Leemans

the SENSE Director of Education

Dr. Ad van Dommelen

The SENSE Research School has been accredited by the Royal Netherlands Academy of Arts and Sciences (KNAW)



K O N I N K L I J K E N E D E R L A N D S E
A K A D E M I E V A N W E T E N S C H A P P E N



The SENSE Research School declares that **Ms. Willemijn Appels** has successfully fulfilled all requirements of the Educational PhD Programme of SENSE with a work load of 43 ECTS, including the following activities:

SENSE PhD Courses

- o Environmental Research in Context
- o Research Context Activity: Designing and writing of competitive proposal *From salt water to fresh water in the province of Zeeland*
- o Uncertainty Modelling and Analysis

Other PhD and Advanced MSc Courses

- o Advanced Soil Physics
- o Sampling for Natural Resource Monitoring
- o NWO talent class Netwerken
- o Conceptual and mathematical models in multiphase flow
- o Characterisation of regional subsurface water
- o PhD competence assessment
- o Techniques for writing and presenting scientific papers

Management and Didactic Skills Training

- o Coordination of Wageningen Water Platform meetings
- o Supervision of two BSc Theses
- o Lecturing for the MSc course *Technical Concepts in Water Engineering*
- o Practical supervision for the BSc courses *Soil and Water 1 & 2* and *Hydrogeology*

Oral Presentations

- o *Puddles and Pools: redistribution of water at the soil surface*, Symposium on the Hydrological Cycle, WIMEK, 29 January 2009, Wageningen
- o *A numerical analysis of ponding and surface runoff*, International Conference on Non-linearities and Upscaling in Porous Media, 6 October 2009, Stuttgart, Germany

SENSE Coordinator PhD Education

Drs. Serge Stalpers